Synthesis and surface treatment of carbon nanotube films for field emission applications

(電界放出の応用を目指したカーボンナノチューブの製造と表面処理)

Sunwoo LEE (李　善雨)

Abstract

Carbon Nanotube (CNT) films were prepared by the catalytic chemical vapor deposition (CVD) method with introduction of ammonia gas during CNT synthesis process. The effect of the surface treatment on the field emission properties of the CNT films was investigated. Chemical treatments (O_2 (gas phase), HNO_3 (liquid phase), and HF (liquid phase) treatment) and plasma processes (Ar, N_2, and H_2 plasma process) were used as the surface treatment methods. The X-ray photoelectron spectroscopy (XPS) analysis was conducted on those surface treated CNT films to understand the change of the chemical bonding state. The scanning electron microscopy (SEM) and the transmission electron spectroscopy (TEM) analyses were carried out to observe the topological changes between the as-prepared CNT film and the treated CNT films.

It was found that the introduction of NH_3 gas during the synthesis of CNTs plays important role to synthesize the pure (including no impurities) and vertically aligned CNT films. Ammonia (NH_3) gas used in this work reduces the carbon ratio by supplying hydrogen, though there is no change of the decomposition rate of acetylene. As ammonia reduces the carbon ratio, the clean and pure CNTs can grow without deactivation. That ammonia also etches the catalyst surface even if the C_2H_2 is decomposed too much.

In all cases of the chemically treated CNT films, the carbon peak (C1s, 284.5 eV) and oxygen peak (O1s, 530 eV) were observed. The stronger oxygen peak than that of the original-CNT for the O_2-CNT, the weak nitrogen peak (trace level) for HNO_3-CNT, and the fluorine peak for HF-CNT were observed, respectively. This means that all of the chemical treatment could attach their functional groups to each CNT films. The surface treatments might affect the field emission property. The field emission current from CNT films could be expressed by using F-N (Flower-Nordheim) emission model. The field emission property in this equation is contributed by the field enhancement factor and the work function. The field enhancement factor is determined by the aspect ratio of the CNT film. As the surface treatment could change the aspect ratio of the CNT films, the field emission performance of the CNT film should be changed.

In the case of the chemical treatment CNT films, the threshold electric fields of the original CNT, O_2-CNT, HNO_3-CNT, and HF-CNT were 2.68, 2.42, 3.18, and 3.38 V/μm,

respectively. Only in the case of the O_2 treatment, the improvement of the field emission performance was acquired.

In the case of the Ar plasma processed CNT films, in order to evaluate the plasma processing time effect on the surface composition, the O1s/C1s ratio and the F1s/C1s ratio were obtained from the above XPS wide scan spectra. The O1s/C1s ratio and the F1s/C1s ratio were increased from 2.64 % to 59.16 % and from 0 % to 10.44 % with increasing plasma processing time, respectively. These results imply that the Ar plasma process could change the surface composition effectively. In the case of the original-CNT, no carbon shift was observed. In the case of the Ar plasma processed CNTs, however the oxygen related carbon shift was observed. This oxygen related carbon shift at higher binding energy implies the increment of amount of the oxygen. The gaps between the carbon shift and the sp^2 peak were observed as 3.9, 3.1, and 3.7 eV at the Ar plasma processed CNT film for 10, 30, and 60 mins, respectively. And in the case of the H_2 plasma processed CNT films, the oxygen related carbon shift moves toward the higher binding energy with increasing H_2 plasma processing time. Thus, the gap between the carbon shift and the sp^2 peak increased with increasing plasma processing time. This means that the bonding strength between carbon and oxygen became stronger with increasing H_2 plasma processing time.

A strong oxygen peak increasing the intensity with increasing the plasma processing time was observed at all of the plasma processed CNT films. The origin of this strong oxygen peak was thought to be the one of the following two possibilities. First one is from the water vapor in the air. And second one is from the wall of the plasma process chamber. In order to identify the origin of oxygen peak at the XPS spectra of the plasma processed CNT films, the CNT films exposed to dry air and wet air were investigated by using the XPS, after the take-off the functional groups attached to the surface of the plasma processed CNT films by ion etching in the XPS inspection chamber. There are no significant changes between dry and wet air exposed CNT films. This result means that the water vapor in the air doesn't play important role in the adhesion of the oxygen to the CNT surface during the plasma process. Therefore we can conclude that the origin of the oxygen peak in the XPS spectra is from the water vapor attached to the chamber wall.

Table of Contents

1. Introduction

1.1 General introduction

Since the discovery of carbon nanotube (CNT) by Iijima [1], many researchers have been attracted to this materials and a large number of studies have been piled up. CNT was first synthesized as a by-product in arc-discharge method in synthesis of fullerenes and are currently being prepared by many kinds of methods including arc-discharge [2-14], laser ablation [15-20], and catalytic decomposition of hydrocarbon [21-27]. In addition, electrolysis [28] and solar energy [29] methods have also been proposed. As for the application of CNT, there has been a remarkable progress in recent days such as that to the field electron emitter [30-34], for instance. Considering such rapid growth in many directions, we can expect that CNT could become one of the most important materials in the 21st century. CNT can be classified into two types: One is a multi walled CNT (MWCNT) [1,2] and another is a single walled CNT (SWCNT) [3]. The former had been discovered earlier that the latter. The MWCNT is comprised of 2 to 30 concentric graphitic layers, diameters of which range from 10 to 50 nm, and the length of more than 10 μm. On the other hand, SWCNT is much thinner with the diameter from 1.0 t0 1.4 nm.

There have been considerable efforts at synthesizing and purifying the MWCNT for the measurement of its physical properties. The time is, however, gradually maturing toward its industrial application. As to SWCNT, it could not be efficiently obtained at first and, furthermore, both of its purification and exact analysis of physical properties were difficult. SWCNT could be efficiently synthesized for the first time in 1996 [14,16]. After then, the SWCNT has become widely studied mainly in the scientific viewpoint.

Electron sources are omnipresent in modern society and play a central role in information display. It is often stated that conventional cathode ray tubes will soon be outclassed by plasma and liquid crystal displays and that the region of electron sources is waning rapidly. Conversely, electron field emitters are now becoming increasingly attractive as electron sources for similar applications. This resurgence is largely due to the recent development of cheap and robust electron field emitters.

Although field emission devices based on micro-fabricated Mo tips are commercially

available, researchers are actively looking for alternative materials. How would the ideal field emitter look like? It should be very long and very thin, made of conductive material with high mechanical strength, be robust, and cheap and easy to process.

Imagine taking a sheet of graphite, a simple planar assembly of carbon atoms disposed in a honeycomb lattice, and rolling it up to form a cylinder. You would obtain a very long, yet very thin cylindrical object. It would have properties similar to those of graphite, be flexible but very hard to stretch. You could assemble these cylinders together in ropes, or nest several of them, with increasing diameters, like a Russian doll.

Since 1991, the dream of fabricating, manipulating characterizing and modifying such cylindrical graphitic structures has become true. These objects were named carbon nanotubes and arose to one of the most fascinating materials that have been discovered in recent years [1]. Nanotubes show exceptional electronic [35-38] and mechanical [39-44] properties that have triggered an ever stronger effort towards applications. The possibilities are varied and promising and range from nanotube composite materials [45,46], nano-electronics [47-49], scanning microscope probes [50,51], chemical [52] and/or biological sensors [53,54], to electron sources.

The power of carbon nanotubes as electron field emitters was already apparent from the first articles reporting extremely low turn-on fields and high current densities in 1995 [55-57]. Only a few studies followed during the next two years. From 1998 on, the perspective to use nanotubes as field emission devices spurred efforts worldwide: a first crude display as well as a lighting element were presented. Later studies addressed issues of large scale production compatible with micro-fabrication technology and strove towards better understanding of the emission mechanism.

In this work, an application of CNT films to FED (field Emission Display) devices which is the most attractive one of the CNT's applications will be described. There are two parameters which determine the CNT's field emission property. The first one is a field enhancement factor concerning the surface topology of the tip which is determined by the aspect ratio of the tip. The other one is a work function concerning the chemical state of the surface.

Therefore, studies about the improvement of the field emission property will be executed in these two ways. The studies about the improvement of the field emission property by the control of the aspect ratio of the CNT tip have been conducted and

reported energetically. However, the improvement method concerning the work function has not been developed.

In order to improve the field emission property in this work, the work function control method was examined by using the chemical treatment and the plasma process.

1.2 What is carbon nanotube

As numerous researches have been reported on new physical phenomena and advanced properties of materials in the extremely infinitesimal areas of nanoscale size in recent years, a new area called nanotechnologies came into being. These nanotechnologies have emerged as a future leader in areas, such as electronic information communications, medicine, material, production process, environment, and energy. As new material properties of carbon nanotubes, in particular, can be realized among other nanotechnologies, both the importance in basic research and industrial applicability are being in the great limelight.

1.2.1 History of carbon nanotubes

After Kroto and Smalley discovered Fullerene [58], one of carbon allotropes(a cluster of 60 carbon atoms : C_{60}) for the first time in 1985, Dr. Iijima [59], a researcher of this new material, of the NEC laboratories in Japan, in 1991 discovered thin and long straw-shaped carbon nanotubes during a TEM analysis of carbon clusters synthesized by the arc-discharge method. This discovery was published in Nature for the first time. The nanotubes range in length from a few tens of nanometers to several micrometers, and in outer diameter from about 2.5 nm to 30 nm. A carbon atom in nanotubes forms a hexagonal honeycomb lattice of sp2 bond with 3 other carbon atoms. As the outer diameters of the tubes are extremely thin down to about several nanometers, the tubes are called nanotubes. In 1992, Ebbesen and Ajayan [60] reported that increasing the pressure in the chamber of an arc-evaporation had greatly improved the nanotube yield on the cathode of graphite. The year 1993 witnessed that Bethune of IBM and Iijima of NEC independently synthesized carbon nanotubes, of which the diameters are 1nm, using arc-discharge methods [61]. Subsequently, Smalley's group in 1996 reported a high yield method of preparing single-walled nanotubes with unusually uniform diameters by the laser-vaporization of graphite [62]. These tubes had a tendency to from aligned bundles, and led Smalley to christen the bundles 'rope'. Using the plasma-enhanced chemical vapor deposition, Ren et al. in 1998 made a breakthrough in synthesis and application of carbon nanotubes by growing highly pure carbon nanotubes vertically aligned on a glass substrate [63]. Since then, researches into synthesis and application have been vigorously conducted around the world.

1.2.2 Carbon related materials

Fig. 1.1 shows images of different carbon related materials. The graphite sheets of carbon nanotubes are actually rolled into a nano-scale cylinder with sp^2 bonding structures. Whether carbon nanotubes are electrically conductors or semiconductors depends on the angle and form at which their graphite sheets are rolled up. Carbon nanotubes can be also classified into Single-walled, Multi-walled, and Rope nanotubes in their rolled shape.

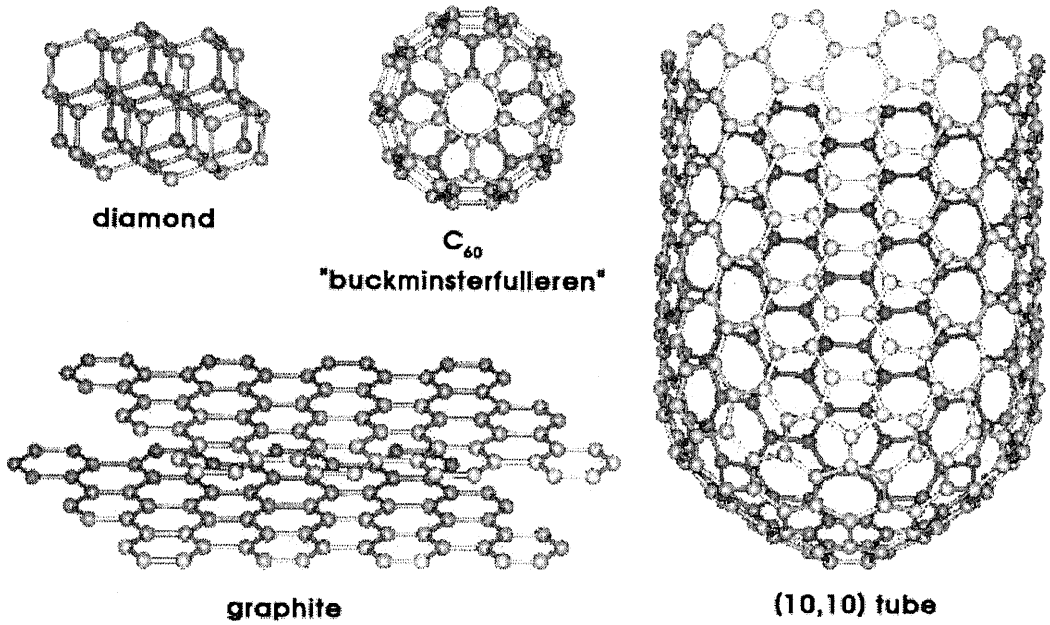

Fig. 1.1 Carbon related materials

1.2.3 Structures of carbon nanotubes

Fig. 1.2 shows the structures of carbon nanotubes. In order to simplify the understanding of the structure of carbon nanotubes, the structure of single walled carbon nanotubes will be used. If we neglect the two ends of a carbon nanotube (CNT) and focus on the large aspect ratio of the cylinder (i.e., length/diameter which can be as large as 10^4 - 10^5), these nanotbes can be considered as one-dimensional nanostructures [58].

An interesting and essential fact about the structure of a CNT is the orientation of the six-membered carbon ring (hereafter called a hexagon) in the honeycomb lattice relative

to the axis of the nanotube. Three examples of SWCNTs are shown in Fig. 1.3.

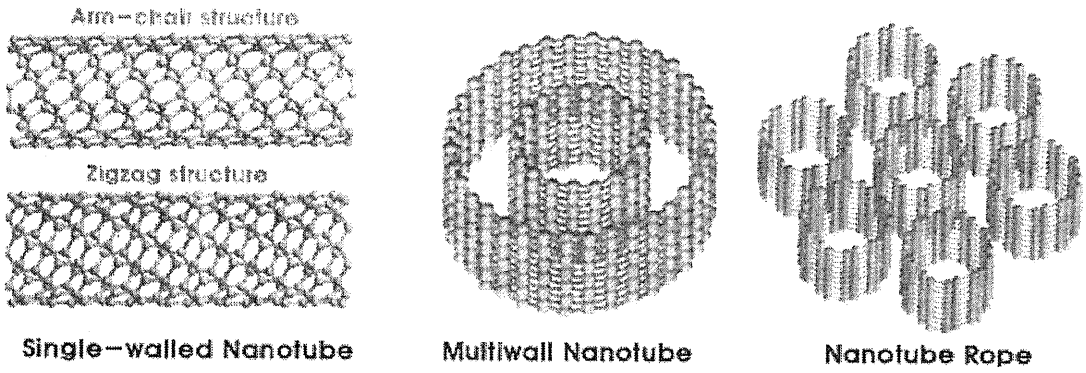

Fig. 1.2 Structures of carbon nanotubes

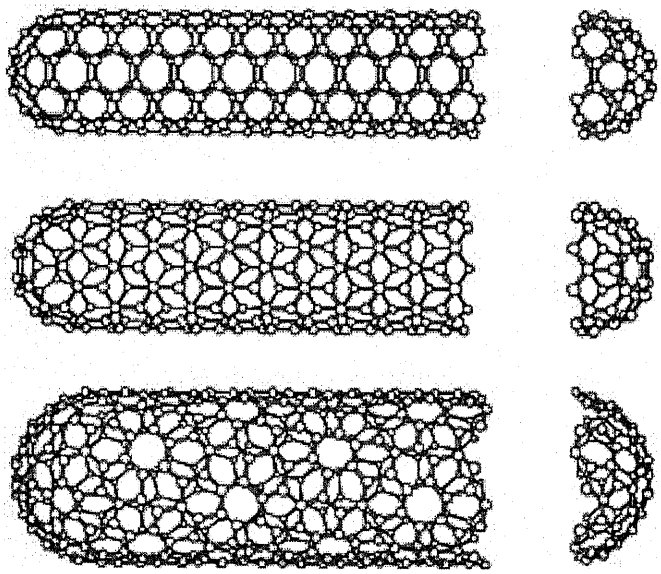

Fig. 1.3 Classfication of carbon nanotubes: (a) armchair, (b) zigzag, and (c) chiral nanotubes. From the figure it can be seen that the orientation of the six-membered ring in the honeycomb lattice relative to the axis of the nanotube can be taken almost arbitrarily.

From the Fig. 1.3, it can be seen that the direction of the hexagon in the honeycomb lattice can be taken almost arbitrarily, without any distortion of the hexagons except for the distortion due to the curvature of the CNT. This fact provides many possible structures for CNTs, even though the basic shape of the CNT wall is a cylinder. Fig. 1.3

shows the terminations of each of the three nanotubes. The terminations are often called caps or end caps and consist of a "hemisphere" of a fullerene. Each cap consists six pentagons and an appreciate number and placement of hexagons that are selected to fit perfectly to the long cylindrical section. In this section, the periodic structure along the nanotube axis was focused on.

The primary symmetry classification of a CNT is as either being achiral (symmorphic) or chiral (non-symmorphic). An achiral CNT is defined by a CNT whose mirror image has an identical structure to the original one. There are only two cases of achiral nanotubes; armchair and zigzag nanotubes, as shown in Fig. 1.3(a) and (b), respectively. The name of armchair and zigzag arise from the shape of the cross-sectional ring, as is shown at the edge of the nanotubes in Fig. 1.3(a) and (b), respectively. Chiral nanotubes exhibit a spiral symmetry whose mirror image cannot be superposed on the original one. We call this tube a chiral nanotube, since such structures are called axially in the chemical nomenclature. Axial chirality is commonly discussed in conection with optical activity. We have thus a variety of geometries in CNTs which can change diameter, chirality and cap structures.

1.3 Physical properties of carbon nanotubes

1.3.1 Optical properties

1.3.1.1 The fundamental gap

The study by Wilder *et al.* showed that nanotubes of type n-m=3*l*, where *l* is zero or any positive integer, were metallic and therefore conducting. The fundamental gap (HOMO-LUMO) would therefore be 0.0 eV. All other nanotubes, they showed, behaved as a semi-conductor. The fundamental gap, they showed, was a function of diameter, where the gap was in the order of about 0.5 eV. Their data were shown in Fig. 1.4 [64].

This graph can be modeled by the function: $E_{gap}=2\ y_0\ a_{cc}\ /\ d$, where y_0 is the C-C tight bonding overlap energy (2.7 ± 0.1 eV), a_{cc} is the nearest neighbor C-C distance (0.142 nm), and d is the diameter. This shows that the fundamental gap ranged from around 0.4 eV - 0.7 eV, which they said was in good agreement with the values obtained from one-dimensional dispersement relations. They concluded that the fundamental gap of semi-conducting nanotubes was determined by small variations of the diameter and bonding angle.

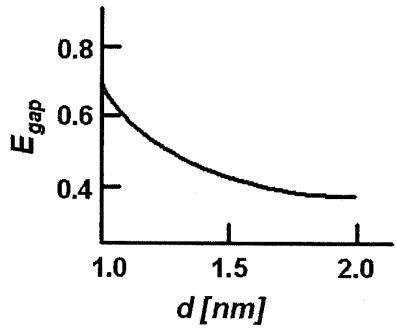

Fig. 1.4 Energy gap as a function of the diameter of SWNT

In a study published at the same time by Odom, Huang, and Lieber [65], they also agreed that the semiconducting properties of carbon nanotubes were determined by the formula stated above. In addition, they suggested that a small gap would exist at the Fermi level in metallic nanotubes. This would be because of the π/σ bonding orbitals and π^*/σ^* anti-bonding orbitals mixing due to the curvature in the graphene sheet of a SWNT. They noted, however, that they had not observed any evidence to support this as of the time of publishing (1998). More interesting to note, in the study by Wilder *et al.*, they reported that the conducting nanotubes shows E_{gap} to range from 1.7 - 2.0 eV,

which could be the evidence Odom *et al.* was predicting.

1.3.1.2 The density of states and spectroscopic transitions

At the Fermi Energy (the highest occupied energy level), the density of states is finite for a metallic tube (though very small), and zero for a semi-conducting tube. As energy is increased, sharp peaks in the density of states, called Van Hove singularities, appear and specific energy levels. The Van Hove singularities in metallic and semiconducting nanotubes are shown in Fig. 1.5.

The optical spectrum is given by $\hbar \times \Omega = \Delta E$, where ΔE is the energy difference between occupied and unoccupied states, especially near the peaks. The spectrum is dominated by the transitions between the Van Hove singularites. [66,67]

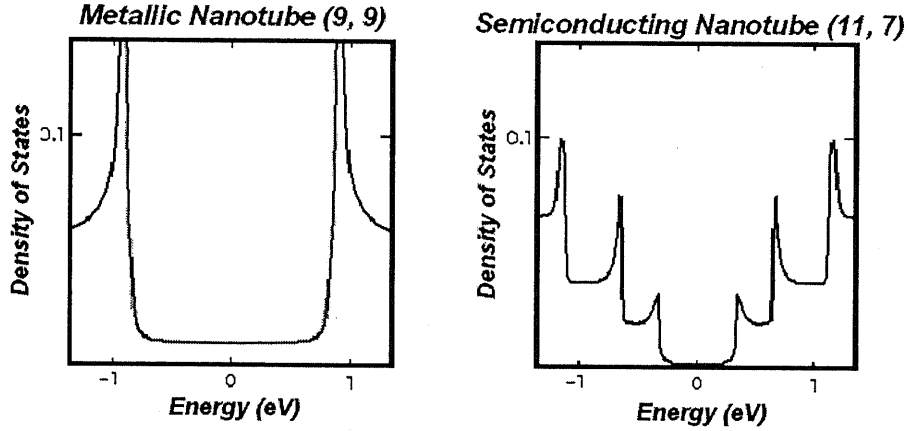

Fig. 1.5 The Van Hove singularities in metallic and semiconducting nanotubes

1.3.2 Electrical transport

The eletrical transport properties of SWNTs has been recently studied has raised some controversy. The conductance of a tube is quantized, and a nanotube acts as a ballistic conductor. Nanotubes also have a constant resistivity, and a tolerance for very high current density.

1.3.2.1 Ballistic conductance

In 1998, Stephan Frank *et al.* experimented on the conductance of nanotubes. [68] Using a SPM, he carefully contacted nanotube fibers with a mercury surface. His results revealed that the nanotube behaved as a ballistic conductor with quantum behavior. The MWNT conductance jumped by increments of 1 G_0 as additional nanotubes were

touched to the mercury surface. The value of G_0 was found to be 1/12.9 $k\Omega^{-1}$, where $G_0 = 2e^2/h$. The coefficent of the conductance quantum was found to have some suprising integer and non-integer values, such as 0.5 G_0.

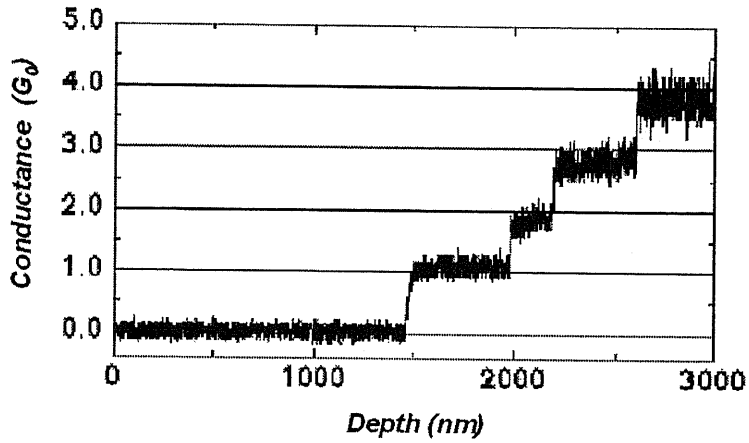

Fig. 1.6 A carbon nanotube is a quantum conductor. The conductance rises by 1 G_0 as the depth increases sufficiently

Later, in 1999, Sanvito, Kwon, Tomanek, and Lambert, [69] used a scattering technique to calculate the ballistic quantum conductance of MWTNs. They found that their results explained these unexpected conductance values found by Frank in 1998. Sanvito *et al.* stated that some of the quantum conductance channels were blocked by interwall reactions. Also, the interwall reactions of MWNTs were found to redistribute the current over individual tubes across the structure nonuniformly.

1.3.2.2 Resistivity and maximum current density

Relatively early in the research of nanotubes, Thess *et al.* calculated the resistivity of ropes of metallic SWNTs to be in the order of 10^{-4} Ωcm at 300 K. [70] They did this by measuring the resistivity directly with a four-point technique. One of their values they measured was 0.34 x 10^{-4}, which they noted would indicate that the ropes were the most highly conductive carbon fibers known, even factoring in their error in measurement. In the same study his measurements of the conductivity, Frank *et al.* [68] was able to have reach a current denisty in the tube greater than 10^7 A/cm^2. Later, Phaedon Avouris [71] suggested that stable current densities of nanotubes could be pushed as high as 10^{13} A/cm^2.

1.3.3 Thermal transport

The thermal conductivity of carbon nanotubes is dependent on the temperature and the large phonon mean free paths. On the graph of thermal conductivity vs temperature, the slope of the line at low temperatures can be modeled using the heat capacity, sound velocity, and relaxation time of the tube.

There seems to be some disagreement into the exact nature of the thermal conductivity of carbon nanotubes, although most agree that thermal conductivity seems to change depending on temperature, and possible also on current and vacancy concentration. In 1999, J. Hone, M. Whitney, and A. Zettle [72] found that the thermal conductivity was temperature dependent, and was almost a linear relationship.

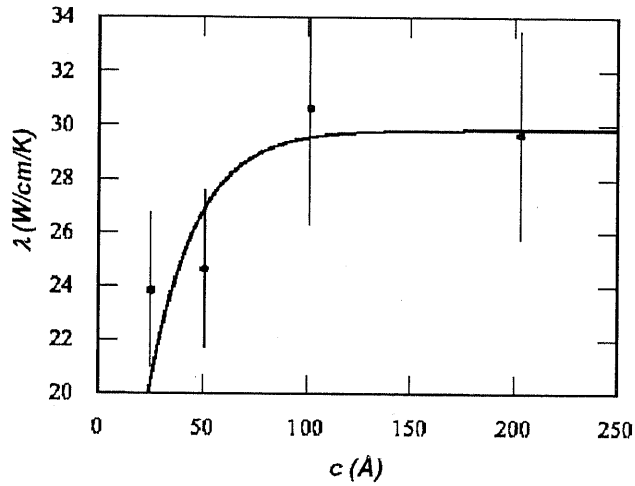

Fig. 1.7 The thermal conductivity as a function of current passed through the nanotube

They suggested that the conductivity was linear in temperature from 7 K to 25 K. From 25 K to 40 K, the line increases in slope, and it arises monotonically with temperature to above room temperature. They proposed a model to explain the low temperature behavior, which is:

$$k_{zz} = \sum C v_z^2 \tau$$

Where $\mathbf{k}_{zz}$ is the slope of the line on the graph, **C** is the heat capacity, is the sound velocity (Hone *et al.* used 1, 2, and 0.8 x 10^6cm/s), and is the relaxation time, which is approximately 10^{-11} s. They also found that the thermal conductivity for a single rope at room temperature could vary between 1800 - 6000 W/m-K.

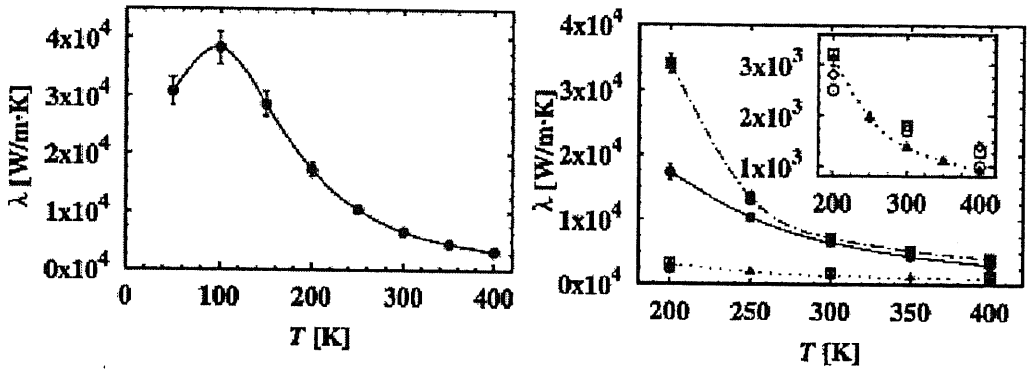

Fig. 1.8 The thermal conductivity as a function of temperature according to Berber, Kwon, and Tomannek [74]

Also that year, Che, Cagin, and Goddard [73] numerically calculated the thermal conductivity of a (10, 10) nanotube to approach 2980 W/m-K as the current applied to it is increased (see figure at right.) In 2000, Berber, Kwon, and Tomanek [74] determined the thermal conductivity of carbon nanotubes and its dependence on temperature. They confirmed the suggestion of Hone *et al.* in 1999 by suggesting an unusually high value of 6,600 W/m-k for the thermal conductivity at room temperature. They theorized that these high values would be due to the large phonon mean free paths, which would concur with Hone's model suggested above. Both groups stated that these values for thermal conductivity are comparable to diamond or a layer of graphite. However, Berber *et al.* suggested that the graphs of the temperature dependence of thermal conductivity looked much less linear than previously proposed by Hone *et al.* Instead of a near-linear graph with a positive slope, their graph showed a positive slope from low temperatures up to 100K, where it peaks around 37,000 W/m-K. Then, the thermal conductivity drops dramatically down to around 3000 W/m-k when the temperature approaches 400 K.

1.3.4 Elastic Behavior

Determining the Elastic Properties of SWNTs has been one of the most hotly disputed areas of nanotube study in recent years. On the whole, SWNTs have are stiffer than steel and are resistant to damage from physical forces. Pressing on the tip of the nanotube will cause it to bend without damage to the tip or the whole CNT. When the force is removed, the tip of the nanotube will recover to its original state. [67]

Quantizing these effects, however, is rather difficult and an exact numerical value cannot be agreed upon. The Young's modulus (elastic modulus) of SWNTs lies close to 1 TPa. The maximum tensile strength is close to 30 GPa.

The results of various studies over the years have shown a large variation in the value reported. In 1996, researchers at NEC in Princeton and the University of Illinois measured the average modulus to be 1.8 TPa. [75] This was measured by first allowing a tube to stand freely and then taking a microscopic image of its tip. The modulus is calculated from the amount of blur seen in the photograph at different temperatures. In 1997, G. Gao, T. Cagin, and W. Goddard III [77] presented a talk at the Fifth Foresight Conference on Molecular Nanotechnology where they reported three variations on the Young's Modulus to five decimal places that were dependent on the chiral vector. They concluded that a (10,10) armchair tube had a modulus of 640.30 GPa, a (17,0) zigzag tube had a modulus of 648.43 GPa, and a (12,6) tube had a value of 673.94 GPa. These values were calculated from the second derivatives of potential. Using these two different methods, a discrepancy arises.

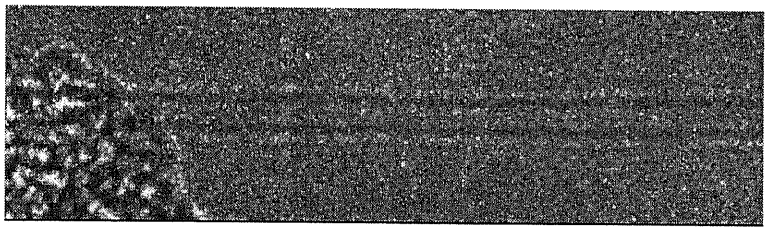

(a) TEM image of SWNT

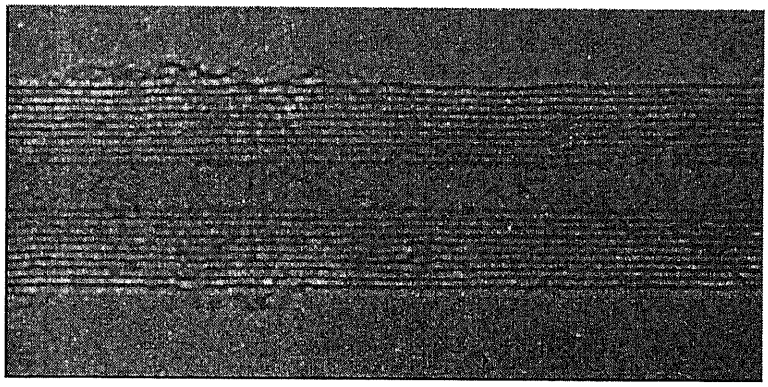

(b) TEM image of MWNT

Fig. 1.9 TEM images of SEM and TEM images from the Zettle research group [73]

Further studies were conducted. In 1998, Treacy *et al.* [76] reported an elastic modulus of 1.25 TPa using the same basic method as done two years earlier. This compared well with the modulus of MWNTs (1.28 TPa), found by Wong *et al.* in 1997. Using an AFM, they pushed the unanchored end of a freestanding nanotube out of its equilibrium position and recorded the force that the nanotube exerted back onto the tip. [78] In 1999, E. Hernandez and Angel Rubio showed using tight-binding calculations, the Young's Modulus was dependent on the size and chirality of the SWNT, ranging from 1.22 TPa for the (10, 0) and (6, 6) tubes to 1.26 TPa for the large (20,0) SWNT. However, using first principal calculations, they calculated a value of 1.09 TPa for a generic tube. [79]

The previous evidence would lead us to assume that the diameter and shape of the nanotube was the determining factor for it's elastic modulus. However, when working with different MWNTs, Forro *et al.* noted that their modulus measurements of MWNTs in 1999 (using AFM) did not strongly depend on the diameter, as had been recently suggested. Instead, they argued that the modulus of MWNTs correlates to the amount of disorder in the nanotube walls. However, their evidence showed that the value for SWNTs does in fact depend on diameter; an individual tube had a modulus of about 1 TPa while bundles (or ropes) of 15 to 20 nm in diameter had a modulus of about 100 GPa.[80]

It has been suggested that the controversy into the value of the modulus is due to the author's interpretation of the thickness of the walls of the nanotube. If the tube is considered to be a solid cylinder, then it would have a lower Young's modulus. If the tube is considered to be hollow, the modulus is gets higher, and the thinner we treat the walls of the nanotube, the higher the modulus will become. [66]

1.4 Applications of carbon nanotubes

Fig. 1.10 shows applications of carbon nanotubes. As carbon nanotubes have various physical properties, they show their unlimited applicabilities, such as electron emitter, VFD(Vacuum Fluorescent Display), FED(Field Emission Display), Lithium ion secondary battery electrode, hydrogen storage fuel cell, nano-wires, nano tweezers, AFM/STM tip, single electron device, gas sensor, medical/engineering microscopic parts, etc. In the 21st century marked by cutting-edge electronic information era, flat panel displays, such as LCD(Liquid Crystal Display), LED(Light Emitting Diode), PDP(Plasma Display Panel) and FED(Field Emission Display) are expected to emerge as main players, substituting for CRT(Cathode Ray Tube), a current typical display device. Among them, FED is drawing a great attention as a new generation information display device, featuring high definition, high efficiency, and low power consumption.

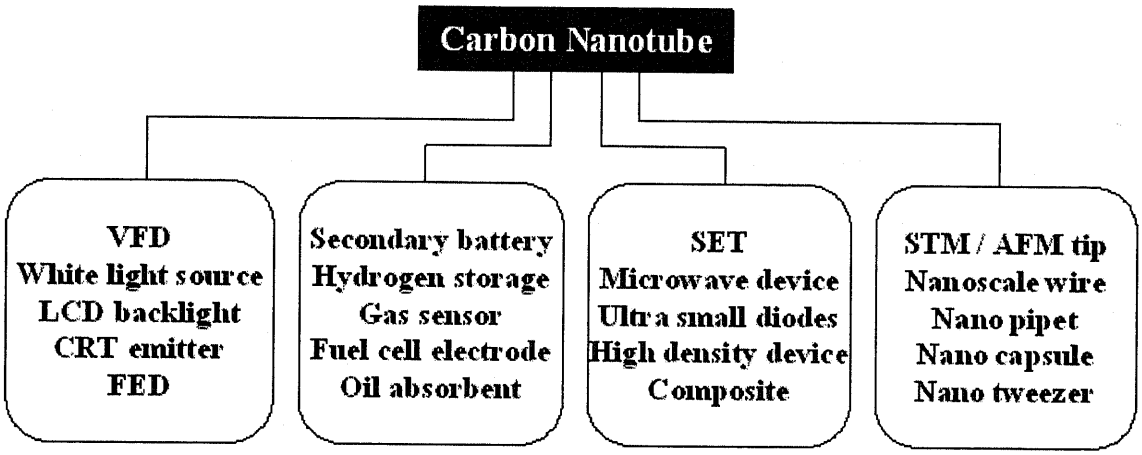

Fig. 1.10 Applications of carbon nanotubes

Its core technologies are based on producibility and stability of tips for electron emission. As conventional silicon or molybdenum tips have big problems in durability and stability and are not efficient in electron emission, efforts to use carbon nanotubes as an electron emission source are getting a great attention. Carbon nanotubes are expected to show excellent characteristics when used as secondary battery electrode or fuel cell. If carbon nanotubes could be used in secondary cell instead of the current hydrogen adsorption alloy, the weight would be lighter and charge performance better. Therefore, carbon nanotubes are highly expected to be used as secondary car battery

electrodes, rechargeable dry cells, batteries for small portable electronic devices, like a notebook computer.

As hydrogen storage capacity is essential in the application, it could be expanded if hollow spaces of carbon nanotubes would be used for storage. As carbon nanotubes not only are light in weight, but have a lot of spaces for storage in them, charge storage capacity per unit mass is outstanding. Accordingly, a fuel cell using carbon nanotubes would emerge as an excellent alternative energy source. The fact means that carbon nanotubes can be used as electric/electronic devices. As the electrical properties of carbon nanotubes can be adjusted for their diameter sizes and coiled forms and their diameters can be grown to scores of nm, an extremely small single electron transistor or a tera-bit memory device could be expected, replacing the current silicon device. The application of carbon nanotubes to a tip of STM or AFM, using their excellent electronic conductivity and mechanical strength could be achieved. It is also expected that the micro-scale length of carbon nanotubes can be used in the application to microscopic pipes and liquid injection devices of a ultra-microscopic system. Advanced applications to a gas sensor and parts as various medical devices, using the gas adsorbility and the carbon compatibility with bio organizations, can be also expected. In addition, the application of carbon nanotubes to high functional composites would create a great sensation in industry. In summary, carbon nanotubes are a new basic material for various industrial applications, such as the cutting-edge electronic information technology which creates high added values.

1.5 A time line for carbon nanotubes researches [81]

In this section, some historical events on the research of carbon nanotubes were given. Also the position of my research was schematically shown in Fig. 11.

1991 **Discovery of multi-wall carbon nanotubes**

"Helical microtubules of graphitic carbon", S. Iijima, Nature 354, 56 (1991).

1992 **Conductivity of carbon nanotubes**

"Are fullerene tubules metallic?", J. W. Mintmire, B. I. Dunlap and C. T. White, Phys. Rev. Lett. 68, 631 (1992).

"New one-dimensional conductors - graphitic microtubules", N. Hamada, S. Sawada and A. Oshiyama, Phys. Rev. Lett. 68, 1579 (1992).

"Electronic structure of graphene tubules based on C_{60}", R. Saito, M. Fujita, G. Dresselhaus and M. S. Dresselhaus, Phys. Rev. B 46, 1804 (1992).

1993 **Structural rigidity of carbon nanotubes**

"Structural Rigidity and Low Frequency Vibrational Modes of Long Carbon Tubules", G. Overney, W. Zhong, and D. Tománek, Z. Phys. D 27, 93 (1993).

1993 **Synthesis of single-wall nanotubes**

"Single-shell carbon nanotubes of 1-nm diameter", S Iijima and T Ichihashi Nature, 363, 603 (1993).

"Cobalt-catalysed growth of carbon nanotubes with single-atomic-layer walls", D S Bethune, C H Kiang, M S DeVries, G Gorman, R Savoy and R Beyers, Nature, 363, 605 (1993).

1995 **Nanotubes as field emitters**

"Unraveling Nanotubes: Field Emission from an Atomic Wire", A.G. Rinzler, J.H. Hafner, P. Nikolaev, L. Lou, S.G. Kim, D. Tománek, P. Nordlander, D.T. Colbert, and R.E. Smalley, Science 269, 1550 (1995).

1996 **Ropes of single-wall nanotubes**

"Crystalline ropes of metallic carbon nanotubes", Andreas Thess, Roland Lee, Pavel Nikolaev, Hongjie Dai, Pierre Petit, Jerome Robert, Chunhui Xu, Young Hee Lee, Seong Gon Kim, Daniel T. Colbert, Gustavo Scuseria, David

Tománek, John E. Fischer, and Richard E. Smalley, Science 273, 483 (1996).

1997 **Quantum conductance of carbon nanotubes**

"Individual single-wall carbon nanotubes as quantum wires", SJ Tans, M H Devoret, H Dai, A Thess, R E Smalley, L J Geerligs and C Dekker, Nature, 386, 474 (1997).

1997 **Hydrogen storage in nanotubes**

"Storage of hydrogen in single-walled carbon nanotubes", A C Dillon, K M Jones, T A Bekkendahl, C H Kiang, D S Bethune and M J Heben, Nature, 386, 377 (1997).

1998 **Chemical Vapor Deposition synthesis of aligned nanotube films**

"Synthesis of large arrays of well-aligned carbon nanotubes on glass", Z F Ren et al., Science, 282, 1105 (1998).

1998 **Synthesis of nanotube peapods**

"Encapsulated C_{60} in carbon nanotubes", B.W. Smith, M. Monthioux, and D.E. Luzzi, Nature 396, 323 (1998).

2000 **Thermal conductivity of nanotubes**

"Unusually High Thermal Conductivity of Carbon Nanotubes", Savas Berber, Young-Kyun Kwon, and David Tománek, Phys. Rev. Lett. 84, 4613 (2000).

2000 **Macroscopically aligned nanotubes**

"Macroscopic Fibers and Ribbons of Oriented Carbon Nanotubes" , Brigitte Vigolo, Alain Pénicaud, Claude Coulon, Cédric Sauder, René Pailler, Catherine Journet, Patrick Bernier, and Philippe Poulin, Science 290, 1331 (2000).

2001 **Integration of carbon nanotubes for logic circuits**

"Engineering Carbon Nanotubes and Nanotube Circuits Using Electrical Breakdown", P.C. Collins, M.S. Arnold, and P. Avouris, Science 292, 706 (2001).

2001 **Intrinsic superconductivity of carbon nanotubes**

M. Kociak, A. Yu. Kasumov, S. Guéron, B. Reulet, I. I. Khodos, Yu. B. Gorbatov, V. T. Volkov, and H. Bouchiat, Phys. Rev. Lett. 86, 2416 (2001).

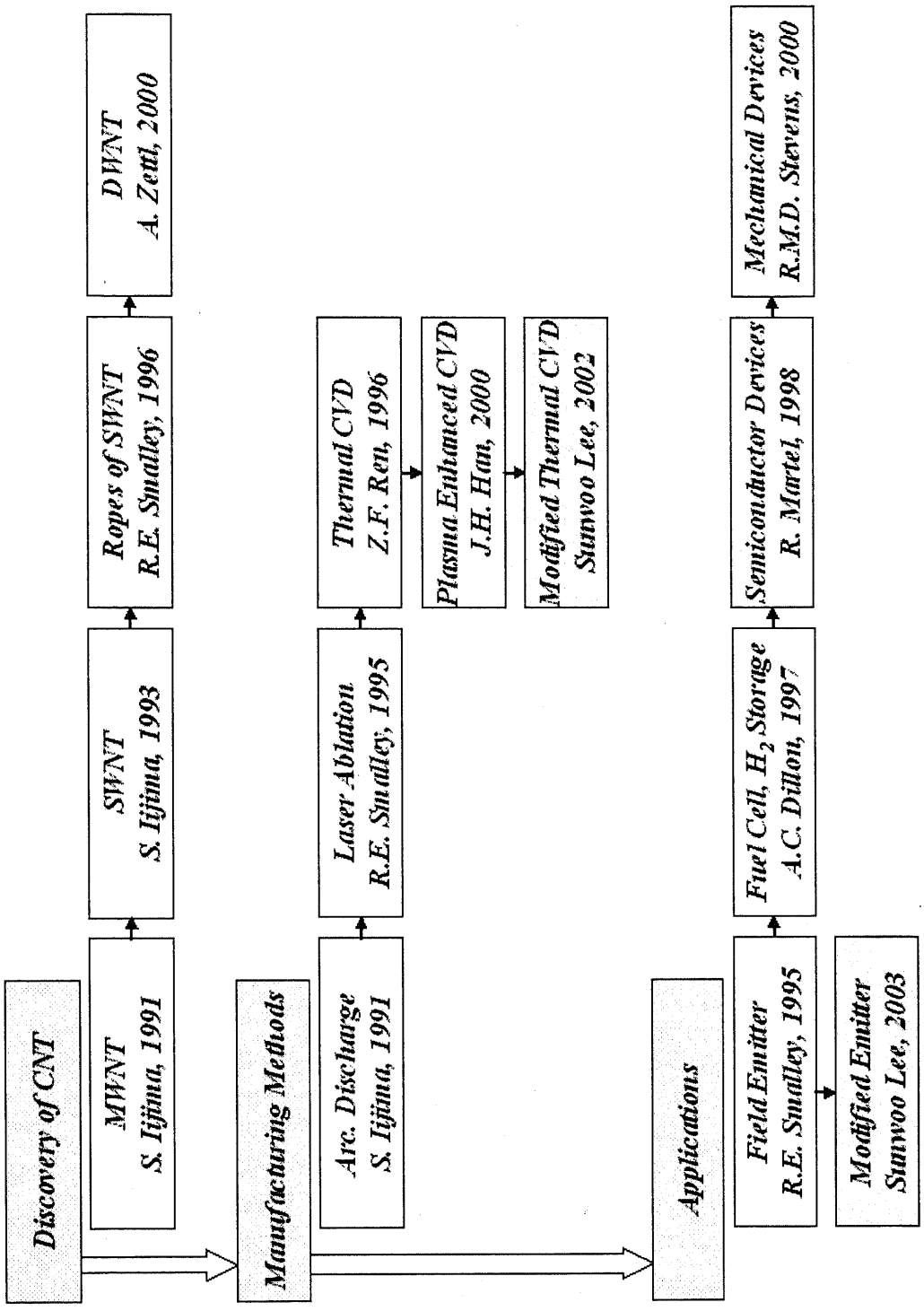

Fig. 11 Schematic diagram of the position of my research.

References

[1] Iijima S., Nature, 1991, 354, 56.

[2] Zhao X., Ohkohchi M., Wang M., Iijima S., Ichihashi T. and ando Y., Carbon, 1997, 35, 775.

[3] Iijima S. and Ichihashi T., Nature, 1993, 363, 603

[4] Bethune D.S., Kiang C.H., de Varies M.S., Gorman G., Savoy R., Vazquez J., and Beyers R., Nature, 1993, 363, 605.

[5] Kiang C.H., Goddard III. W.A., beyers R., Bethune D.S., Carbon, 1995, 33, 903.

[6] Imamura M., Shimada H., Matsubayashi N., Yumura M., Uchida K., Ohshima S., Kuriki Y., Yoshimura Y., Sato T., Nishijima A., Jpn. J. Appl. Phys., 1994, 33, L1016.

[7] Lin X., Wang K., Dravid V.P., Chang R.P.H. and Ketterson J.B., Appl. Phys. Lett., 1994, 64, 181.

[8] Seraphin S., J. electrochem. Soc., 1995, 142, 290.

[9] Seraphin S. and Zhou D., Appl. Phys. Lett., 1994, 64, 2087.

[10] Saito Y., Kawabata K., Okuda M., J. Phys. Chem., 1995, 99, 16076.

[11] Ajayan P.M., Lambert J.M., Bernier P., Barbedette L. and Colliex C., Chem. Phys. Lett., 1993, 215, 509.

[12] Lambert J.M., Ajayan P.M., Bernier P., Planeix J.M., Brotons V., Coq B. and Castaing J., Chem. Phys. Lett., 1994, 226, 364.

[13] Maser W.K., Bernier P., Lambert J.M., Stephan O., Ajayan P.M., Colliex C., Brotons V., Planeix J.M., Coq B., Molinie P. and Lefrant S., Synth. Met., 1996, 81, 243.

[14] Jounet C., Maser W.K., Bernier P., Loiseau A., de la Chapelle M. Lamy, Lefrant S., Deniard P., Lee R. and Fischer J.E., Nature, 1997, 388, 756.

[15] Kroto H.W., Heath J.R., Brien S.C., Curl R.F. and Smalley R.E., Nature, 1985, 318, 162.

[16] Thess A., Lee R., Nikolaev P., Dai H., Petit P., Robert J., Xu C., Lee Y.H., Kim S.G., Rinzler A.G., Colbert D.T., Scuseria G.E., Tomanek D., Fischer J.E. and Smalley R.E., Science, 1996, 273, 483.

[17] Guo T., Nikoraev P., Rinzler A.G., Tomanek D., Colbert D.T. and Smalley R.E., J.

Phys. Chem., 1995, 99, 10694.

[18] Guo T., Nikoraev P., Thess A., Colbert D.T. and Smalley R.E., Chem. Phys. Lett., 1995, 243, 49.

[19] Yudasaka M., Komatsu T., Ichihashi T. and Iijima S., Chem. Phys. Lett., 1997, 278, 102.

[20] Yudasaka M., Komatsu T., Ichihashi T., Achiba Y. and Iijima S., J. Phys. Chem. B., 1998, 102, 4892.

[21] Endo M., Takeuchi K., Kobori K., Takahashi K., Kroto H.W. and Sakar A., Carbon, 1995, 33, 873.

[22] Foneska A., Hernadi K., Piedigrosso P. and Colomer J.F., Appl. Phys. A, 1998, 67, 11.

[23] Ivanov V., Foneseca A., Nagy J.B., Lucas A., Lambin P., Bernaerts D. and Zhang X.B., Carbon. 1995, 33, 1727.

[24] Muller T.E., Reid D.G., Hsu W.K., Hare J.P., Kroto H.W. and Walton D.R.M., Carbon, 1997, 35, 951.

[25] Li W.Z., Xie S.S., Qian L.X., Chang B.H., Zou B.S., Zhou W.Y., Zhao R.A. and Wang G., Science, 1996, 274, 1701.

[26] Terrones M., Grobert N., Olivares J., Zhang J.P., Terrones H., Kordatos K., Hsu W.K., Hare J.P., Townsend P.D., Prassides K., Cheetham A.K., Kroto H.W. and Walton D.R.M., Nature, 1997, 388, 52.

[27] Cheng H.M., Li F., Su G., Pan H.Y., He L.L., Sun X. and Dresselhaus M.S., appl. Phys. Lett., 1998, 72, 3282.

[28] Hsu W.K., Hare J.P., Terrones M., Kroto H.W. and Walton D.R.M., Nature, 1995, 377, 687.

[29] Laplaze D., Bernier P., Maser W.K., Flamant G., Guillard T. and Loiseau A., Carbon, 1998, 36, 685.

[30] Saito Y., Hamaguchi K., Hata K., Uchida K., Tasaka Y., Ikazaki F., Yumura M., Kasuya A. and Nishima Y., Nature, 389, 554.

[31] Saito Y., Hamaguchi K. and Uemura S., Jpn. J. Appl. Phys., 1998, 37, L346.

[32] Saito Y., Hamaguchi K. and Uemura S., Uchida K., Tasaka Y., Ikazaki F., Yumura M., Kasuya A. and Nishima Y., Appl. Phys. A, 1998, 67, 95.

[33] Wang Q.H., Setlur A.A., Lauerhaas J.M. and Dai J.Y., appl. Phys. Lett., 1998, 72,

2912.

[34]Service R.F., Science, 1998, 281, 940.

[35]Hamada N., Sawada S.J., Oshiyama A., Phys. Rev. Lett., 1992, 68, 1579.

[36]Saito R., Fujita M., Dresselhaus G., Cresselhaus M.S., Appl. Phys. Lett., 1992, 60, 2204.

[37]Wildoer J.W.G., Venema L.C., Rinzler A.G., Smalley R.E., Dekker C., Nature, 1998, 391, 59.

[38]Odom T.W., Lin H.J., Kim P., Lieber C.M., Nature, 1998, 391, 62.

[39]Treacy M.M.J., Ebbesen T.W., Gibson J.M., Nature, 1996, 381, 678.

[40]Falvo M.R., Clary G.J., Taylor II R.M., Chi V., Brooks Jr F.P., Washburn S., Superfine R., Nature, 1997, 389, 582.

[41]Wong E.W., Sheehan P.E., Liever C.M., Science, 1997, 277, 1971.

[42]Salvetat J.P., Kulik A.J., Bonard J.M., Briggs G.A.D., Stockli T., Metenier K., Bonnamy S., Beguin F., Burnham N.A., Forro L., Adv. Mater., 1999, 11, 161.

[43]Salvetat J.P., Briggs G.A.D., Bonard J.M., Bacsa R.R., Kulik A.J., Stockli T., Burnham NA, Forro L., J. Phys. Rev. Lett., 1999, 82, 944.

[44]Yu M.F., Lourie O., Dyer M.J., Moloni K., Kelly T.F., Ruoff R.S., Science, 2000, 287, 637.

[45]Andrews R., Jacques D., Rao A.M., Rantell T., Derbyshire F., Chen Y., Chen J., Haddon R.C., Appl. Phys. Lett., 1999, 75, 1329.

[46]Laurent C., Peigney A., Dumortier O., Rousset A. J., Eur. Ceram. Soc., 1998, 18, 2005.

[47]Tans S.J., Verschueren R.M., Dekker C., Nature, 1998, 393, 49.

[48]Martel R., Schmidt T., Shea H.R., Hertel T., Avouris P., Appl. Phys. Lett. 1998, 73. 2447.

[49]Roschier L., Penttila J., Martin M., Hakonen P., Paalanen M., Tapper U., Kauppinen E.I., Journet C., Bernier P., Appl. Phys. Lett., 1999, 75, 728.

[50]Dai H., Hafner J.H., Rinzler A.G., Colbert D.T., Smalley R.E., Nature, 1996, 384, 147.

[51]Cooper E.B., Manalis S.R., Fang H., Dai H., Matsumoto K., Minne S.C., Hunt T., Quate C.F., Appl. Phys. Lett., 1999, 75, 3566.

[52]Kong J., Franklin N.R., Zhou C., Chapline M.G., Peng S., Cho K., Dai H., Science,

2000, 287, 622.

[53] Wong S.S., Joselevich E., Woolley A.T., Li C.C., Lieber C.M., Nature, 1998, 394, 52.

[54] Wong S.S., Woolley A.T., Joselevich E., Lieber C.M., Chem. Phys. Lett., 1999, 306, 5.

[55] Chernozatonskii L.A., Gulyaev Y.V., Kosakovskaya Z.Y., Sinitsyn N.I., Torgashov V., Zakharchenko Y.F., Fedorov E.A., Valchuk V.P., Chem. Phys. Lett., 1995, 233, 63.

[56] Rinzler A.G., Hafiner J.H., Nikolaev P., Lou L., Kim S.G., Tomanek D., Nordlander P., Colbert D.T., Smalley R.E., Science, 1995, 269, 1550.

[57] De Heer W.A., Chatelain A., Ugarte D., Science, 1995, 270, 1179.

[58] Kroto H.W., Heath J.R., Brien S.C., Curl R.F. and Smalley R.E., Nature, 1985, 318, 162.

[59] Iijima S., Nature, 1991, 354, 56.

[60] Ebbesen T.W. and Ajayan P. M., Nature, 1992, 358, 220.

[61] Bethune D.S., Kiang C.H., de Varies M.S., Gorman G., Savoy R., Vazquez J., and Beyers R., Nature, 1993, 363, 605.

[62] Thess A., Lee R., Nikolaev P., Dai H., Petit P., Robert J., Xu C., Lee Y.H., Kim S.G., Rinzler A.G., Colbert D.T., Scuseria G.E., Tomanek D., Fischer J.E. and Smalley R.E., Science, 1996, 273, 483.

[63] Ren Z.F., Huang Z.P., Xu J.W., Wang J.H., Bush P., Siegal M.P. and Provencio P.N., Science, 1998, 282, 1105.

[64] Wilder J.W.G., Venema L.C., Rinzler A.G., Smalley R.E., Dekker C., Nature, 1998, 391, 6662, 59.

[65] Odom T.W., Huang J.L., Kim P., Lieber C.M., Nature, 1998, 391, 6662, 62.

[66] David Tomànek Web Site: http://www.pa.msu.edu/~tomanek/tomanek.html

[67] Dekker C., Physics Today, 1999, p22, May.

[68] Frank S. et al., Science, 1998, 280, 1744.

[69] Sanvito S., Kwon Y.K., Tománek D. and Lambert C.J., Phys. Rev. Lett., 2000, 84, 1974.

[70] Petit D.P., Robert J., Xu C., Lee Y.H., Kim S.G., Rinzler A.G., Colbert D.T., Scuseria G., Tománek D., Fischer J.E., Smalley R.E., Science 1996, 273, 483.

[71]Lecture given at Michigan State University by Phaedon Avouris, a nanotube researcher at the IBM labs. [2000]

[72]Hone J., Whitney M., Zettle A., Synthetic Metals, 1999, 103 2498.

[73]"Thermal Conductivity of Carbon Nanotubes", by Che J., Cagin T, and Goddard IIIW.A., Location: http://www.foresight.org/Conferences/MNT7/Papers/Che/index.html

[74]Berber S., Kwon Y.K. and Tomànek D., Phys. Rev. Lett. 2000, 84.

[75]"TEM & SEM Images of Nanotubes", Zettle Research Group

[76]Location: http://www.physics.berkeley.edu/research/zettl/projects/imaging.html

[77]"Physics News Update, The American Institute of Physics Bulletin of Physics News, Number 279 (Story #2)", July 15, 1996 by Schewe P.F. and Stein B. Location: http://www.aip.org/enews/physnews/1996/split/pnu279-2.htm Energetics, Structure, Mechanical and Vibrational Properties of Single Walled Carbon Nanotubes (SWNT)", by Gao G., Cagin T. and Goddard III W.A., 1997 Location: http://www.wag.caltech.edu/foresight/foresight_2.html

[78]Dujardin E., Ebbesen T.W., Krishnan A., Yianilos P.N., and Treacy M.M.J., Physical Review B 1998, 58, 20.

[79]"Nanotubes: Mechanical and Spectroscopic Properties" ,Hernández E. and Rubio A., 1999 Location: http://www.fam.cie.uva.es/~arubio/psi_k/node5.html

[80]Tomànek D. and Enbody R.J., Science and Application of Nanotubes, New York, Kluwer Academic/Plenum Publishers, 2000

[81]http://www.pa.msu.edu/cmp/csc/nttimeline.html

2. Preparation of Carbon Nanotubes

2.1 Introduction

The first experimental identification in 1991 of carbon nanotubes was on multi-wall nanotubes [1]. This report stimulated a large number of theoretical works on the structure and properties of the simpler and more fundamental single-wall carbon nanotubes, one atomic layer in thickness in the radial direction. The experimental discovery of single-wall carbon nanotubes in 1993 [2,3] further stimulated work in the field, though, at first, only small quantities of single-wall nanotubes were available experimentally for systematic studies. These single-wall nanotubes were generally found along with very much larger concentrations of amorphous carbon, carbon nanoparticles and other carbon based materials, and the single-wall constituents contained a distribution of diameters and chiral angles, as explained below. For these reasons most of the experimental studies continued to be done on multi-wall nanotubes.

The recent discovery in 1996 of a much more efficient synthesis route, involving laser vaporization of graphite [4] to prepare arrays or ropes of ordered single-wall nanotubes, offered major new opportunities for quantitative experimental studies of carbon nanotubes. By making the single-wall nanotubes available to many research groups worldwide, progress was made for the first time in quantitative measurements of the physical roperties of single-wall carbon nanotubes.

The detailed mechanisms responsible for the growth of these nanotubes are not yet well understood. Therefore we can expect extensive research to be carried out on the growth mechanism and on the development of new growth techniques that provide more controlled growth of nanotubes. Whereas multi-wall nanotubes require no catalyst for their growth, catalyst species are necessary for the growth of the single-wall nanotubes, and more than one catalytic species seem to be necessary to grow ropes of single-wall nanotubes.

Because of the potential interest of carbon nanotubes for practical applications, there is also interest in developing continuous synthesis methods more appreproate for scale-up and low cost, and this may perhaps be accomplished by vapor growth methods [5].

2.2 Growth Mechanisms

It is postulated that the formation and growth of nanotubes is an extension of other known processes in which graphitic structures are formed over metal surfaces at temperatures below about 1100°C from carbon that is produced by the decomposition of a carbon-containing precursor. It is also proposed that the form of graphite that is produced is closely related to the physical dimensions of the metal catalytic particles. This hypothesis builds on a considerable volume of research that has been conducted over the past two to three decades on the formation of graphitic carbon over metal substrates [6,7]. The most effective metals have been shown repeatedly to be iron, nickel and cobalt [8]. The peculiar ability of these metals to form ordered carbon is thought to be related to a combination of factors. These include their catalytic activity for the decomposition of volatile carbon compounds, the fact that they form metastable carbides, and that carbon is able to diffuse through and over the metals extremely rapidly [6-8]. The latter property allows ordered carbon to be produced by a mechanism of diffusion and precipitation. This also means that graphitic structures are only formed in proximity to the metal surface. If there is significant reaction away from the metal, other undesirable forms of carbon, such as amorphous carbon nanoparticles, will be co-produced. Restriction of the reaction to the surface is controlled through the choice of the carbon precursor, its partial pressure and the reaction temperature.

Over thin metal foils, which in the present context can be considered as bulk metal, carbon dissolves to form a solid solution [8]. On cooling, it precipitates on the surface as a continous thin film of highly crystalline graphite in which the graphite basal planes are oriented parallel to the substrate. The high degree of crystalline perfection that is obtained in a matter of seconds demonstrated that carbon atoms are extremely mobile and can move easily over and through the metal.

When the metal is present as particles of diameter in the range of tenth of a micron, the carbon is produced as filaments of similar diameter [5,6]. The metal particles can be supported on a substrate or introduced as floating particles in a gas stream that flows through the reactor [9,10]. If the particles are considered to be spherical or pear shaped, the deposition of carbon atoms takes place on one half of the surface (on the lower curvature face for pear shapes). The carbon diffuses along the concentration gradient and precipitates on the opposite half, around and below the bisecting diameter. However,

it dose not precipitate from the apex of the hemisphere, which accounts for the hollow core that is characteristic of these filaments.

In the filament structure, the graphite crystallites precipitate with the basal plane tangential to the curved surface (as opposed to parallel to the surface for metal substrates with much larger dimensions). In cross-section, the filaments are composed of a series of crystallites whose <c> axis tends to follow the radial vector of the filament and whose basal planes follow the circumference, approximating the curved surface of the filament. The <c> axis may also be tilted at an angle to the radical vector, giving rise to a chevron type structure. For supported metals, filaments can form either by extrusion in which the fiber grows upwards from metal particles that remain attached to the substrate, or the particles detach and move at the head of the growing fibers, labeled tip-growth. These mechanisms are illustrated graphically in Fig. 2.1 [6].

It is postulated that the catalyst particle size determines the size of the filament. As the particle diameter is reduced, the filament curvature increases, imposing an increasing strain on the basal planes of the crystallites. Eventually, a continuous surface is energetically more favorable and MWCNTs are formed. Logically, if the particle size is reduced still further, SWCNTs will be formed.

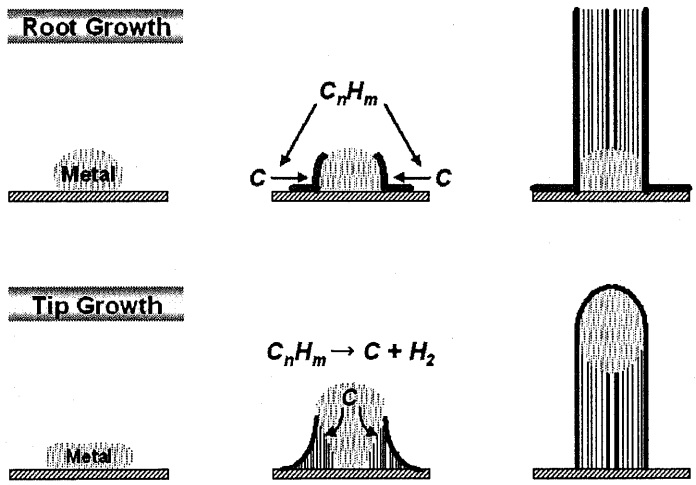

Fig. 2.1 Schematics of root-growth and tip-growth mechanisms for carbon filament growth ([6])

2.3 Preparation methods of carbon nanotubes

2.3.1 Laser Vaporization Synthesis Method

An efficient route for the synthesis of bundles of single-wall carbon nanotubes with a narrow diameter distribution employs the laser vaporization of a graphite target.

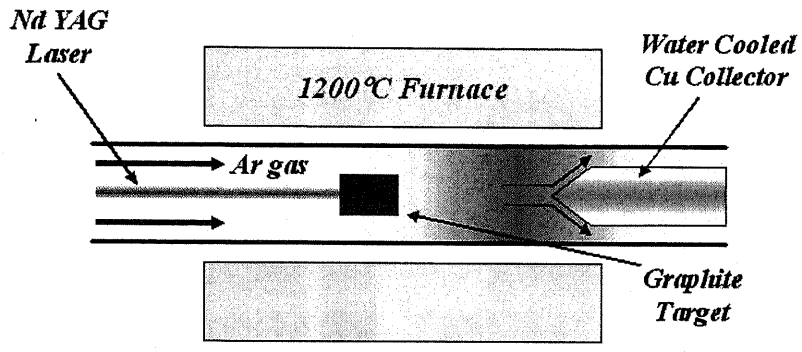

Fig. 2.2 Schematic diagram of laser vaporization apparatus using a graphite target and a cooled collector [13].

In the early reports of the laser synthesis technique [11], high yields with >70% - 90% conversion of graphite to single-wall nanotubes were reported in the condensing vapor of the heated flow tube (operating at 1200°C). A Co-Ni/graphite composite laser vaporization target was used, consisting of 1.2 atom % Co-Ni alloy with equal amounts of Co and Ni added to the graphite (98.8 atom %) [11]. Two sequenced lase pulses were used to evaporate a target containing carbon mixed with a small amount of transition metal from the target (see Fig. 2.2). Flowing argon gas sweeps the entrained nanotubes from the high temperature zone to the water-cooled Cu collector downstream, just outside the furnace [11-13].

The material thus produced appears in a scanning electron microscope (SEM) image as a mat of ropes 10-20 nm in diameter and up to 100 μm or more in length. Under transmission electron microscope (TEM) examination, each rope is found to consist primarily of a bundle of single-wall carbon nanotubs aligned along a common axis.

X-ray diffraction (which views many ropes at once) and transmission electron microscopy experiments (which views a single rope) show [11] that the diameters of the single-wall nanotubes have a strongly peaked distribution at 1.38±0.02 nm, very close to the diameter of an ideal (10, 10) nanotube which is defined in Fig. 2.3. A detailed transmission electron microscopy study of carbon nanotubes prepared by the laser

vaporization method [11] has shown that the carbon nanotube chiral indices (n, m) are mainly (10, 10) (~44%), (9, 9) (~20%), and some (12, 8) [14], while others, presumably using different growth conditions, have reported chiral angles in the range $\Delta\theta = 7.3°$.

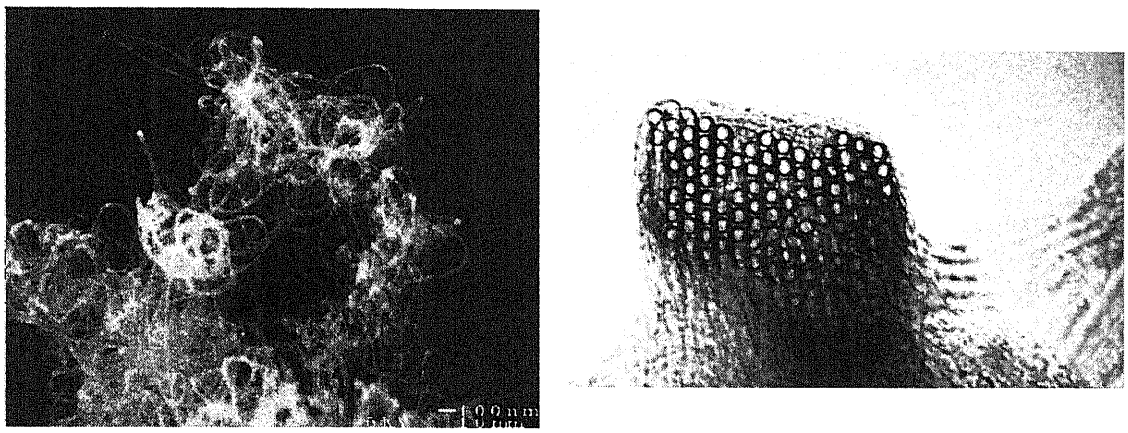

Fig. 2.3 (a) Ropes of single wall carbon nanotubes observed by scanning electron microscopy (SEM). The ropes are 10-20 nm thick and ~100 μm long. (b) At higher magnification, the TEM image shows that each rope contains a bundle of single wall nanotubes with diameters of ~1.4 nm, arranged in a triangular lattice (with lattice constant 1.7 nm). Such an image is seen when the rope bends through the image plane of the microscope [11].

Thus for nanotube diameters ranging from that for the (8, 8) to (11, 11) armchair nanotubes, there are only 17 possible nanotubes [14]. The single-wall nanotubes are held together by weak van der Waals inter-nanotube bonds to form a two-dimensional triangular lattice with a lattice constant of 1.7 nm, and an inter-tube separation of 0.315 nm at cloest approach within a rope [11]. By varying the growth temperature, the catalyst composition and other growth parameters, the average nanotube diameter and diameter distribution can be varied [15]. It is found that the spread in nanotube diameters within a single rope is smaller than between ropes grown at the same time and under the same nominal growth conditions.

2.3.2 Arc Method of Synthesizing Carbon Nanotubes

The carbon arc provides a simple and traditional tool for generating the high temperatures needed for the vaporization of carbon atoms into a plasma (>3000 °C)

[16-18]. This technique has been used for the synthesis of single-wall and multi-wall carbon nanotubes, and ropes of single-wall nanotubes [12].

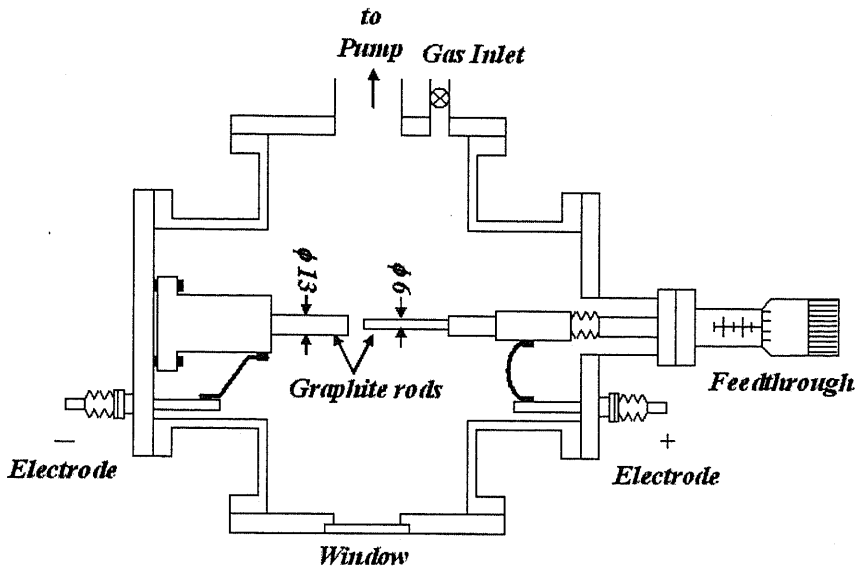

Fig. 2.4 Cross-sectional view of a carbon arc generator that can be used to synthesize carbon nanotubes [17]

Typical conditions for operating a carbon arc for the synthesis of carbon nanotubes include the use of carbon rod electrodes of 5–20 nm diameter separated by ~1 mm with a voltage of 20-25 V across the electrodes and a dc electric current of 50-200 A flowing between the electrodes. The arc is typically operated in ~500 torr He with a flow rate of 5–15 ml/s for cooling purpose. As the carbon nanotubes form the length of the positive electrode (anode) decreases (see Fig. 2.4).

Once the arc is in operation, a carbon deposit forms on the negative electrode. For the multi-wall carbon nanotube synthesis, no catalyst need to be used and the nanotubes are found in bundles in the inner region of the cathode deposit where the temperature is a maximum (2500-3000 °C). The nanotube bundles are roughly aligned in the direction of the electric current flow (see Fig. 2.4) [17,19]. Surrounding the nanotubes is a hard grey shell consisting of nanoparticles, fullerenes and amorphous carbon [19-21]. Adequate cooling of the growth chamber is necessary to maximize the nanotube yield in the arc growth process. The growth of carbon nanotubes appears to be unfavorable under the conditions that are optimized to synthesize fullerene molecules.

Catalysts used to prepare isolated single-wall carbon nanotubes include transition

metals such as Co, Ni, Fe and rare earths such as Y and Gd, while mixed catalysts such as Fe/Ni, Co/Ni and Co/Pt have been used to synthesize ropes of single-wall nanotubes. Although the details of the diameter (and chirality) distribution of the single-wall carbon nanotubes depend on the synthesis conditions, temperature of the arc and the catalyst that is used, the average nanotube diameter is usually small (≤ 1.5 nm) and the diameter distribution is usually narrow.

2.3.3 Vapor Growth and Other Synthesis Methods

Fe, Co, and Ni particles are known to be catalysts for vapor grown carbon fiber synthesis [22-24], in which hydrocarbons (e.g., CH_4, C_6H_6) and H_2 gases are reacted in the presence of Fe, Co, or Ni particles in a reaction tube at 1100 °C. The innermost tubes of vapor grown fibers are considered to be carbon nanotubes. Growth of carbon nanotubes from the vapor phase has also been demonstrated.

2.3.3.1 Vapor Growth Method

The synthesis of carbon nanotubes from the vapor phase utilizes equipment similar to that used for the preparation of vapor-grown carbon fibers, with the furnace temperature held at 1100°C and using Fe catalyst particles, but using a low benzene gas pressure [25,26]. A variety of other hydrocarbons, catalysts and catalyst supports have been used successfully by various groups worldwide to synthesize carbon nanotubes. One big advantage of the vapor growth approach is that carbon nanotubes can be made continuously and thus if the optimum conditions for growing pure carbon nanotubes could be found, this could be a very good way to synthesize large quantities of carbon nanotubes under relatively controlled conditions. Thus the vapor growth method has some advantage for scale-up and commercial production. Many presently identified applications of carbon nanotubes can be met with vapor-grown carbon nanotubes.

2.3.3.2 Other Synthesis Methods

Another method of nanotube synthesis relates to the use of carbon ion bombardment to make carbon whiskers [27,28]. Carbon whiskers are known as a graphite material with high crystallinity whose diameter is ~0.1–1 μm and several mm in length. In the ion bombardment growth method, carbon is vaporized in vacuum through ion or electron

irradiation [29], and the resulting deposit containing carbon nanotubes, along with other structures is collected on a cold surface. Little is known about the optimization of the ion bombardment technique in relation to the preparation of nanotubes.

The use of solar energy for the synthesis of single-wall carbon nanotubes has been reported [30,31], using an experimental chamber where solar energy is focused on the crucible to achieve a temperature of 3000 K on a clear day. A mixture of Ni and Y catalysts is used in an argon temperature (pressure of ~450 mbar). Further research is needed to optimize and control the synthesis process, increase the yield of ropes of single-wall nanotubes, minimize the concentration of carbon nanoparticles and amorphous carbon produced, and to characterize the carbon nanotubes that are produced.

2.4 Carbon nanotube film preparation by CVD nethod

Carbon nanotubes were grown by using thermal decomposition of C_2H_2 at atmospheric pressure. The 15×15 mm size n-type Si (100) wafer was used as the substrate. Nickel was deposited on the substrate by RF sputtering method. In order to make the particle size small, the sputtering conditions are selected as low sputtering power (~10 W) and long sputtering time (~1 h).

CNT was deposited in a horizontal flow reactor. Experimental setup shown in Fig. 2.5 consists of the gas inlet part, reaction part, temperature control part, and exhaustion part.

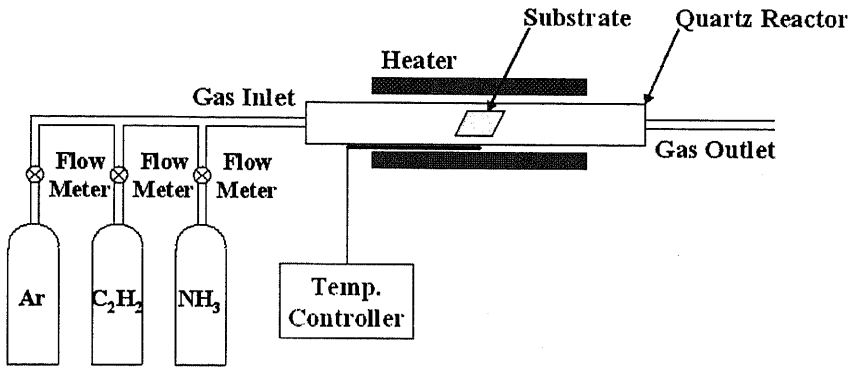

Fig. 2.5 Experimental apparatus for synthesizing the carbon nanotubes

The substrate was placed at the heating zone in the reaction chamber. The reaction chamber was heated up to the reaction temperature ranging 700 to 800°C in Ar environment. The flow rate of the environmental gas (Ar) was 100 sccm. The ammonia gas (NH_3) was added with the flow rate of 50 sccm to synthesize the pure and vertically aligned CNTs. The deposition of the CNT was performed by adding acetylene (C_2H_2) gas with the flow rate of 30 sccm to the environmental gas. The reaction time was selected as 20 mins. The reactor was cooled down slowly to the room temperature (25°C) under Ar ambient after the growth. The grown CNTs on Si substrate were examined by a scanning electron microscope (SEM, Hitachi, S-550, 30kV), to measure the length, the diameter, the alignment, and the uniformity.

SEM image of CNTs prepared by above condition is shown in Fig. 2.6. The prepared CNTs were laid down to the substrate, and the amount of CNTs is not so much. The impurities such as amorphous carbon are also produced.

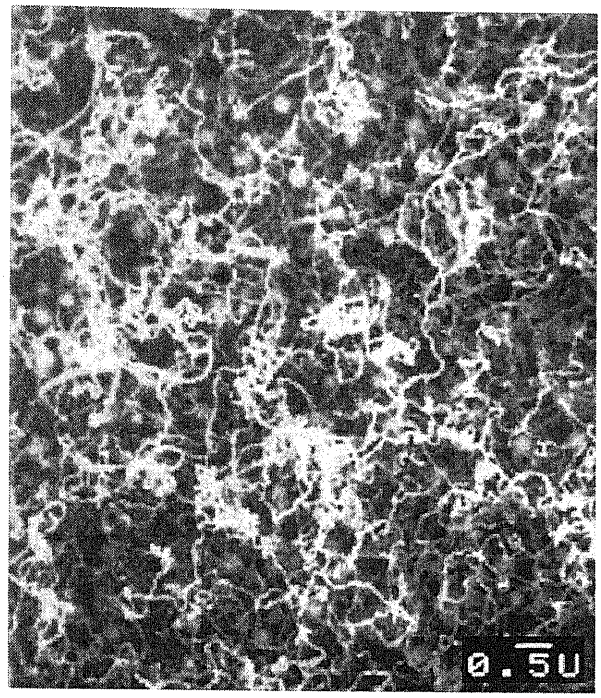

Fig. 2.6 SEM image of carbon nanotubes prepared by above conditions

2.5 Effect of ammonia gas

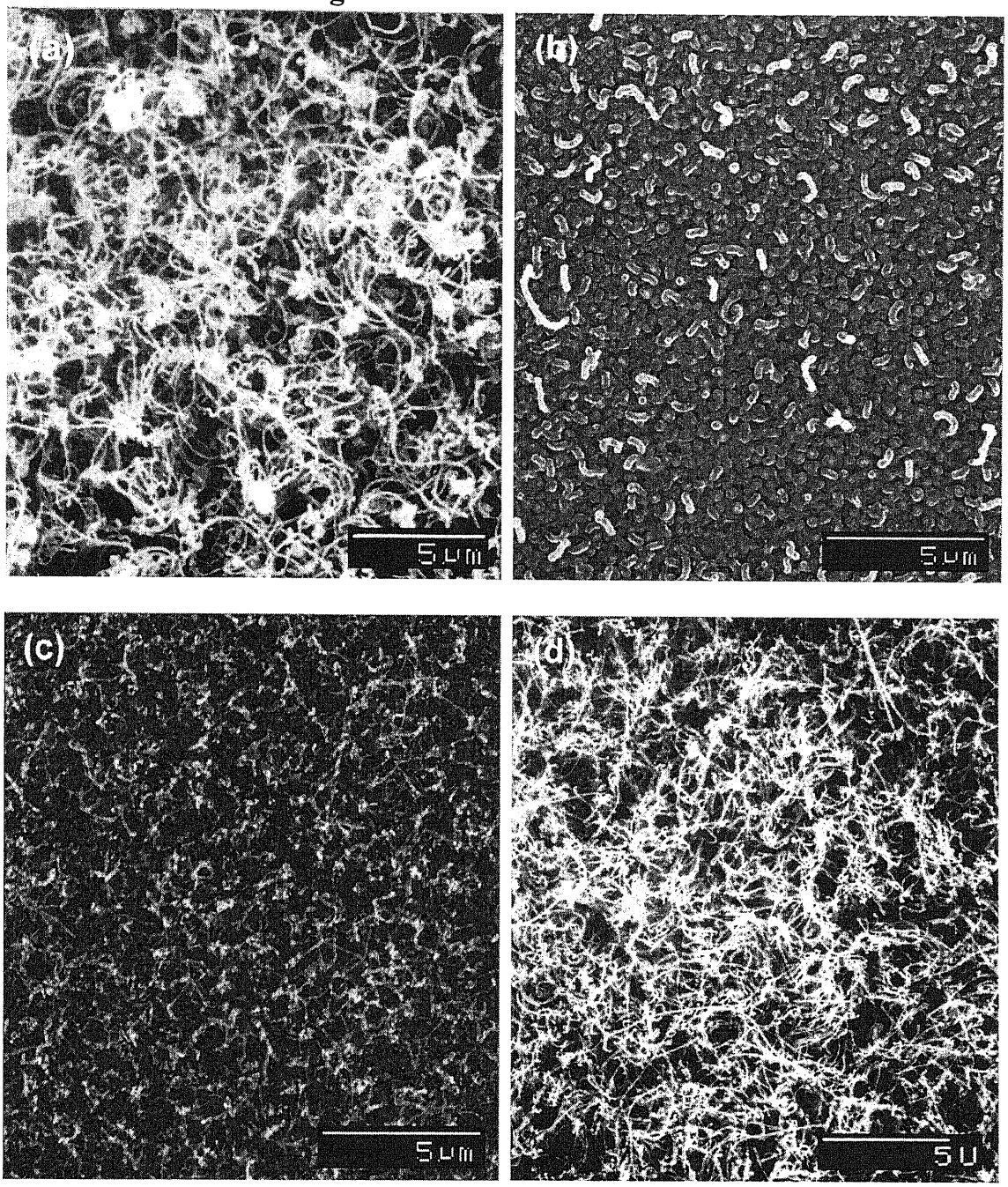

Fig. 2.7 SEM images of CNT films prepared with various flow rates of the ammonia gas; (a) 0 sccm, (b) 10 sccm, (c) 20 sccm, (d) 30 sccm

Fig. 2.7 shows the SEM images of CNT films prepared with various flow rates of the ammonia gas; (a) 0 sccm, (b) 10 sccm, (c) 20 sccm, and (d) 30 sccm. From the result of the Fig. 2.7 (a) (without ammonia gas), there are small amount of non-aligned CNTs

including large amount of impurities. From the result of the Fig. 2.7 (b) (ammonia gas flow rate of 10 sccm), there is no CNT synthesized. From the result of the Fig. 2.7 (c) (ammonia gas flow rate of 20 sccm), vertically aligned CNTs including no impurities were synthesized, but the deviation of diameter is so large. And from the result of the Fig. 2.7 (d) (ammonia gas flow rate of 30 sccm), vertically aligned CNTs with unit diameter and without any impurities were synthesized.

If the amorphous carbon covers the catalyst particles during the reaction process, the CNTs cannot grow, which is called as Deactivation. That deactivation occurs when the decomposition rate of acetylene ($C_2H_2 \rightarrow 2C + H_2$) is too high [32]. That decomposition rate is dependent on a reaction temperature, an acetylene gas (C_2H_2) flow rate, and a hydrogen ratio in the mixed gas [33].

Ammonia (NH_3) gas used in this work reduced the carbon ratio by supplying hydrogen, though there is no change of the decomposition rate of acetylene. As ammonia reduces the carbon ratio, the clean and pure CNTs can grow without deactivation. That ammonia etches the catalyst surface even if the C_2H_2 is decomposed too much. From above results, it is found that the introduction of NH_3 gas during the synthesis of CNTs plays an important role to synthesize the pure (including no impurities) and vertically aligned CNTs.

2.6 Conclusions

By introducing ammonia gas during the CNT synthesis process, the pure CNT films including no impurities such as amorphous carbon could be prepared. The role of the ammonia gas in this CVD process was thought to be the next two possibilities. First, the ammonia gas elevates the hydrogen ratio in the mixed gas during the CNT synthesis process, so that we can control the CNT reaction rate. Also, the ammonia gas, which has an etching ability, etches the catalyst particles and makes them active during the synthesis process.

2.7 References

[1] Iijima S., Nature, 1991, 354, 56.

[2] Iijima S. and Ichihashi T., Nature, 1993, 363, 603.

[3] Bethune D.S., Kiang C.H., de Varies M.S., Gorman G., Savoy R., Vazquez J., and Beyers R., Nature, 1993, 363, 605.

[4] Thess A., Lee R., Nikolaev P., Dai H., Petit P., Robert J., Xu C., Lee Y.H., Kim S.G., Rinzler A.G., Colbert D.T., Scuseria G.E., Tomanek D., Fischer J.E. and Smalley R.E., Science, 1996, 273, 483.

[5] Jounet C., Maser W.K., Bernier P., Loiseau A., de la Chapelle M. Lamy, Lefrant S., Deniard P., Lee R. and Fischer J.E., Nature, 1997, 388, 756.

[6] S.B. Sinnott et al., Chem. Phys. Lett. 315 (1999) 25-30.

[7] R.H. Fowler, L.W. Nordheim, Proc. R. Soc. Lond., Ser. A 119 (1928) 173.

[8] J.M. Bonard, M. Croci, I. Arfaoui, O. Noury, et al., Diamond and Related Materials 11 (2002) 763-768.

[9] H. Ago, T. Kugler, f. Cacialli, et al., J. Phys. Chem. B 103 (1999) 8116-8121.

[10] J. Chen, M.A. Hamon, et al., Science, 282 (1998) 95.

[11] Yakobson B.I. and Smalley R.E., American Scientist, 1997, 85, 324.

[12] Eklund P.C. et al., unpublished, 1997, UK Workshop.

[13] Ebbesen T.W., Annu. Rev. Mater. Sci., 1994, 24, 235.

[14] Ebbesen T.W. and Ajayan P. M., Nature, 1992, 358, 220.

[15] Ebbesen T.W., Hiura H., Fujita J., Ochiai Y., Matsui S. and Tanigaki K., Chem.. Phys. Lett., 1993, 209, 83.

[16] Seraphin S., Zhou D., Jiao J., Withers J.C. and Loufty R., Carbon, 1993, 31, 685.

[17] Ebbesen T.W., Annu. Rev. Mater. Sci., 1994, 24, 235.

[18] Ajayan P.M. and IIjima S., Nature, 1992, 358, 23.

[19] Dravid V.P., Lin X., Wang Y., Wang X.K., Yee A., Ketterson J.B. and Chang R.P.H., Science, 1993, 259, 1601.

[20] Iijima S., Mater. Sci. eng., 1993, B19, 172.

[21] Bethune D.S., Kiang C.H., de Varies M.S., Gorman G., Savoy R., Vazquez J., and Beyers R., Nature, 1993, 363, 605.

[22] Dresselhaus M.S., Dresselhaus G., Sugihara K., Spain I.L. and Goldberg H.A.,

Graphite Fibers and filaments (Spriger-Verlag, Berlin, 1998), Vol. 5 of Springer Series in Materials Science.

[23] Oberlin A., Endo M. and Koyama T., Carbon, 1976, 14, 133.

[24] Endo M., CHEMTECH, 1988, 18, 568. September issue.

[25] Endo M., Takeuchi K., Kobori K., Takahashi K., Kroto H.W. and Sakar A., Carbon, 1995, 33, 873.

[26] Endo M., Takeuchi K., Igarashi S., Kobori K., Shiraishi M. and Kroto H.W., J. Phys. Chem. Solids, 1993, 54, 1841.

[27] Cuomo J.J. and Harper J.M.E., IBM Tech. Disclosure Bulletin, 1977, 20, 775.

[28] Floro J.A., Rossnagel S.M. and Robinson R.S., J. Vac. Sci. Technol., 1983, A1, 1398.

[29] Kosakovskaya Z.Ya, Chernozatonskii L.A. and Fedorov E.A., JETP Lett. (Pis'ma Zh. Eksp. Teor), 1992, 56,26.

[30] Loiseau A., private communication, 1998.

[31] Laplaze D., Bernier P., Maser W.K., Flamant G., Guillard T. and Loiseau A., Carbon, 1998, 36, 685.

[32] T.Y. Kim, K.R. Lee, K.Y. Eun, et al., The 2002 Korea-US Symposium on Phase Transformations of Nano-Materials Proceedings (2002)

[33] K. Tanaka, T. Yamamoto, K. Fukui, The science and technology of carbon nanotubes, Elsevier Science Press (1999)

3 Effect of chemical treatments

3.1 Introduction

After the recent discovery of the Carbon Nanotube (CNT) [1], many researchers have studied about the CNT due to its high aspect ratio, small curvature, good electrical conductivity, strong mechanical property, and chemical stability [2-5]. These CNT's remarkable features made it possible for CNT to apply to the wide range of researches. Especially, CNT has been considered as a superior candidate of a flat display panel and mechanical tip of AFM or STM [6,7].

Although some researches were studied on the field emission properties [8,9], systematical studies on the field emission properties due to the change of surface bonding state on CNT films caused by the attachment of functional groups through the chemical treatment have not been investigated.

Carbon nanotubes consist of very strong covalent bonds, so that they are very stable against to the chemical attacks. Breaking these strong covalent bonds and attaching new functional groups will be expected to bring a significant change on the CNT's physical properties. Therefore they will open the novel application fields. For example, when we use the CNT films as a field emission device, we can control the field emission property of those films by attaching some useful functional groups due to the chemical treatments. The field emission behavior takes place at the cap of the CNT. For this reason, we attach the functional groups to the cap of the CNT. Fortunately, the break of the chemical bonding starts from the pentagons on the cap.

In this paper, two models were proposed. First one is the aspect ratio changed by the surface treatment which causes a change of the field emission property. Another one is the surface bonding state changed by the attachment of the functional groups.

In order to confirm the former mechanism concerning with surface topology, the scanning electron spectroscopy (SEM) analysis was conducted. For the surface bonding analysis, XPS spectra were observed. Those analyses were conducted related with the field emission properties.

3.2 Purpose of chemical treatments

The effect of the chemical treatment on the field emission properties of the CNT was investigated. The CNT samples were chemically treated in O_2 gas, HNO_3 solution or HF solution. The processed samples were named as O2-CNT, HNO_3-CNT, or HF-CNT, respectively.

3.2.1 O_2 treatment

It is well known that the O_2 annealing treatment can be used to purify the raw CNTs including non-wanted impurities such as amorphous carbon. This means that the O_2 treatment can etch the cap of CNT. Therefore we can predict the topological changes (i.e. the change of the curvature of CNTs) of the surface of CNT film.

3.2.2 HNO_3 treatment

The HNO_3 solution is also used to purify the CNTs. Therefore, we can predict the etching effect the same as O_2 treatment. Additionally, the HNO_3 treatment is also expected that the attachment of functional groups occurs at the cap of CNTs. This attachment might bring the change of surface state of the CNT film.

3.2.3 HF treatment

The HF solution is well used in semiconductor process as a very strong etchant. Also, the fluorine atoms (usually functional groups containing the fluorine atom) react with the dangling bonds of graphite structure located at the cap of CNT very actively. Therefore, the HNO_3 treatment is also expected that the attachment of functional groups occurs at the cap of CNTs. This attachment might generate the change of surface state of the CNT film.

3.3 Chemical treatments of carbon nanotube films

3.3.1 O_2 treatment

The O_2 treatment apparatus was the same apparatus as used to synthesize CNTs. The O_2 treatment was done with gas flow rate of O_2:Ar = 20:200sccm at 500^{O}C for 5min. Before treatment, Ar gas flowed through the reaction chamber to hinder the CNT's burning. These treatment conditions were selected for not burning the CNTs, but surface treatment of the CNT film.

3.3.2 HNO_3 treatment

The HNO_3 treatment was done in the 20vol% HNO_3 solution at room temperature for 1hr. The CNT film was dip into the HNO_3 solution. Subsequently, the treated sample was washed in pure ethanol, and was dried at room temperature for 1hr.

3.3.3 HF treatment

The HF treatment was done in 20vol% HF solution at room temperature for 30min. The CNT film was dip into the HNO_3 solution. Subsequently, the treated sample was washed in pure ethanol, and was dried at room temperature for 1hr.

These chemical treatments on the CNT films were summarized and were schematically shown in Fig. 3.1.

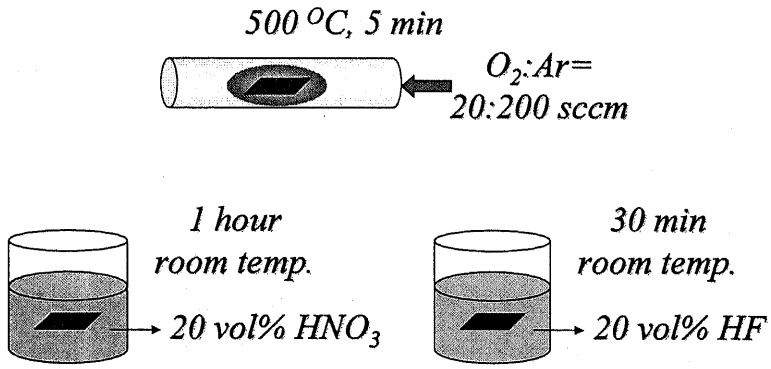

Fig. 3.1 Schematic diagrams of the chemical treatments on the CNT films

3.4 SEM analysis

3.4.1 Original CNT film

Fig. 3.2 shows the SEM images of the original CNT film. We can see the clean (free of amorphous carbon) and vertically aligned CNTs.

3.4.2 O_2 treated CNT film

Fig. 3.3 shows the SEM images of the O_2 treated CNT (O_2-CNT). There isn't any significant change in top view of the SEM image, but the length of the CNTs becomes shorter in the side view of the SEM image than that of the original CNTs as shown in Fig. 3.2.

3.4.3 HNO_3 treated CNT film

In Fig. 3.4, the SEM images of HNO_3 treated CNT (HNO_3-CNT) were given. The top view of the HNO_3-CNT, as shown in Fig. 3.4 (a), shows that CNTs are fallen down. This phenomenon might be caused that the HNO_3, which is a very strong etchant, etches and blows off some CNT from the substrate. The amount of CNTs became smaller than that of original CNT film, therefore steric hindrance supporting CNTs mutually disappears. So that, the vertically aligned CNTs are fell down. This geometrical effect on the field emission property will be discussed later. And we can see from the side view of the SEM image as shown in Fig. 3.4 (b) that the length of the CNTs became shorter than that of the original CNTs.

3.4.4 HF treated CNT film

In fig. 3.5, the SEM images of HF treated CNT (HF-CNT) were given. Similarly to the result of O_2 treatment, there isn't any significant change in top view of the SEM image, but the length of the CNTs becomes shorter in the side view of the SEM image.

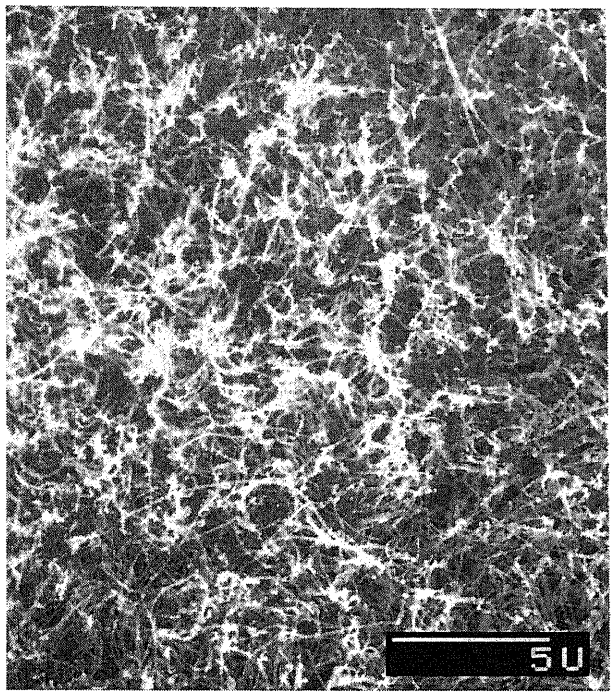

(a) Top view of the original CNT

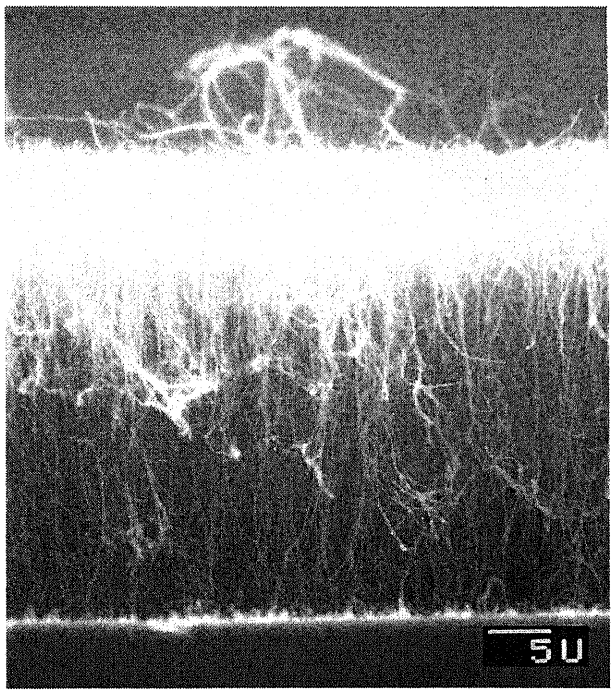

(b) Side view of the original CNT

Fig. 3.2 SEM images of the original CNT; (a) top view and (b) side view

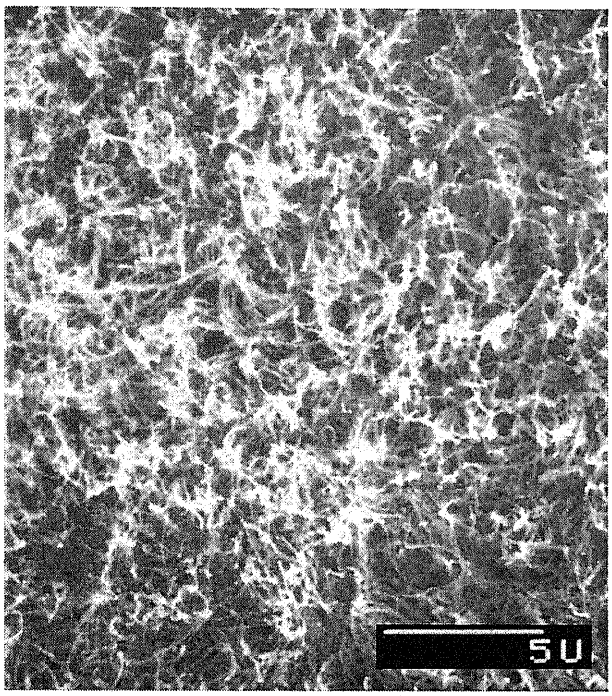

(a) Top view of the O_2-CNT

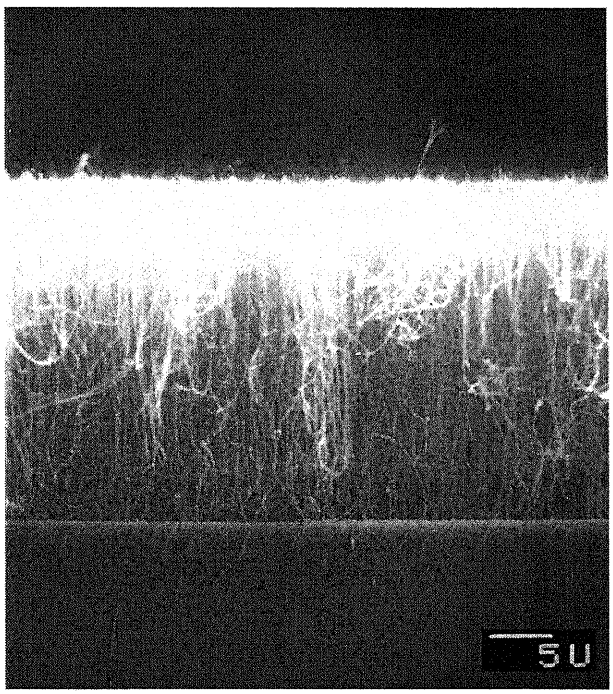

(b) Side view of the O_2-CNT

Fig. 3.3 SEM images of the O_2-CNT; (a) top view and (b) side view

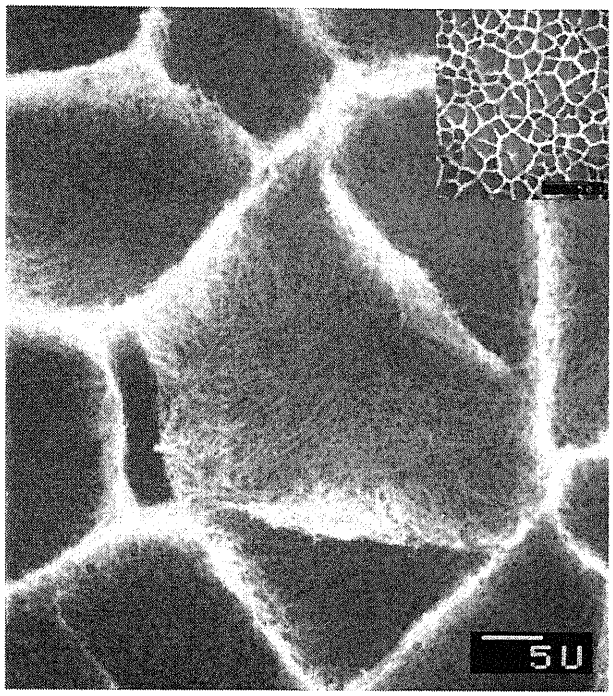

(a) Top view of the HNO_3-CNT

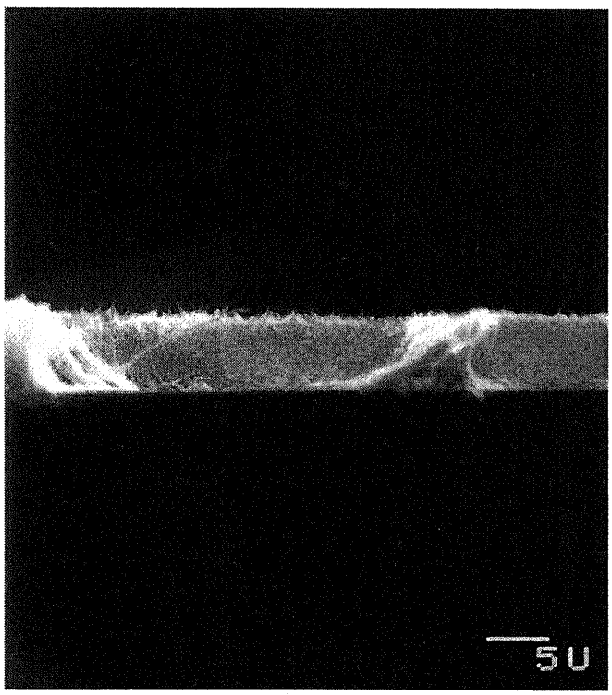

(b) Side view of the HNO_3-CNT

Fig. 3.4 SEM images of the HNO_3-CNT; (a) top view and (b) side view

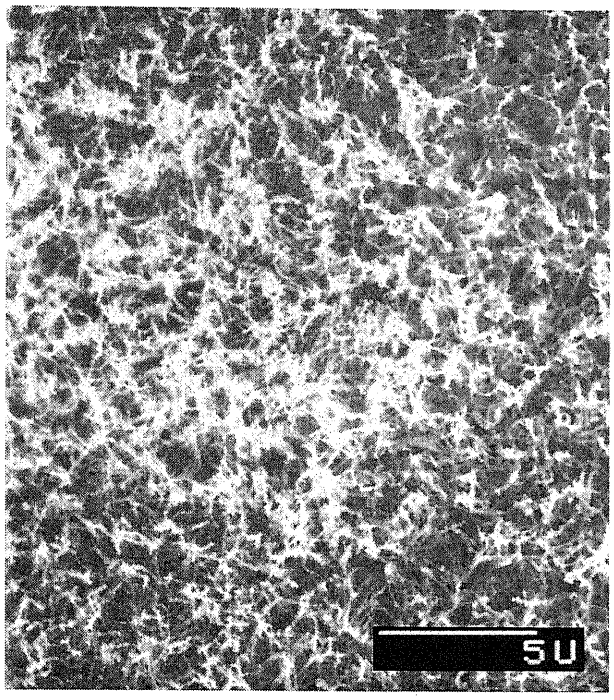

(a) Top view of the HF-CNT

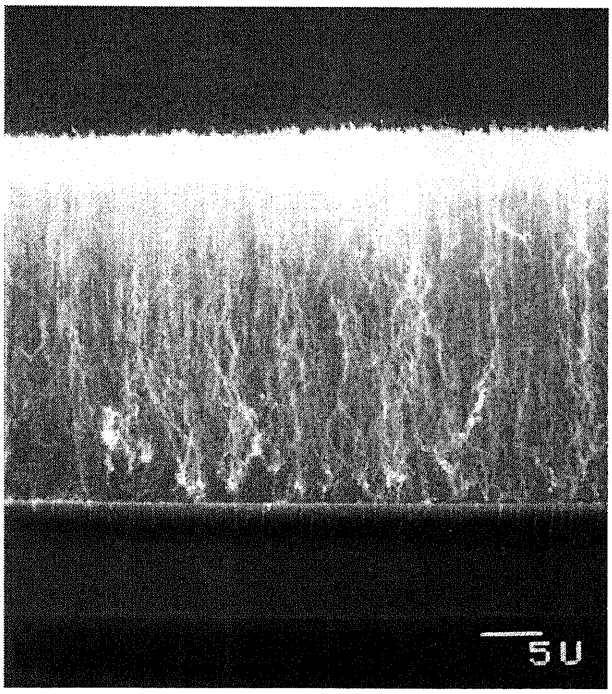

(b) Side view of the HF-CNT

Fig. 3.5 SEM images of the HF-CNT; (a) top view and (b) side view

3.5 XPS analysis

In the case of the use of CNT for field emission devices, it is predicted that the field emission property may be changed by the shift of work function due to the chemical treatment. The field emission property can be changed by the attachment of functional group only to the cap of CNTs, because the field emission behavior takes place at the cap of the CNTs. Fortunately, the most of the attachment of functional group take place at the cap of CNTs.

In this chapter, the change of the surface state of the chemically treated CNT was investigated by using the XPS spectroscopy. Fig. 3.6 - 3.9 show the wide scan (a) and the C1s narrow scan (b) of the XPS spectra for the original CNT, the O_2-CNT, the HNO_3-CNT, and the HF-CNT, respectively. Curve fitting of C1s peaks was executed by using the spectrum analysis software (Microcal Origin, Microcal software Inc., assuming that all of the spectra are in Gaussian distribution). The binding energies of the chemical bonding for carbon are shown in Table 1.

Main peaks observed were sp^2 peak (~284.5 eV), sp^3 peak (~285 eV), and other carbon related peak (CF, ~289 eV). The sp^2 peak, which becomes sharp if the crystallinity increase, is usually observed at the graphite. The sp^3 peak is easy to react and combine other functional groups, because its binding strength is weaker than that of sp^2 peak. For this reason, it is expected that C-O bond, C-N bond, and C-F bond were generated for O_2 treatment, HNO_3 treatment, and HF treatment, respectively.

Table 3.1 The binding energies of the chemical bonding for carbon

C (graphite)	1s	284.5	COO (PMMA)	1s	288.8
C (graphite)	1s	284.2	COO (PBMA)	1s	288.9
SiC	1s	282.5	COO (PET)	1s	288.9
TiC	1s	281.5	COO (PBT)	1s	288.9
VC	1s	282.2	NH-C=O	1s	288.0
WC	1s	283.0	NH-C=O	1s	287.8
Na2CO3	1s	289.4	COOH	1s	288.8
CaCO3	1s	289.4	N-C=O	1s	288.7
CaCO3	1s	289.8	O-COO	1s	290.7
CO2	1s	291.9	C-CN	1s	286.2
CS2	1s	287.0	C-NH	1s	286.1
NaCN	1s	286.2	C-N	1s	285.5
KCN	1s	286.1	C=N	1s	287.3
CH-CH	1s	285.0	C-Cl	1s	285.2
C-O (PMMA)	1s	286.5	C-C-Cl	1s	286.4
C-O (PBMA)	1s	286.4	C-Cl2	1s	285.4
C-O (PET)	1s	286.6	C-C-Cl2	1s	286.5
C-O (PBT)	1s	286.4	C-S	1s	285.3
C-O (PC)	1s	286.4	C-S-O	1s	285.9
C-O (PI)	1s	285.9	CF2	1s	291.6
C-O (EP)	1s	286.3	CHF-CHF	1s	289.2
C-OH (CL)	1s	286.5	CF2-CHF	1s	291.5
O-C-O	1s	287.9	CF3	1s	294.0

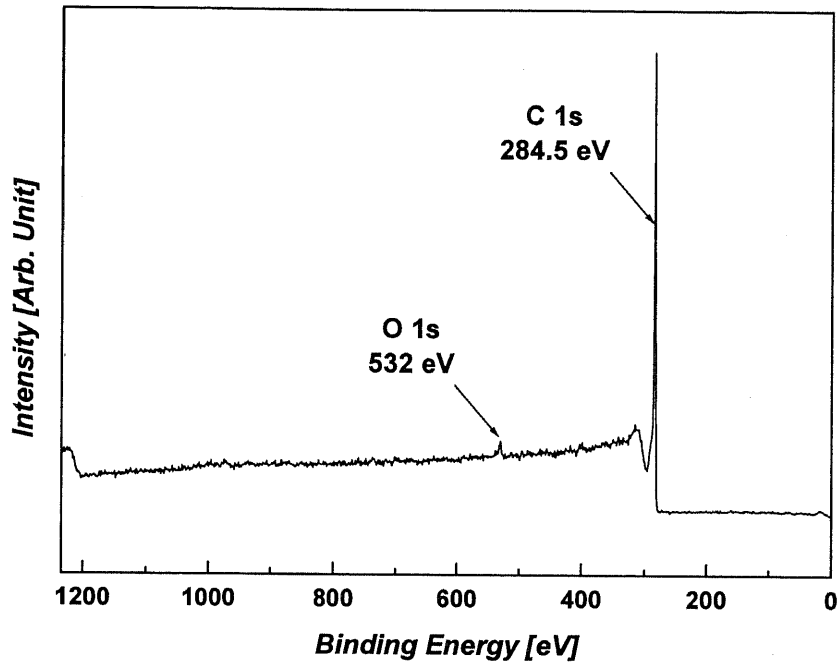

(a) The XPS wide scan spectrum of the Original CNT film

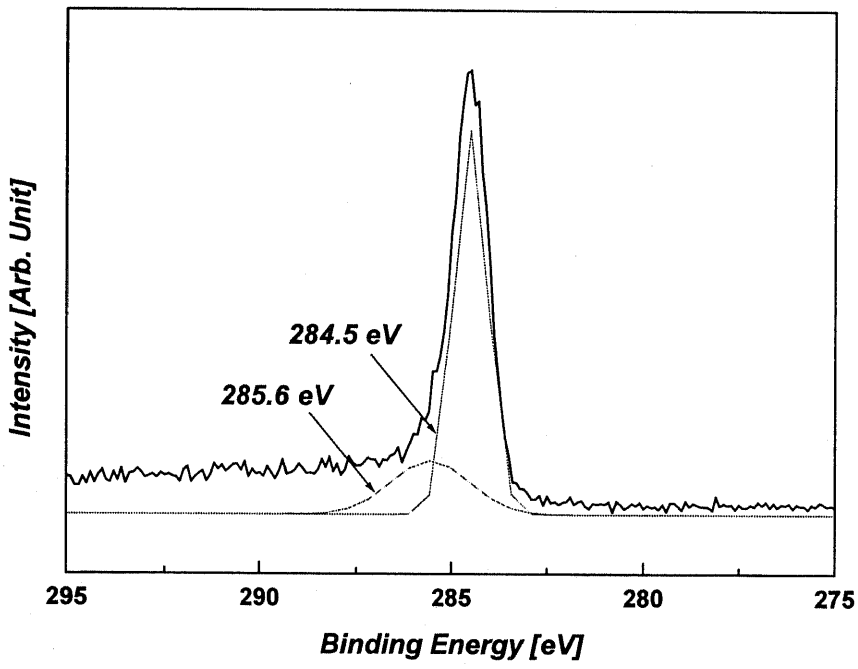

(b) The C1s narrow scan spectrum from the above wide scan spectrum

Fig. 3.6 The wide scan (a) and the C1s narrow scan (b) of the XPS spectra for the original CNT film

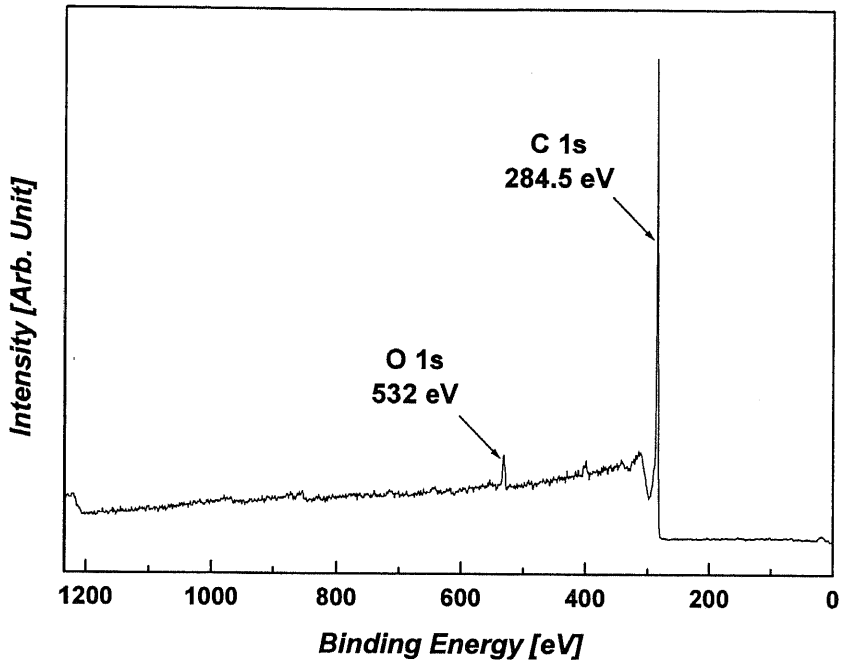

(a) The XPS wide scan spectrum of the O_2-CNT film

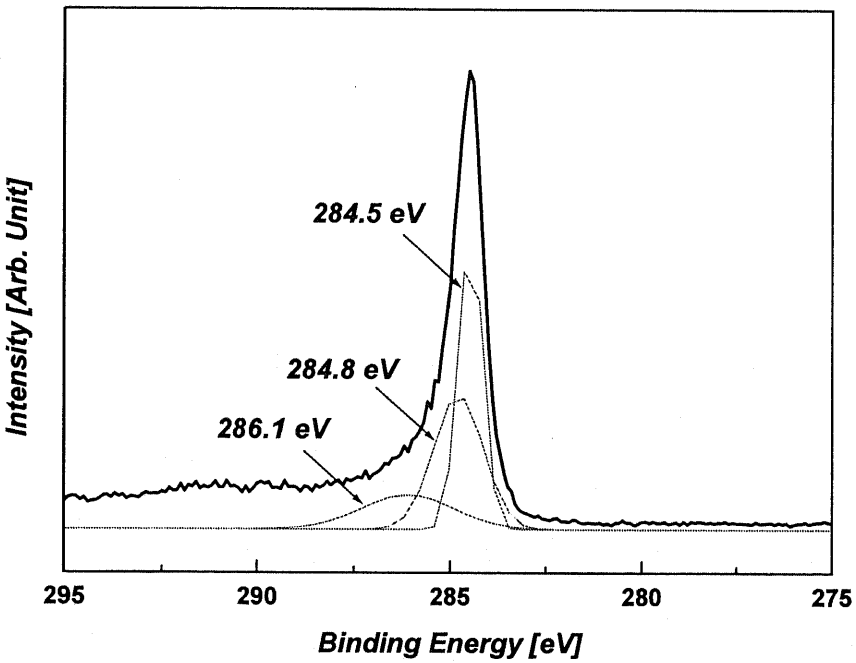

(b) The C1s narrow scan spectrum from the above wide scan spectrum

Fig. 3.7 The wide scan (a) and the C1s narrow scan (b) of the XPS spectra for the O_2-CNT film

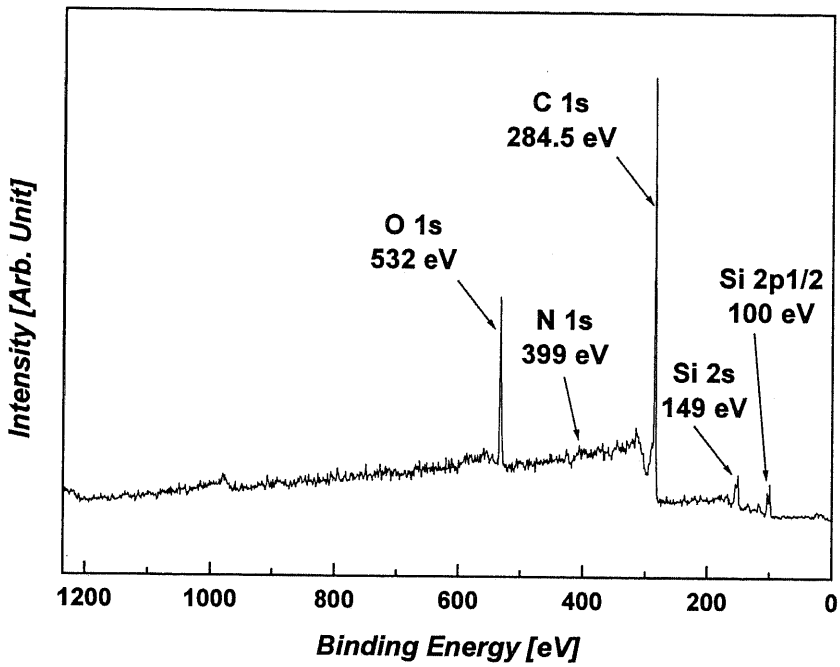

(a) The XPS wide scan spectrum of the HNO_3-CNT film

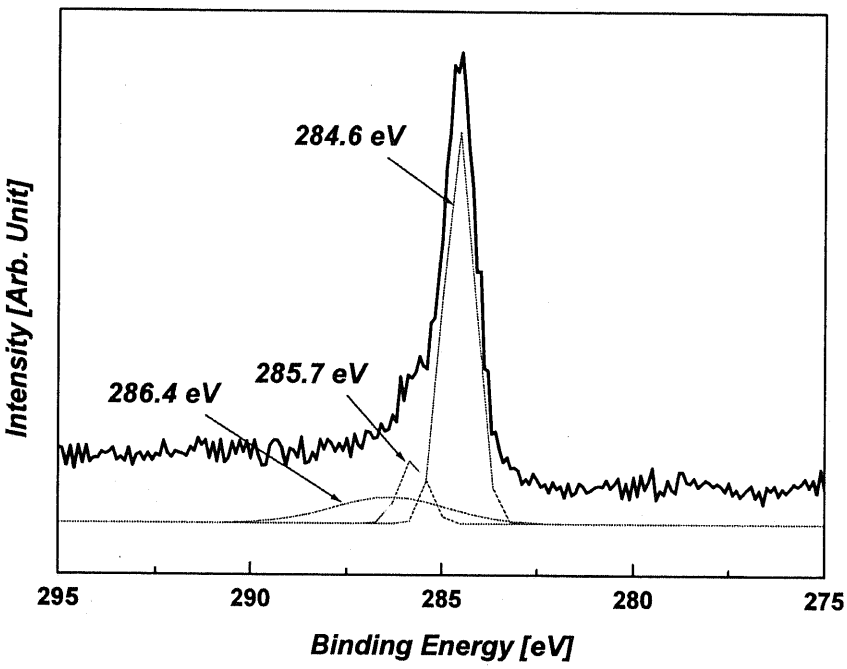

(b) The C1s narrow scan spectrum from the above wide scan spectrum

Fig. 3.8 The wide scan (a) and the C1s narrow scan (b) of the XPS spectra for the HNO_3-CNT film

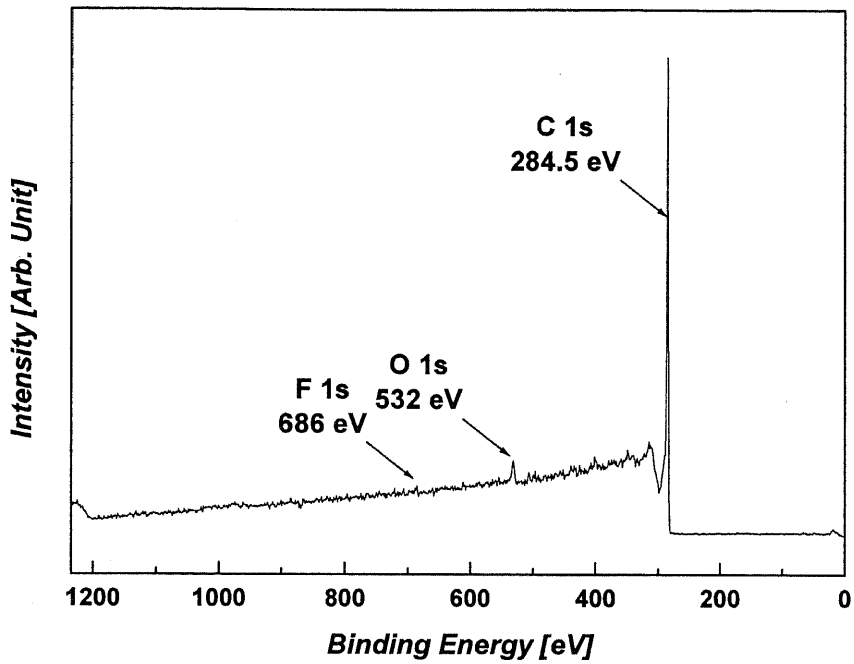

(a) The XPS wide scan spectrum of the HF-CNT film

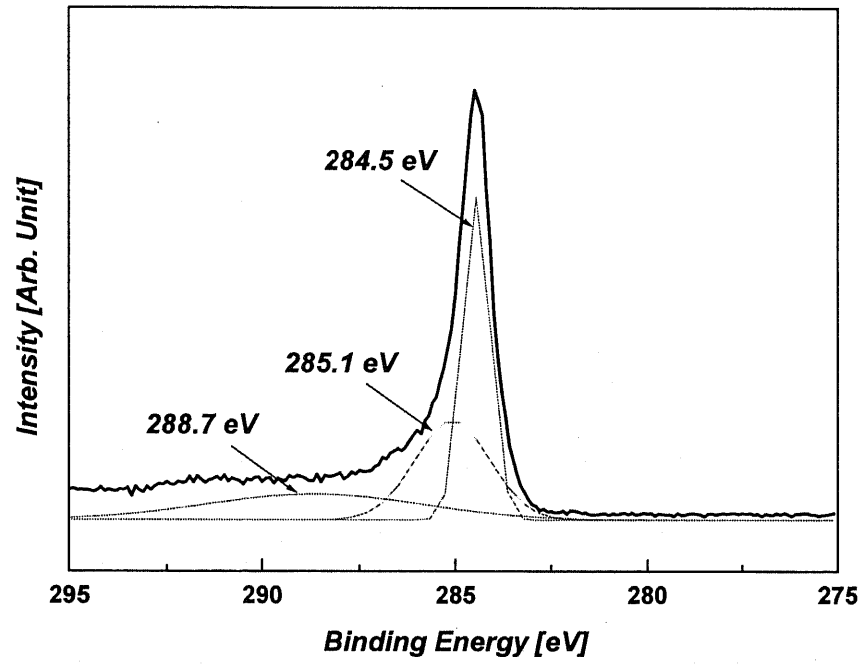

(b) The C1s narrow scan spectrum from the above wide scan spectrum

Fig. 3.9 The wide scan (a) and the C1s narrow scan (b) of the XPS spectra for the HF-CNT film

In all cases, the carbon peak (C1s, 284.5 eV) and oxygen peak (O1s, 530 eV) were observed. The stronger oxygen peak than that of the original-CNT film for the O_2-CNT film, the weak nitrogen peak (trace level) for HNO_3-CNT film, and the fluorine peak (trace level) for HF-CNT film were observed, respectively. This means that all of the chemical treatments could attach their functional groups to each film. Especially in the case of HNO_3-CNT film, there exist strong oxygen peak and silicon peaks. One possible explanation for these peaks is the loss of some CNTs, which was aligned vertically to the substrate, by the HNO_3 treatment. In order to verify this possibility, the XPS spectrum of the silicon wafer was investigated. The ratio of the silicon peak to the oxygen peak in the HNO_3-CNT film is same as the ratio in the silicon substrate. From the result of comparing oxygen peak intensity and silicon peak intensity, it is found that the oxygen peak and the silicon peak were introduced from the Si substrate. (See Fig. 3.10)

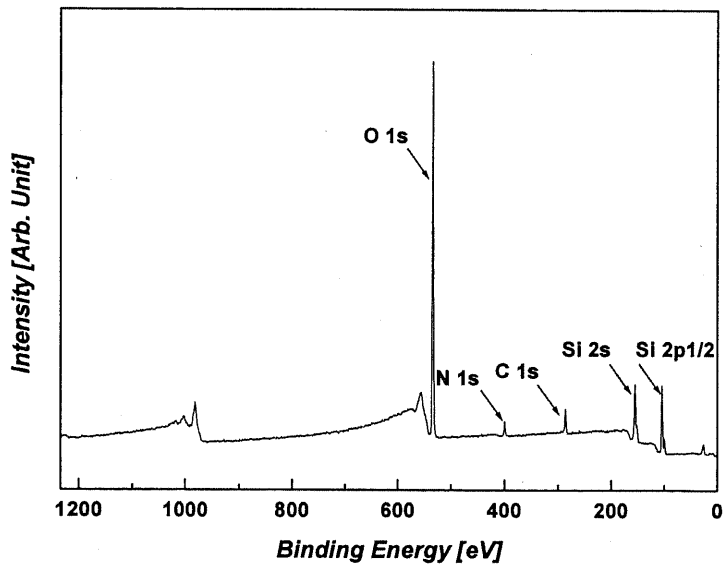

Fig. 3.10 XPS spectrum of silicon substrate

Curve fitting of C1s peaks was executed by using the spectrum analysis software (Microcal Origin, Microcal software Inc., assuming that all of the spectra are in Gaussian distribution). Main peaks observed were sp^2 peak (~284.5 eV), sp^3 peak (~285 eV), and other carbon related peak (286~289 eV). The sp^2 peak, which becomes sharp if the crystallinity increase, is usually observed at the graphite. The sp^3 peak is easy to

react and combine other functional groups, because its binding strength is weaker than that of sp^2 peak. For this reason, it is expected that C-O bond, COO- bond or C-OH bond, and CHF-CHF bond were generated for O_2 treatment, HNO_3 treatment, and HF treatment, respectively.

From the curve fitted C1s spectra, the composition ratio of the carbon-containing surface groups was derived and summarized in Table 2. At the surface of all of the chemically treated CNT films excluding the HNO_3-CNT film, the sp^2 bond which represents the hexagon structure of CNT decreased by the chemical treatments. However, the sp^3 bond which represents the carbon single bond (dangling bond) and the carbon shift which represents the attachment of functional groups increased by the chemical treatments. In the case of the HNO_3-CNT film, the sp^3 bond and the chemical shift were undervalued because the CNTs were fallen down. As a result, it was found that the chemical treatments on the CNT film were very effective to increase the amount of the dangling bonds which is thought to be the field emission sites. From these results, we can predict that the chemical treatment on the CNT film improve the field emission performance.

Table 3.2 Composition ratio of the carbon-containing surface groups

Sample	sp^2 (%)	sp^3 (%)	Carbon shift (%)
Original CNT film	76	24	0
O_2-CNT film	42	39	19
HNO_3-CNT film	72	11	17
HF-CNT film	41	34	25

3.6 Conclusions

The surface treatment of the CNT films by chemical treatment was investigated by using the XPS analysis. A strong oxygen peak, a weak nitrogen peak, and a fluorine peak in trace level were observed for the O_2 treated CNT film, the HNO_3 treated CNT film, and the HF treated CNT film, respectively. Carbon shifts such as C-O, COO-, or CHF-CHF were observed from the C 1s narrow scan spectra for O_2-CNT film, HNO_3-CNT film, and HF-CNT film. This fact implies that every element observed in the XPS wide scan spectra has a chemical bond with the carbon on the CNT films.

In order to verify the effect of the chemical treatment on the field emission property, the field emission current was measured. All of the chemically treated CNT films show the better field emission property than the original CNT film. Although the field emission from O_2-CNT film occurs at the lower electric field, field emission from HNO_3-CNT film and HF-CNT film occurs at the higher electric field. The threshold of the electric field of the original CNT film, O_2-CNT film, HNO_3-CNT film, and HF-CNT film are 3.55, 2.41, 3.17, and 3.34 V/μm, respectively. As the field emission occurs at pentagons or dangling bonds of the cap, increment of the dangling bonds means the improvement of the field emission performance. And it was thought that the difference of the field emission performance between the CNT film treated in liquid phase and the CNT films treated in gas phase was due to the attached functional groups. The CNT films treated in liquid phase such as HNO_3-CNT film and HF-CNT film may have carboxyl groups (–COOH). On the other hand, the CNT film treated in gas phase such as O_2-CNT film may have hydroxyl groups (–OH). Since the carboxyl group has more oxygen atoms than the hydroxyl group, it is predicted that the CNT film treated in liquid phase has deeper trap than that treated in gas phase. As a result, the CNT film treated in liquid phase degraded the field emission performance.

3.7 References

[1] S. Iijima, Nature 354 (1991)

[2] J.M. Bonard, F. Maier, T. Stockli, et al., Ultramicroscopy 73 (1998)

[3] J.M. Bonard, H. Kind, T. Stockli, L.-O. Nilsson, Solid State Electronics 45 (2001)

[4] W.B. Choi, D.S. Chung, J.H. Kang, et al., Appl. Phys. Lett. 75, 20 (1999)

[5] Milne WI, Teo KBK, Chhowalla M, et al., Current Appl. Phys. 2, 6 (2002)

[6] R.M.D. Stevens, N.A. Frederick, B.L. Smith, et al., Nanotechnology 11 (2000)

[7] S. Akita, H. Nishijima and Y. Nakayama, J. Phys. D: Appl. Phys. 33 (2000)

[8] Tong Y, Liu C, Hou PX, et al., Physica B 323, 1-4 (2002)

[9] Dean KA, Chalamala BR, Coll BF, et al., New Diam Front C Tec 12, 4 (2002)

4 Effect of plasma processes

4.1 Introduction

Carbon nanotubes consist of very strong covalent bonds, so that they are very stable against to the chemical attacks [1]. Breaking these strong covalent bonds and attaching new functional groups will be expected to bring a significant change on the CNT's physical properties [2]. Therefore they will open the novel application fields. For example, when we use the CNT films as a field emission device, we can control the field emission performance of those films by attaching some useful functional groups due to the plasma processes [3]. The field emission behavior takes place at the cap of the CNT [4]. For this reason, we attach the functional groups to the cap of the CNT. Fortunately, the break of the chemical bonding starts from the pentagons on the cap [5].

In this paper, we investigate the surface change of the CNT films caused by the Ar plasma process. And then, the effect of the surface change on the field emission property was investigated. The plasma process was carried out in the Ar gas circumstance with varying the processing time. The surface change of the plasma processed CNT films was analyzed by using the XPS spectroscopy. Finally, we discuss the relation between the surface change and the field emission property.

4.2 Purpose of plasma process

It is expected that the plasma process can make the CNT film active. It is also expected that the plasma process can change the surface composition of the CNT film by their attached functional groups from the gas used to generate the plasma plum. In this paper, in order to study the effect of these surface compositional changes on the field emission property of the CNT film, the relation between the surface compositional changes analyzed by the XPS and the field emission properties was investigated.

4.3 Plasma processes

The plasma process was performed by using the apparatus shown in Fig. 4.1. AC voltage amplified by through the neon transformer was supplied to generate plasma. The inter-electrodes distance was 2 cm. Carbon nanotube films were plasma processed in Ar circumstance for various time conditions. Plasma reaction chamber was evacuated

to the vacuum level of 1×10^{-2} Pa. And then Ar gas was introduced up to the vacuum level of 20 Pa. At this vacuum level, the plasma process carried out at the electric field of 2.4 kV/cm. The Ar plasma processing time was varied from 10 mins to 60 mins. After the plasma process, the CNT sample was stabilized for 1 h. In this paper, three types of plasma processes were carried out. Those were Ar, N_2, and H_2 plasma processes.

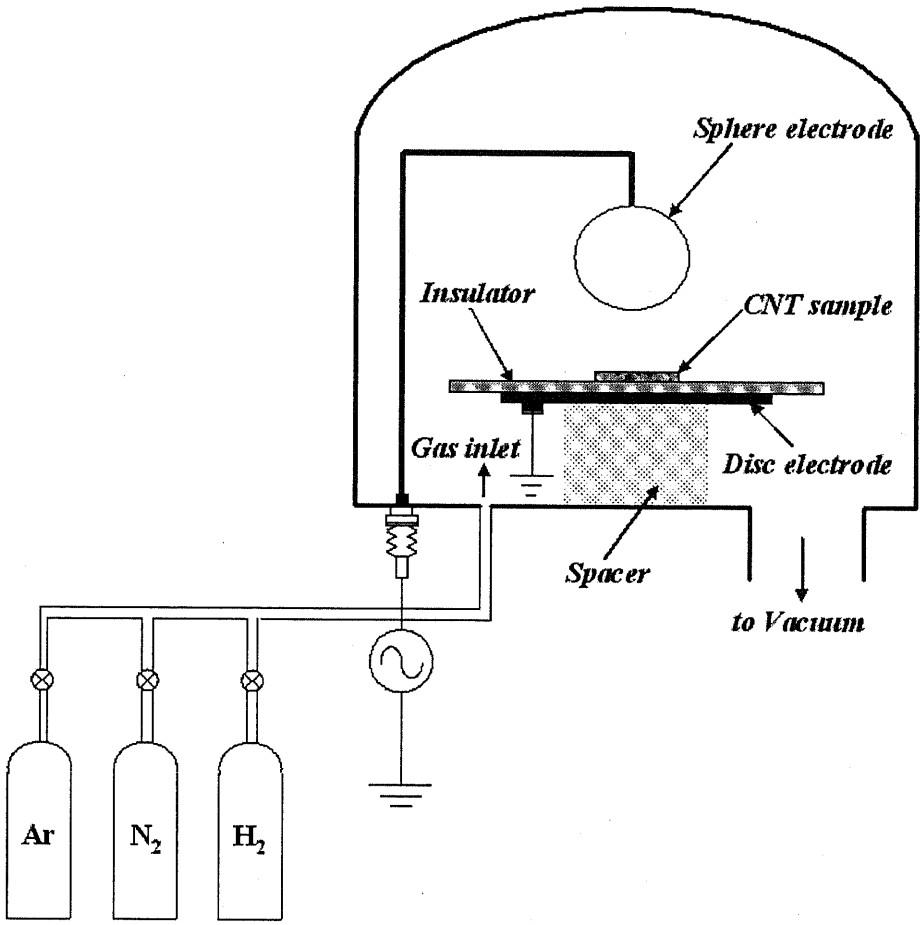

Fig. 4.1 Plasma process apparatus used in this work.

4.4 XPS analysis

4.4.1 Ar plasma process

Fig. 4.2 shows the XPS wide scan spectra of the original CNT film and the plasma processed CNT films for 10, 30, and 60 mins, respectively. In the case of the original CNT film there is very small oxygen peak, but in the case of the Ar plasma processed CNT films, the iron peak, the fluorine peak, and the oxygen peaks were observed. The iron might come from the stainless ball-type electrode used to generate the plasma plum. The fluorine peak might come from the Teflon sheet used as insulating material. And here, the origin of the oxygen peak is a problem to be verified. There are two possible ways that the oxygen attaches to the CNT samples during the plasma process. First one is from the water vapor included in the air. The other one is from the water vapor attached at the wall of the vacuum chamber. In order to verify these two possibilities, the ion etching process was done in the XPS inspection chamber. The result of the ion etching process will be described in the section 4.4.2.

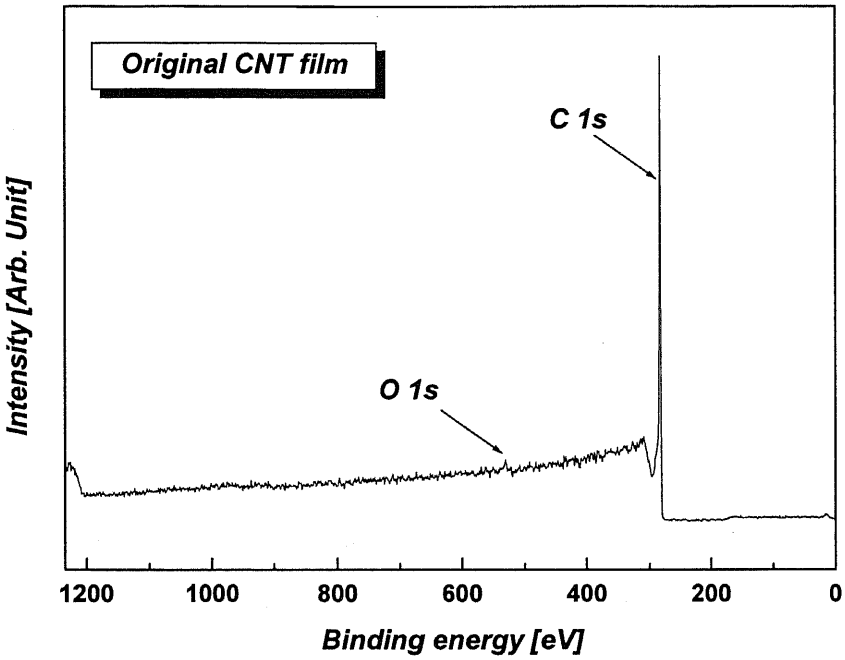

(a) Original CNT film

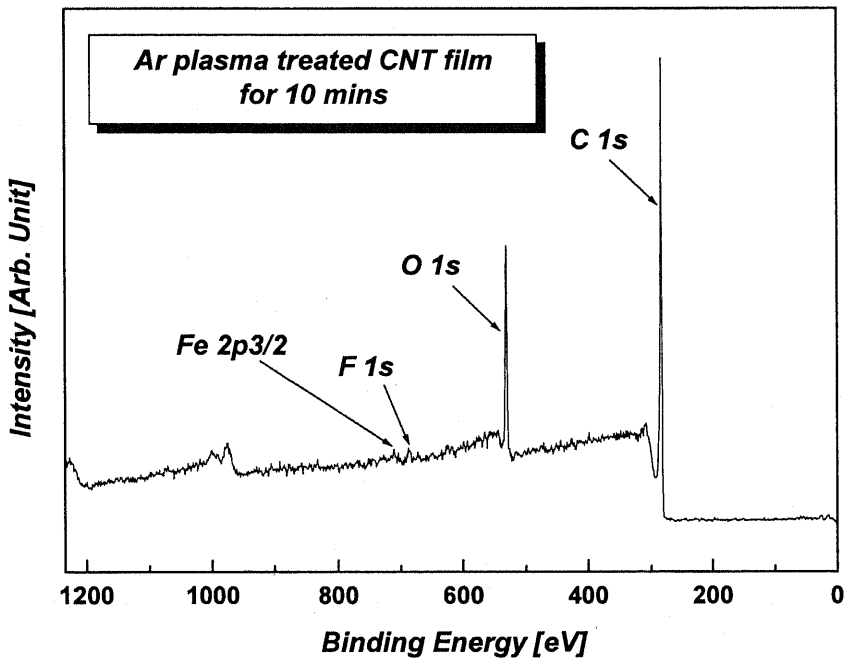

(b) Ar plasma processed CNT film for 10 mins

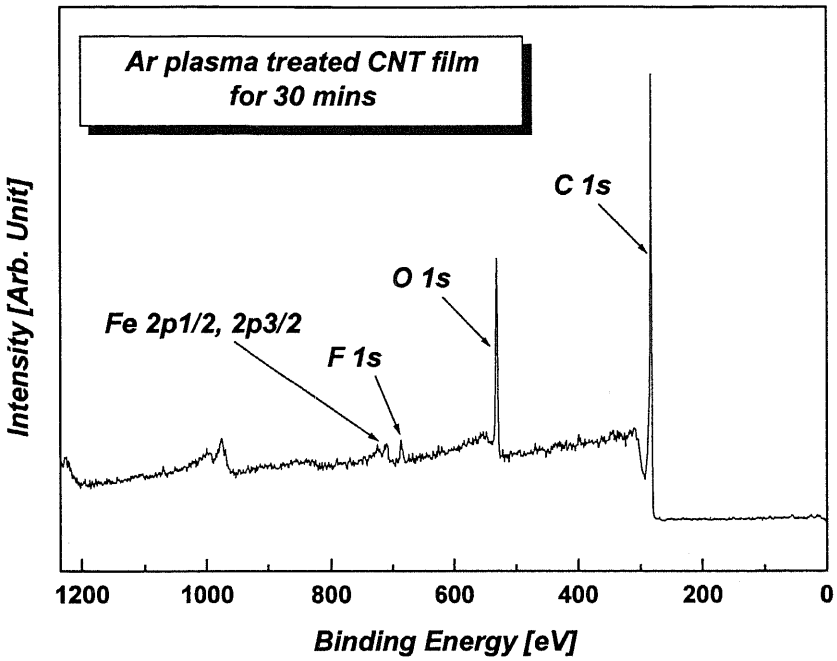

(c) Ar plasma processed CNT film for 30 mins

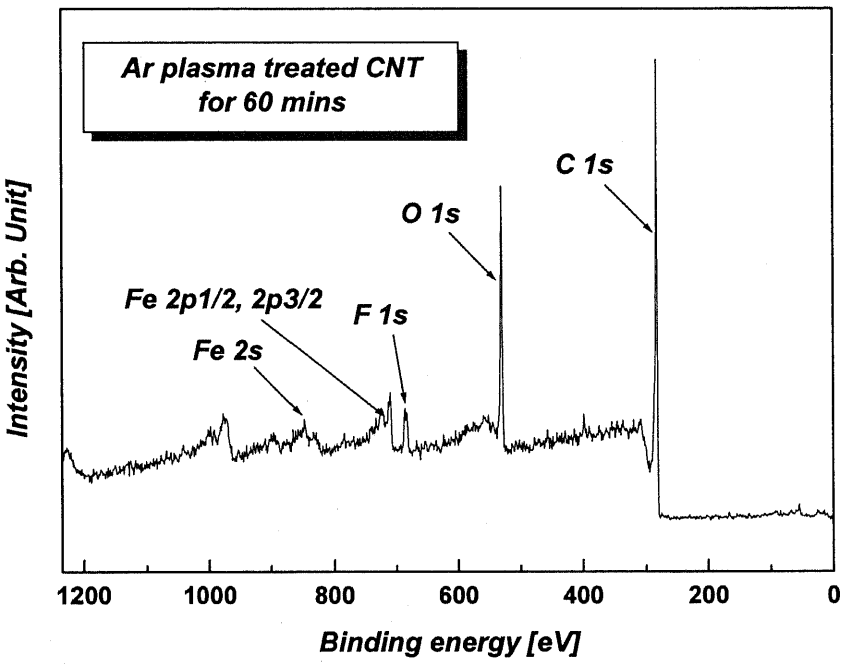

(d) Ar plasma processed CNT film for 60 mins

Fig. 4.2 XPS wide scan spectra of (a) the original CNT film and the plasma processed CNT films for (b) 10, (b) 30, and (d) 60 mins.

In order to evaluate the plasma processing time effect on the surface composition, the O1s/C1s ratio and the F1s/C1s ratio were obtained from the above XPS wide scan spectra. Each ratio was calculated by using the peak intensities. These results were shown in Fig. 4.3. The O1s/C1s ratio and the F1s/C1s ratio were increased from 2.64 % to 59.16 % and from 0 % to 10.44 % with increasing plasma processing time, respectively. These results imply that the Ar plasma process could change the surface composition effectively.

Next, the C1s narrow scan spectra of the Ar plasma processed CNT samples, which gives us the information about the bonding state of the carbon and attached atoms, were described. The C1s peak can be divided to sp^2 and sp^3 peak. Additionally, the carbon shift exists at the higher binding energy region (about 286 ~ 289eV).

The XPS narrow scan spectra of the original-CNT film and the Ar plasma processed CNT films were shown in Fig. 4.4. Every peak was curve fitted and divided into sp^2, sp^3, and carbon shift. In the case of original-CNT film, no carbon shift was observed. In the case of the Ar plasma processed CNT films however, the oxygen related carbon shift was observed. This oxygen related carbon shift at higher binding energy implies increment of amount of the oxygen. The gap between the carbon shift and the sp^2 peak was observed as 3.9, 3.2, and 3.7 eV at the Ar plasma processed CNT film for 10, 30, and 60 mins, respectively.

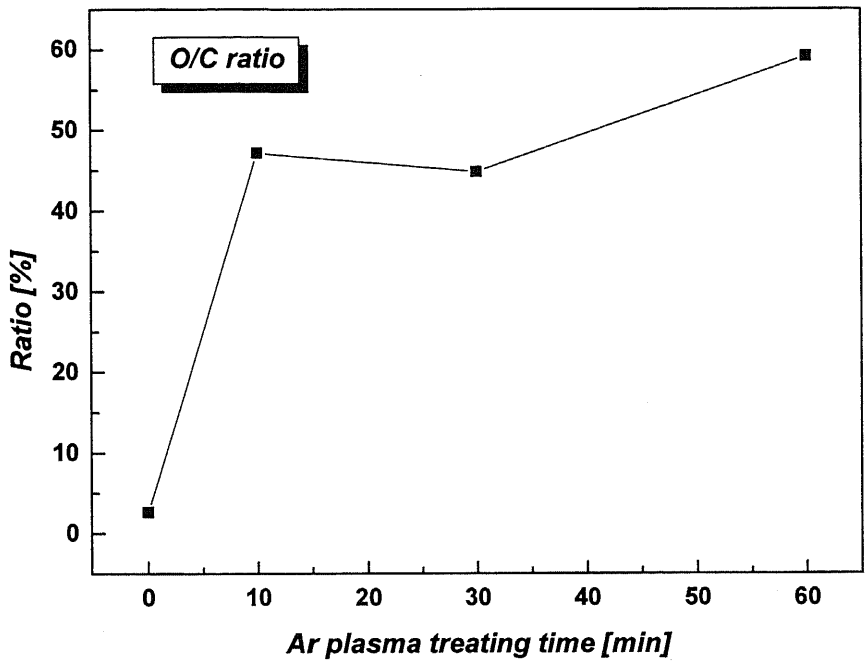

(a) O1s/C1s ratio change

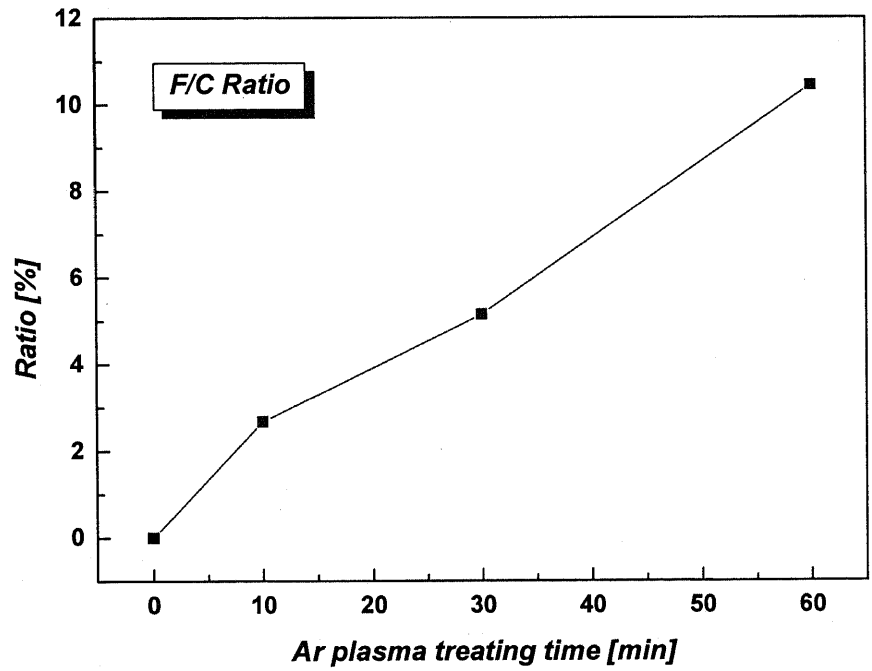

(b) F1s/C1s ratio change

Fig. 4.3 Surface composition changes by the Ar plasma process in terms of the O1s/C1s ratio and the F1s/C1s ratio.

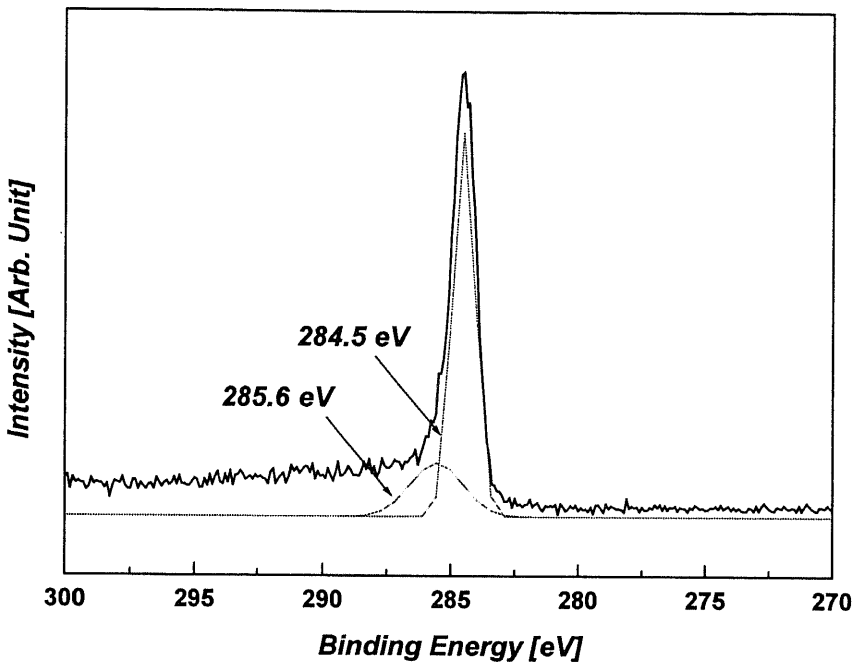

(a) Original CNT film

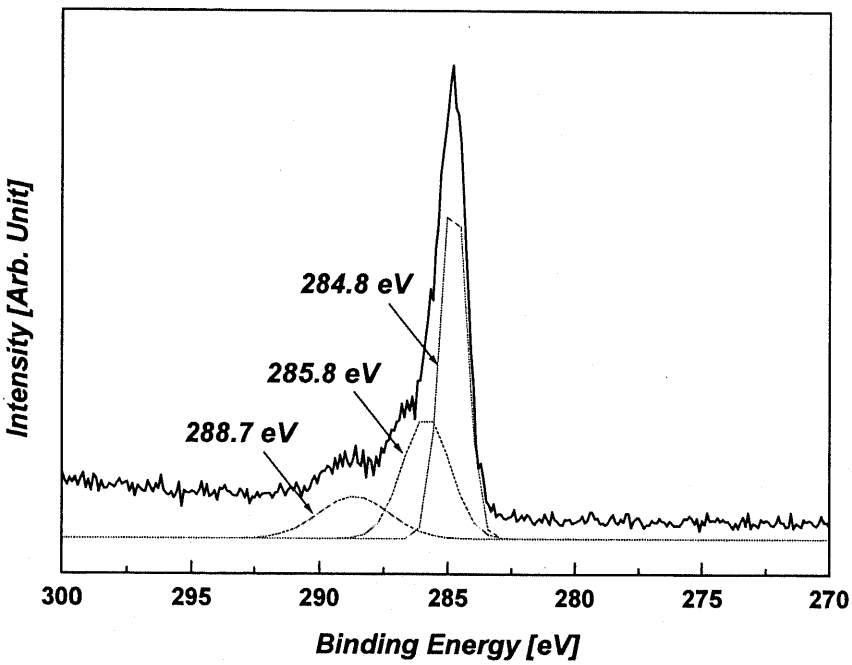

(b) Ar plasma processed CNT film for 10 mins

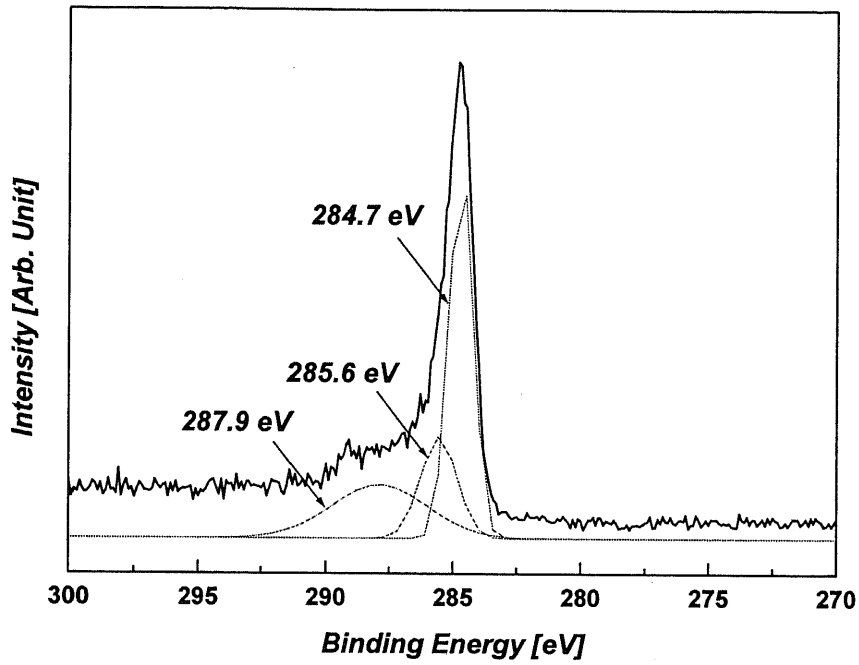

(c) Ar plasma processed CNT film for 30 mins

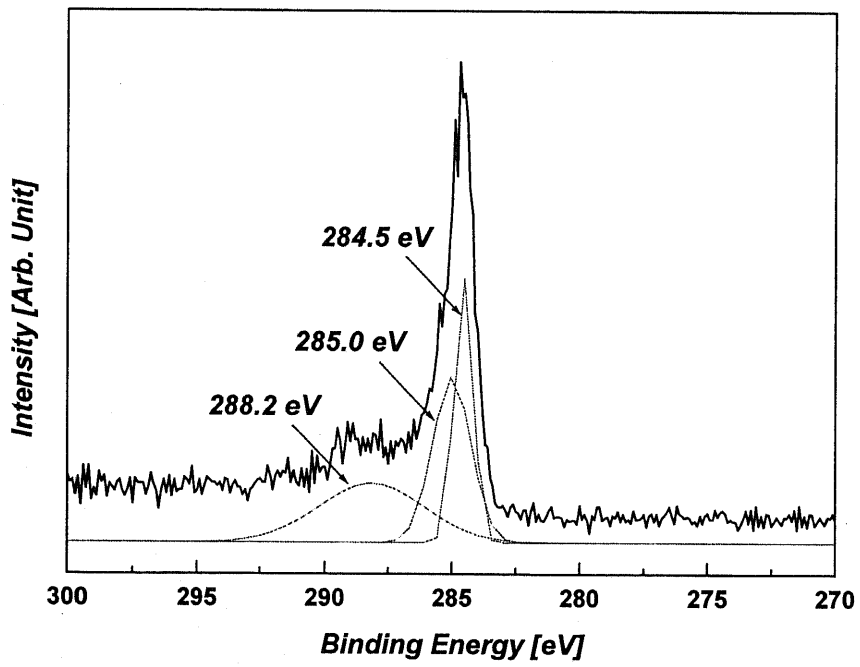

(d) Ar plasma processed CNT film for 60 mins

Fig. 4.4 XPS narrow scan spectra of the original CNT film and the Ar plasma processed CNT films.

4.4.2 N_2 plasma process

The N_2 plasma process was executed with the same conditions of the Ar plasma process. The N_2 plasma process was done to verify the origin of the oxygen peak using ion etching in the XPS inspection chamber. As described earlier, there can be two possibilities in the origin of the oxygen, i.e. i) water vapor in air, and ii) water vapor attached to the wall of the plasma process chamber.

Dry air and wet air were used to compare the effect of water in air. After ion etching in the XPS inspection chamber, the samples were pulled out to the preliminary chamber. The samples were exposed to dry or wet air by introducing the dry or wet air in this chamber. After the exposing process, the samples were loaded into the XPS inspection chamber again. Finally, the XPS spectra of before and after the ion etching and the exposing process were compared.

Fig. 4.5 shows the XPS wide scan spectra of the original CNT film and the N_2 plasma processed CNT films for 10, 30, and 60 mins. In the case of the original CNT film there is very small oxygen peak, but in the case of the N_2 plasma processed CNT films oxygen, nitrogen, fluorine, iron, and chrome peaks are observed. The fluorine peak might come from the Teflon plate used as insulation material. The iron and chrome peak might come from the stainless ball-type electrode used to generate Ar plasma. And the oxygen peak was thought to come from the water vapor attached to the vacuum chamber wall. With increasing processing time, oxygen/carbon ratio increased. This means that the amount of oxygen increased with the plasma processing time.

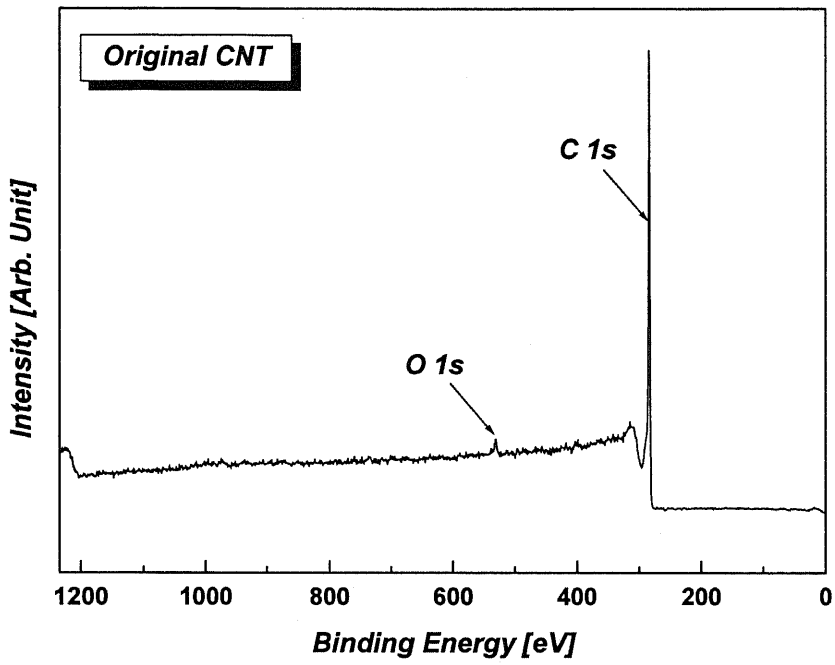

(a) Original CNT film

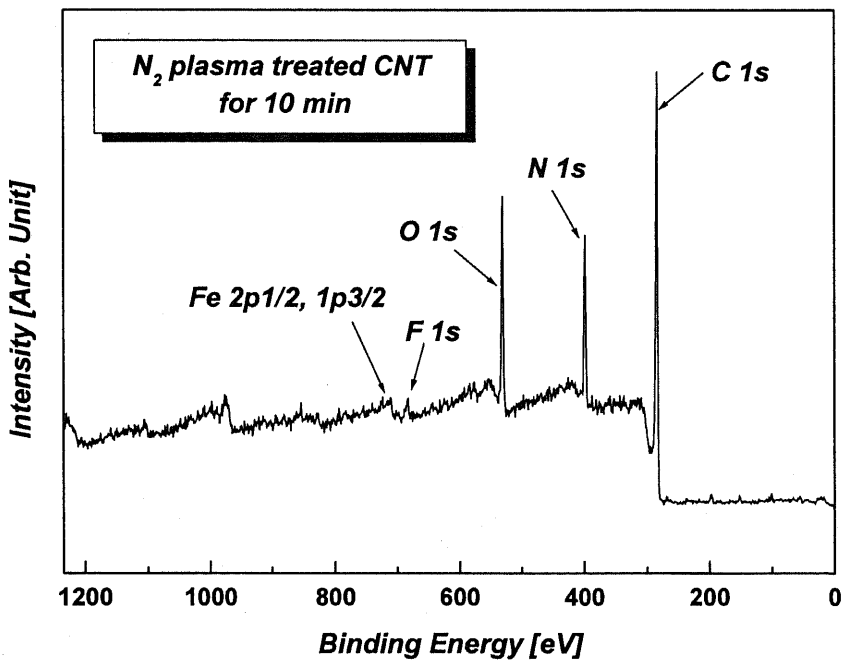

(b) N_2 plasma processed CNT film for 10 mins

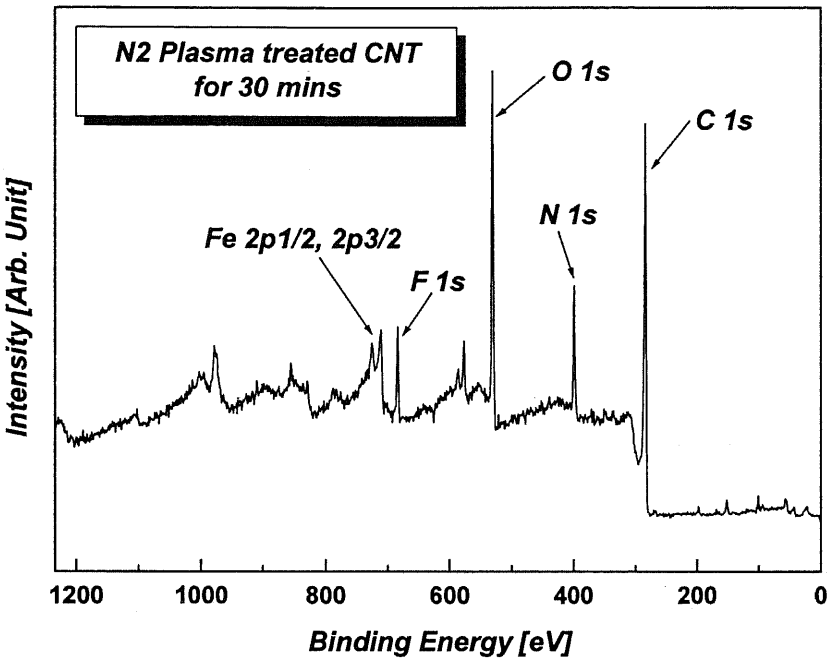

(c) N_2 plasma processed CNT film for 30 mins

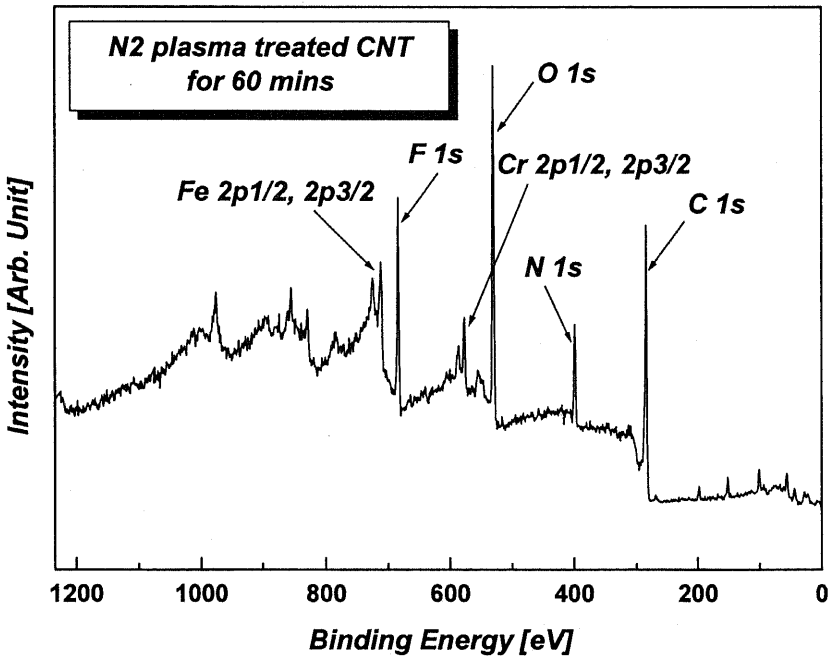

(d) N_2 plasma processed CNT film for 60 mins

Fig. 4.5 XPS wide scan spectra of (a) the original CNT film and the N_2 plasma processed CNT films for (b) 10, (c) 30, and (d) 60 mins.

In order to identify the origin of oxygen peak at the XPS spectra of N_2 plasma processed CNT films, the original CNT film and plasma processed CNT films were investigated by the XPS before and after the etching process in the XPS inspection chamber. The etching process was done for 400 sec (40 secs × 10 times). This etching process blows off the attached functional groups from the CNT surface, and makes the surface state of CNT film active, so as to react with oxygen energetically during the exposing process.

Fig. 4.6 and 4.7 show the XPS wide scan spectra of the original CNT film and the N2 plasma processed CNT films after the exposing process to dry and wet air, respectively. There are no significant changes between dry and wet air exposed samples. This means that the water vapors in the air don't play an important role in the adhesion of the oxygen to the CNT surface during the plasma process. Therefore we can conclude that the origin of the oxygen peak in the XPS spectra is from the water vapor attached to the chamber wall.

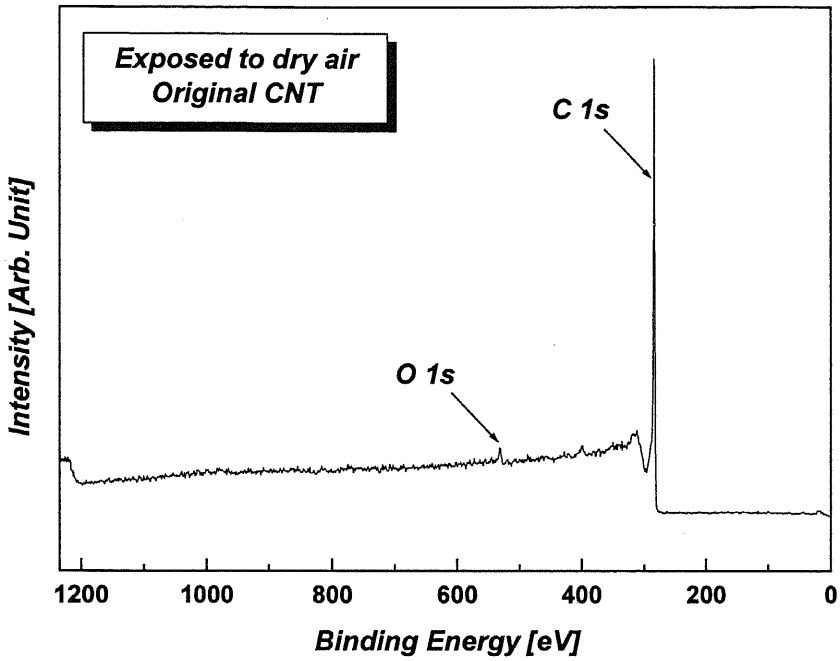

(a) Original CNT film

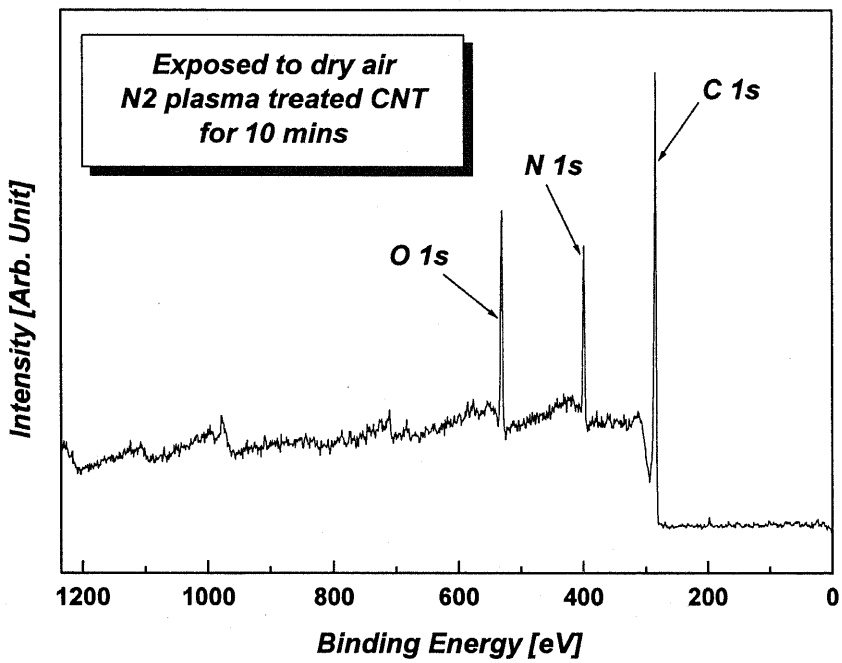

(b) N_2 plasma processed CNT film for 10 mins

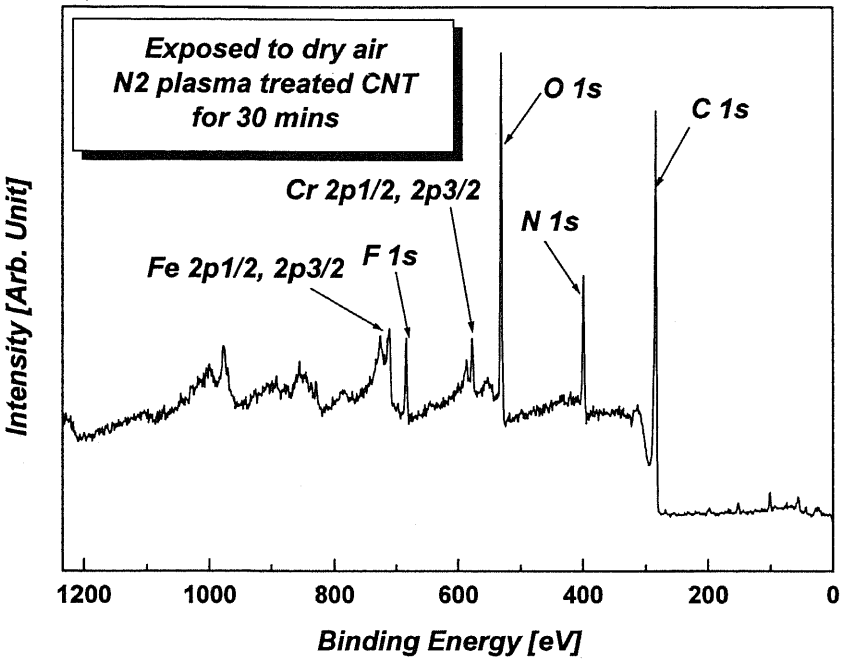

(c) N_2 plasma processed CNT film for 30 mins

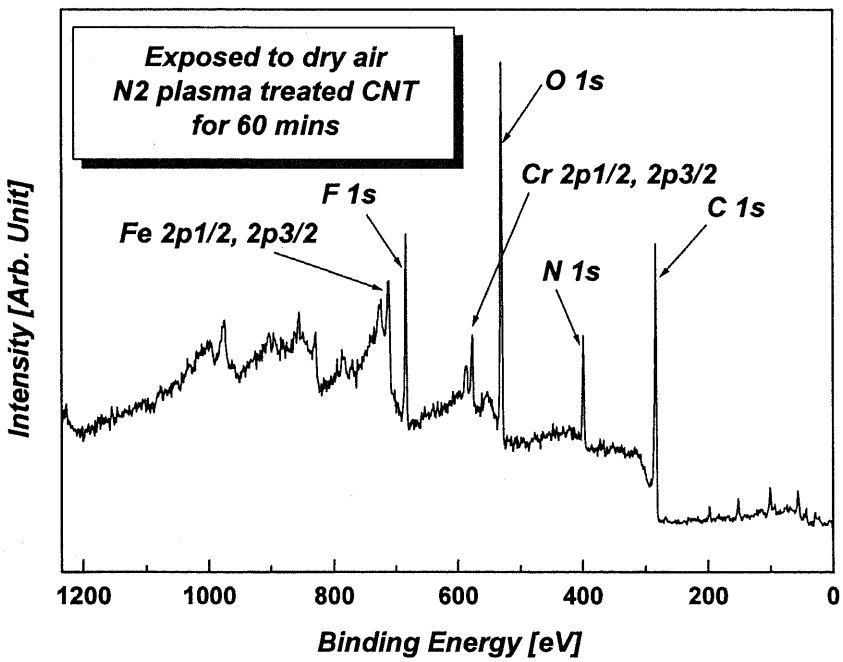

(d) N_2 plasma processed CNT film for 60 mins

Fig. 4.6 XPS wide scan spectra of (a) the original CNT film and the N_2 plasma processed CNT films for (b) 10 mins, (c) 30 mins, and (d) 60 mins after the exposing process to dry air.

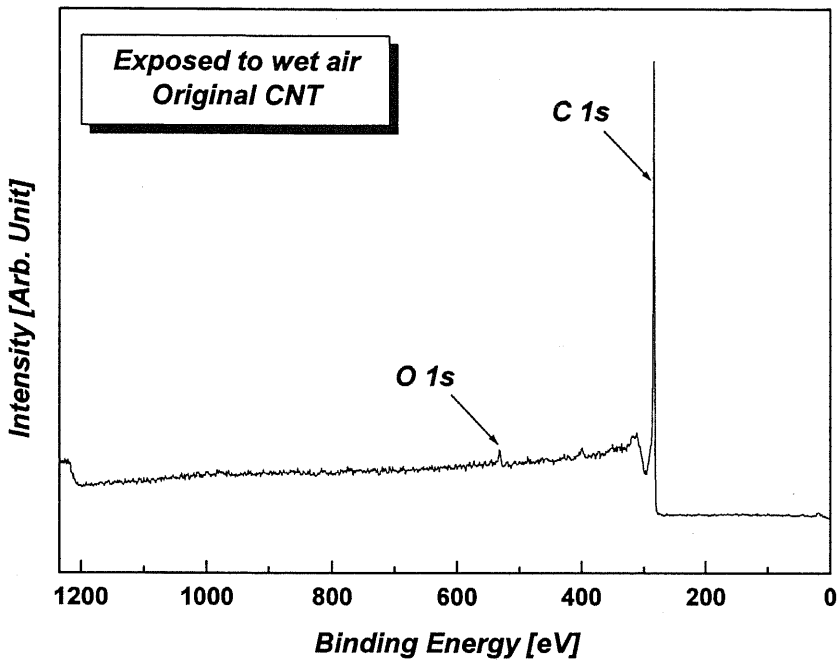

(a) Original CNT film

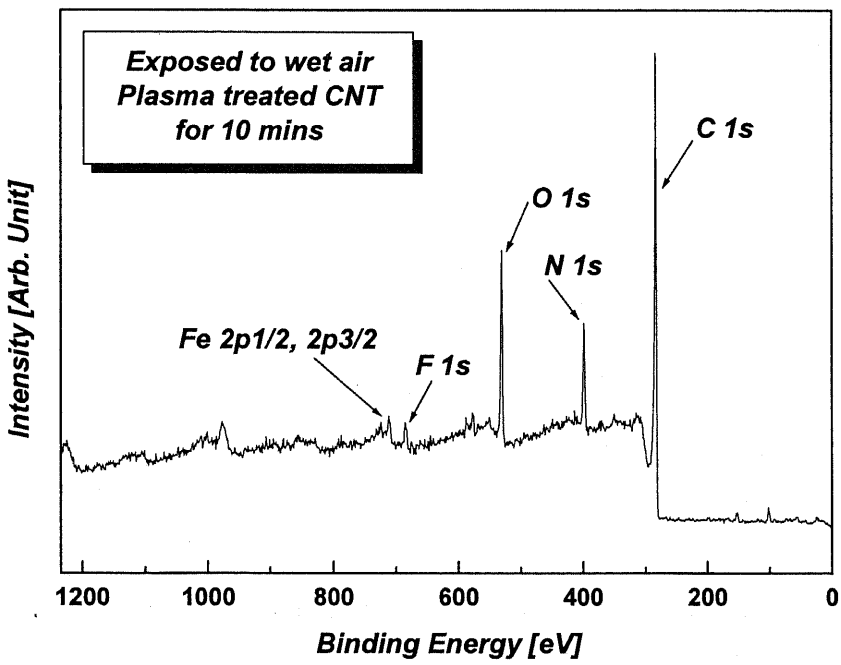

(b) N_2 plasma processed CNT film for 10 mins

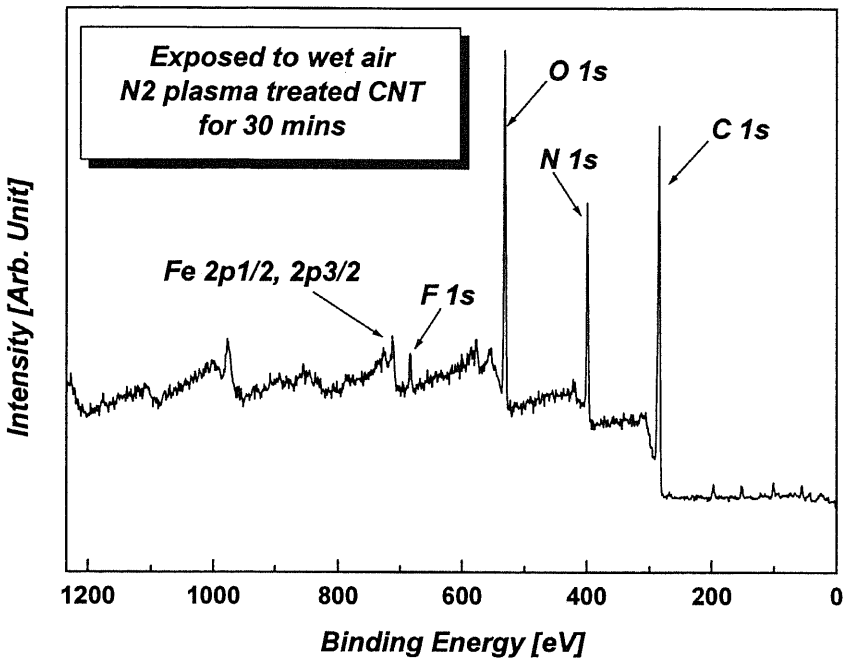

(c) N_2 plasma processed CNT film for 30 mins

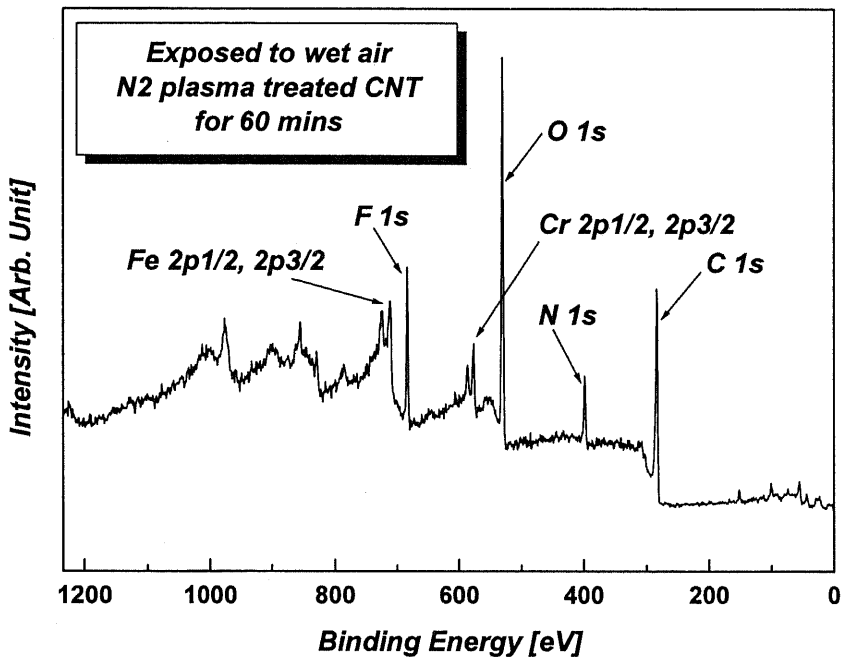

(d) N_2 plasma processed CNT film for 60 mins

Fig. 4.7 XPS wide scan spectra of the original CNT film (a) and the N_2 plasma processed CNT films for 10 (b), 30 (c), and 60 mins (d) after the exposing process to wet air.

Also in N_2 plasma process, in order to evaluate the plasma processing time effect on the surface composition, the N1s/C1s ratio, the O1s/C1s ratio, and the F1s/C1s ratio in the samples exposed to dry and wet air were obtained from the above XPS wide scan spectra. These results were shown in Fig. 4.8. These results imply that the N_2 plasma process could change the surface composition effectively.

Ion etching process is very effective to blow off the oxygen from the Silicon wafer surface. But in this case of CNT, the etching process makes no significant change between the results of before and after the etching process. This means that the oxygen related functional groups (or molecules) are attached very strongly or, very deep places from the film surface.

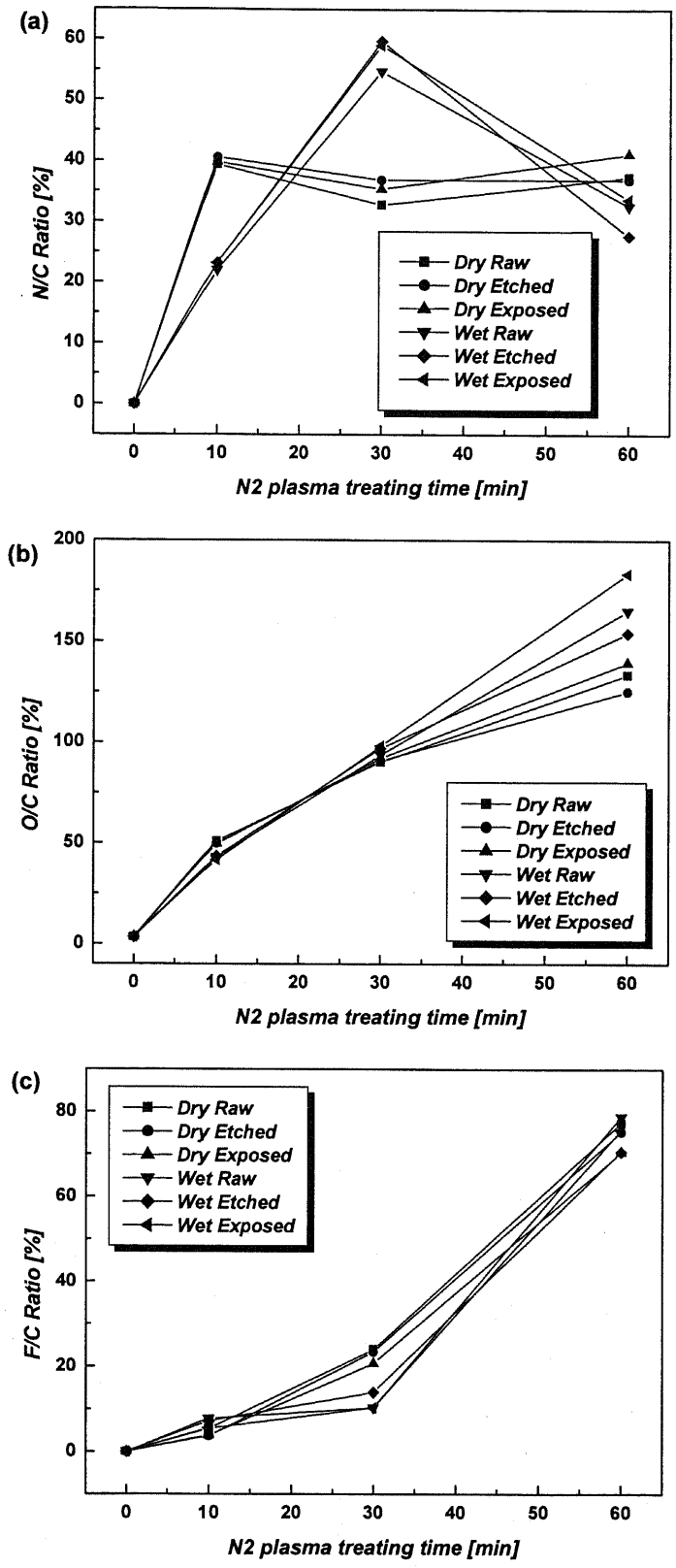

Fig. 4.8 Surface composition changes by the N_2 plasma process in terms of (a) the O1s/C1s ratio, (b) the O1s/C1s ratio and (c) the F1s/C1s ratio.

4.4.3 H_2 plasma process

The H_2 plasma process was executed with the same conditions of the Ar plasma process. Fig. 4.9 shows the XPS wide scan spectra of the original CNT film and the H_2 plasma processed CNT films for 10, 30, and 60 mins.

In the case of the original CNT film there is very small oxygen peak, but in the case of the H_2 plasma processed CNT films, oxygen, fluorine, chrome and iron peaks were observed. This result is similar to that of Ar and N_2 plasma processed CNT films.

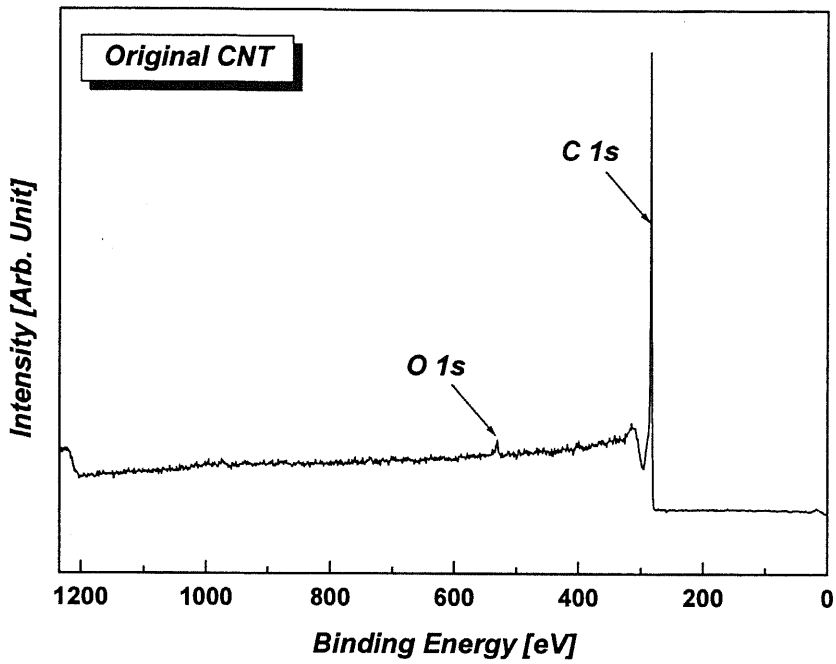

(a) Original CNT film

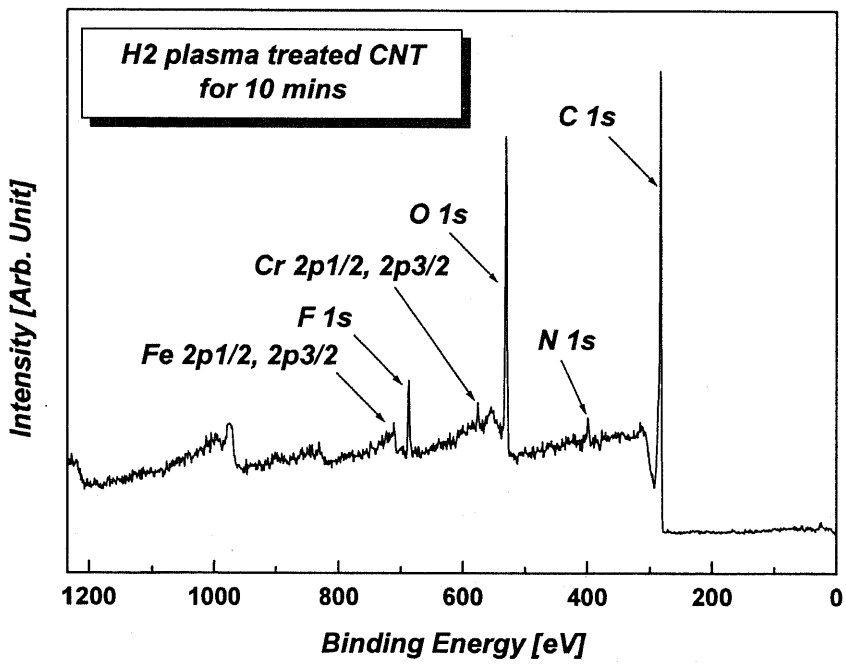

(b) H_2 plasma processed CNT film for 10 mins

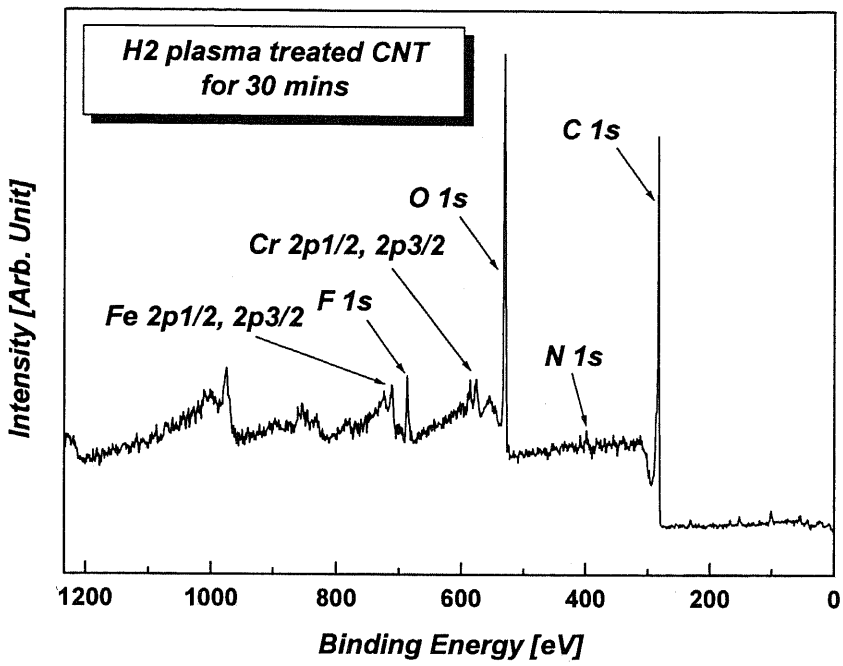

(c) H_2 plasma processed CNT film for 30 mins

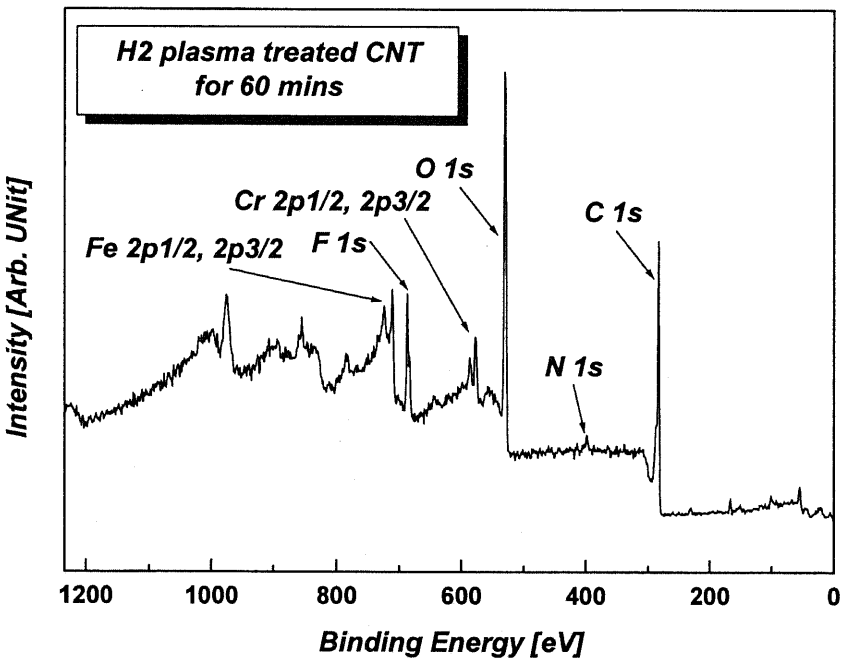

(d) H_2 plasma processed CNT film for 60 mins

Fig. 4.9 XPS wide scan spectra of (a) the original CNT film and the H_2 plasma processed CNT films for (b) 10, (c) 30, and (d) 60 mins.

The XPS narrow scan spectra of the original-CNT film and the H_2 plasma processed CNT films were shown in Fig. 4.10. Every peak was curve fitted and divided into sp^2, sp^3, and carbon shift. In the case of original-CNT, no carbon shift was observed. In the case of the H_2 plasma processed CNTs however, the oxygen related carbon shift was observed. This oxygen related carbon shift to higher binding energy implies the increment of amount of the oxygen. The binding energy gap in the XPS narrow scan spectra of the H_2 plasma processed CNT films were shown in Fig. 4.11.

The oxygen related carbon shift moves toward the higher binding energy with increasing H_2 plasma processing time. Thus, the gap between the carbon shift and the sp^2 peak increased with increasing plasma processing time. This means that the bonding strength between carbon and oxygen became stronger with increasing H_2 plasma processing time.

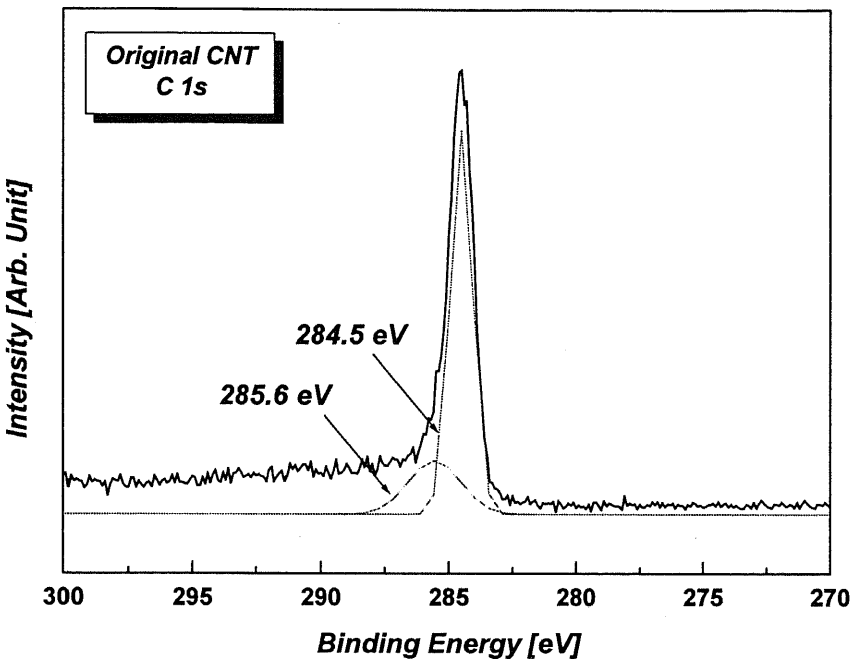

(a) Original CNT film

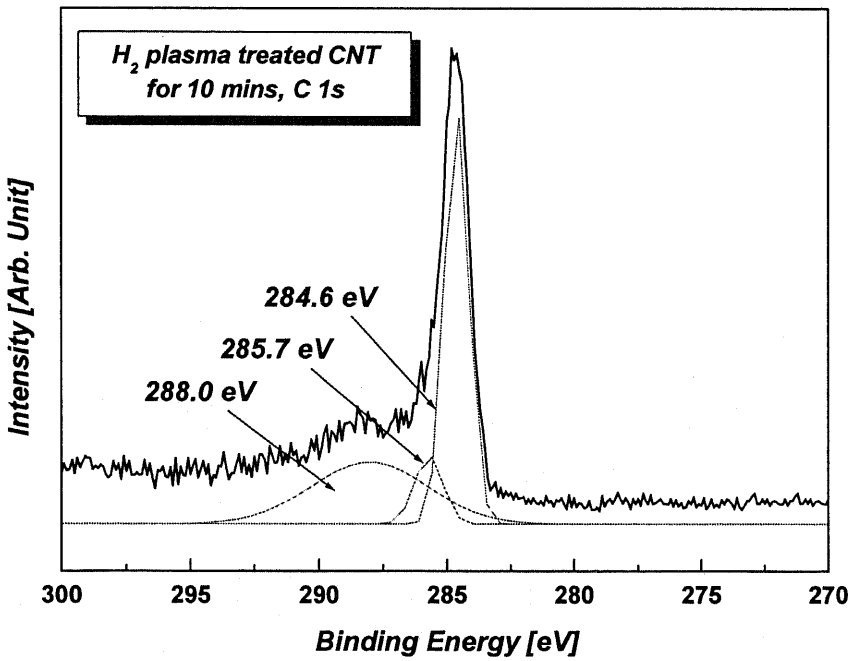

(b) H_2 plasma processed CNT film for 10 mins

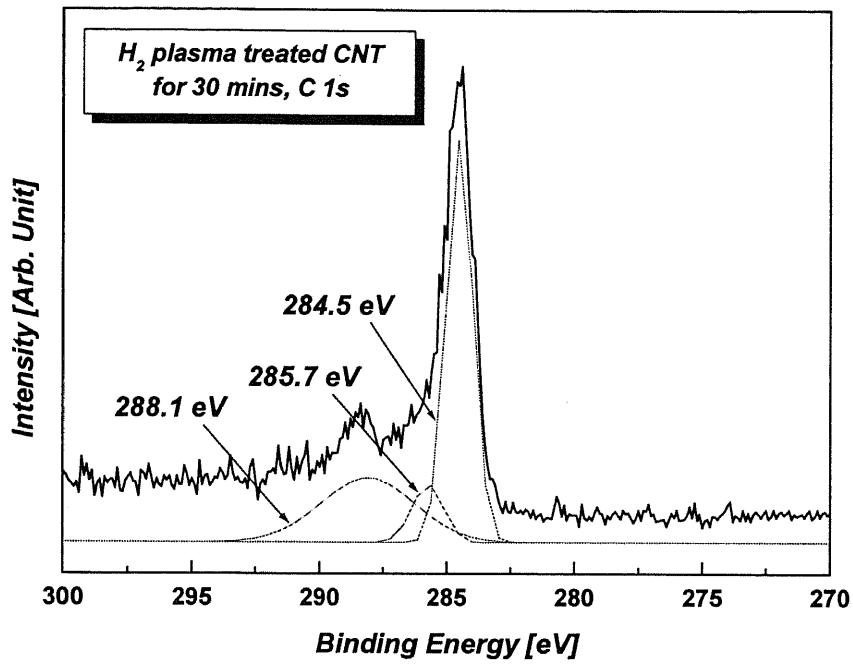

(c) H_2 plasma processed CNT film for 30 mins

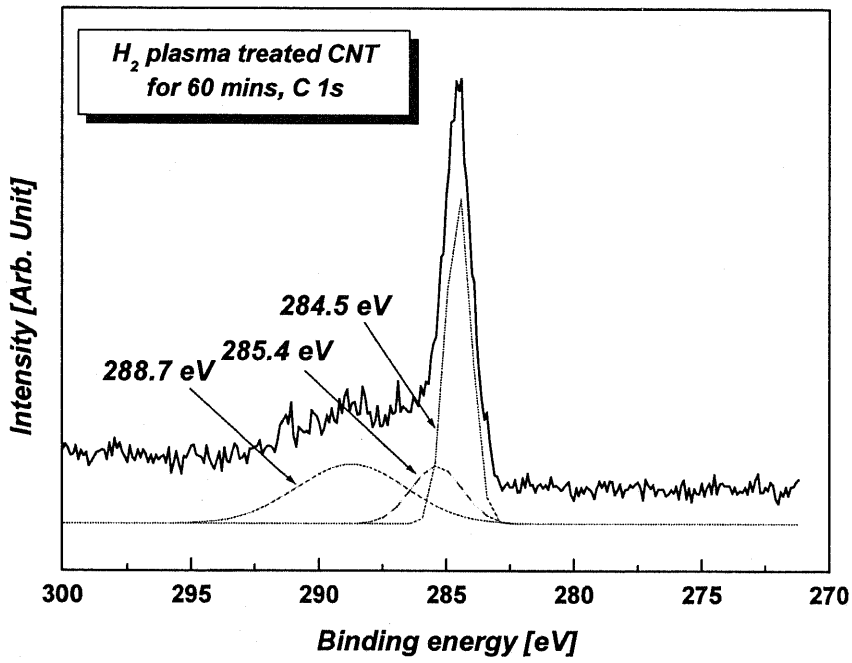

(d) H_2 plasma processed CNT film for 60 mins

Fig. 4.10 XPS narrow scan spectra of the original CNT film and the H_2 plasma processed CNT films.

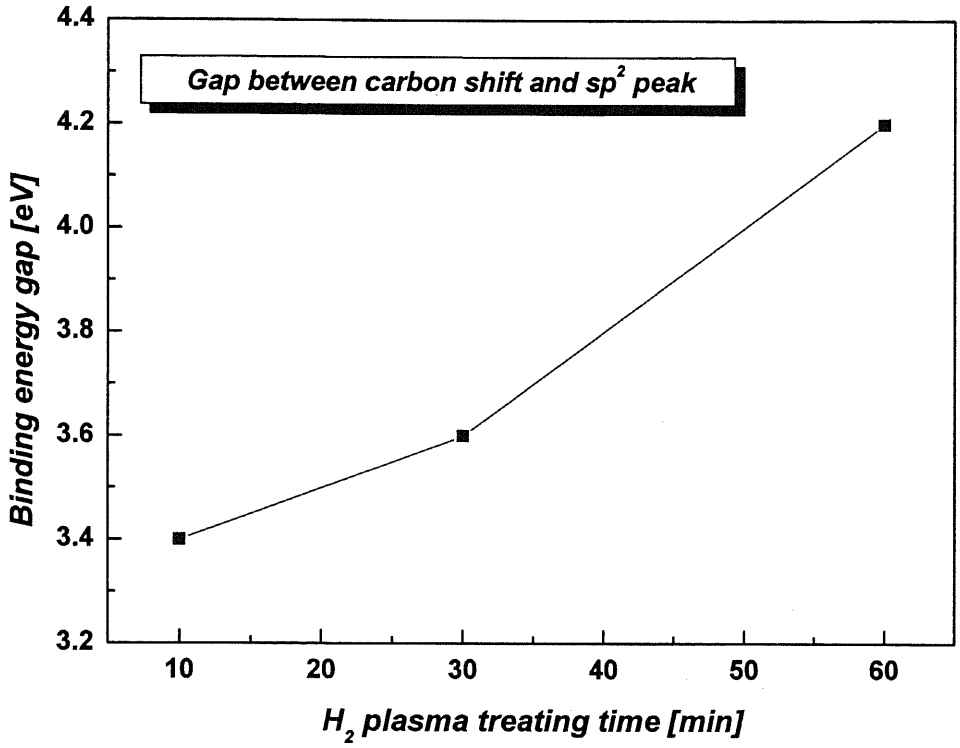

Fig. 4.11 Binding energy gap in the XPS narrow scan spectra of the H_2 plasma processed CNT films.

In H_2 plasma process, in order to evaluate the plasma processing time effect on the surface composition, the O1s/C1s ratio and the F1s/C1s ratio in the CNT films were obtained from the above XPS wide scan spectra. These results were shown in Fig. 4.12. These results imply that the H_2 plasma process could change the surface composition effectively. The O1s/C1s ratio increased from 0 % to 139 % for the H_2 plasma processed CNT films for 0 mins to 60 mins, respectively.

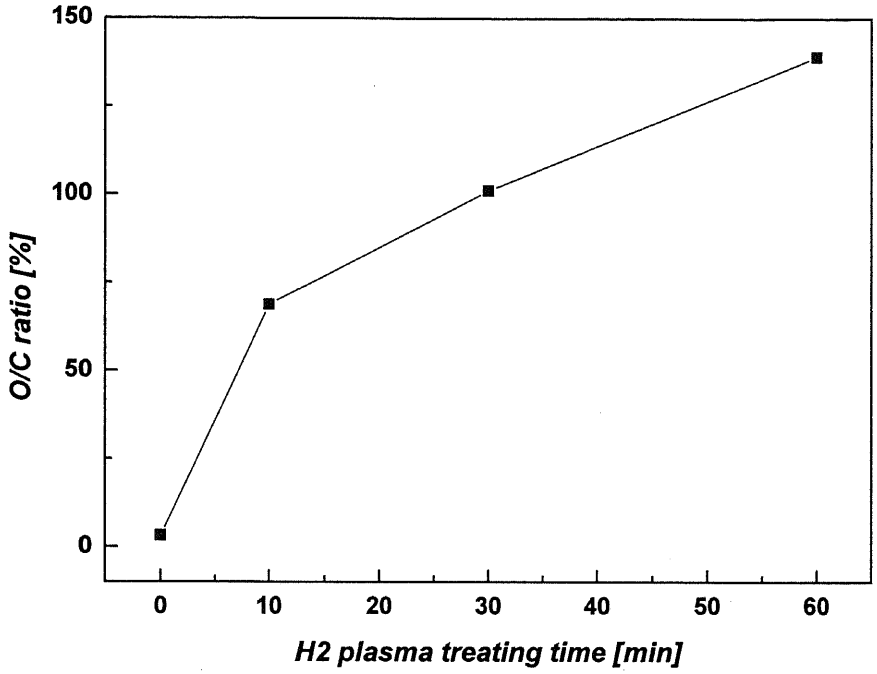

(a) The O1s/C1s ratio change

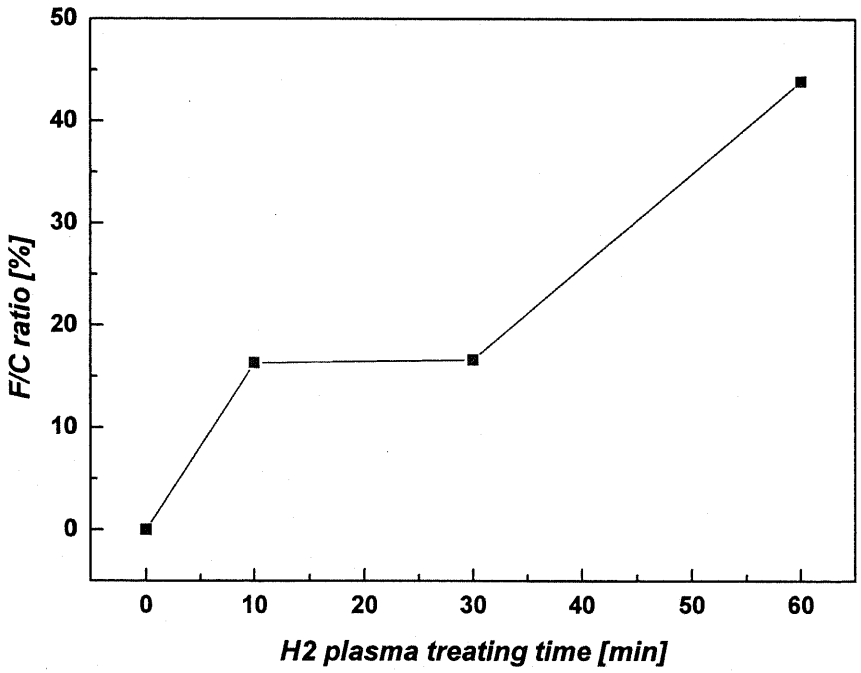

(b) The F1s/C1s ratio change

Fig. 4.12 Surface composition changes by the H_2 plasma process in terms of the O1s/C1s ratio and the F1s/C1s ratio.

4.5 Conclusions

Ar, N_2, and H_2 plasma processes were conducted as a surface treatment, the change of the surface state on the plasma processed CNT film was investigated by using XPS analysis. For the plasma processed CNT films, very strong oxygen peaks were observed. From the additional experiment, the origin of this strong oxygen peak was thought to be come from the water vapor attached at the chamber surface of the plasma process setup.

4.5.1 Ar plasma process In the case of the original CNT film, there was very small oxygen peak, but in the case of the Ar plasma processed CNT films, the strong oxygen peak was observed. In order to evaluate the plasma time effect on the surface composition, the O1s/C1s ratio and the F1s/C1s ratio were obtained from the XPS wide scan spectra. The O1s/C1s ratio and the F1s/C1s ratio were increased from 2.64 % to 59.16 % and from 0 % to 10.44 % with increasing plasma processing time, respectively. These results imply that the Ar plasma process could change the surface composition effectively. From the result of the C 1s narrow scan spectra, every peak was curve fitted and divided into sp^2, sp^3, and carbon shift. In the case of original-CNT film, no carbon shift was observed. In the case of the Ar plasma processed CNT films however, the oxygen related carbon shift was observed. This oxygen related carbon shift at higher binding energy implies increment of amount of the oxygen.

4.5.2 N_2 plasma process The N_2 plasma process was done to verify the origin of the oxygen peak using ion etching in the XPS inspection chamber. The water vapors in the air don't play an important role in the adhesion of the oxygen to the CNT surface during the plasma process. Therefore we can conclude that the origin of the oxygen peak in the XPS spectra is from the water vapor attached to the chamber wall.

4.5.3 H_2 plasma process In the case of the original CNT film, there was very small oxygen peak, but in the case of the H_2 plasma processed CNT films, a very strong oxygen peak was observed. This result is similar to that of Ar and N_2 plasma processed CNT films. The oxygen related carbon shift moves toward the higher binding energy with increasing H_2 plasma processing time. Thus, the gap between the carbon shift and the sp^2 peak increased with increasing plasma processing time. This means that the bonding strength between carbon and oxygen became stronger with increasing H_2 plasma processing time.

4.6 References

[1] P.M. Ajayan, Chem. Rev. 99 (1999) 1787-1799

[2] D.E. Hill, Y. Lin, A.M. Rao, L.F. Allard, and Y.P. Sun, Macromolecules 35 (2002) 9466-9471

[3] S. Lee and T. Oda, J. Phys. D : Appl. Phys. (Under submission)

[4] Y. Saito and S. Uemura, Carbon 38 (2000)

[5] S.C. Kung and K.C. Hwang, Appl. Phys. Lett. 80, 25 (2002) 4819-4821

5. Field emission properties

5.1 Introduction

Nanotubes were produced and studied before Iijima identified them in 1991, and this applies probably also to field emission studies. In that respect, it is interesting to note that Chernotazonskii et al. reported field emission from "tubulene" films [1], i.e., from very dense MWNT films deposited on Si substrates [2] in 1995. The tube caps protruded only a few nm above the surface [3] and consequently the voltages needed to extract the current were very high [4]. De Heer et al. observed electron emission from a continuous film of randomly oriented arc discharge MWNT, with macroscopic current densities as high as 100 mA/cm^2 [5].

Most reports on the field emission describe the fabrication method of the film emitter and present a typical *I-V* curve. A short overview of results is given in Table 1 for each nanotube type, in chronological order.

Table 1 shows that field emission is excellent for nearly all types of naontubes. The threshold fields are as low as 1 V/μm and turn-on fields around 5 V/μm are typical. Nanotube films are capable of emitting current densities up to a few A/cm^2 at fields below 10 V/μm.

One interesting parameter is the actual emitter density on the films. Typically, a film has a nanotube density of 10^8 -10^9 cm^{-2} [6].

5.2 Field emission from carbon nanotubes

5.2.1 Field emission from carbon nanotubes

Let us first recall that field emission involves the extraction of electrons from a solid by tunneling through the surface potential barrier (for reviews on field emission see Refs. [7-11]). The emitted current depends directly on the local electric field at the emitting surface, E, and on its work function, ϕ, as shown in Fig. 5.1. In fact, a simple model (the Fowler-Nordheim model) shows that the dependence of the emitted current on the local electric field and the work function is exponential-like. As a consequence, a small variation of the shape or surrounding of the emitter (geometric field enhancement) and/or the chemical state of the surface has a strong impact on the emitted current.

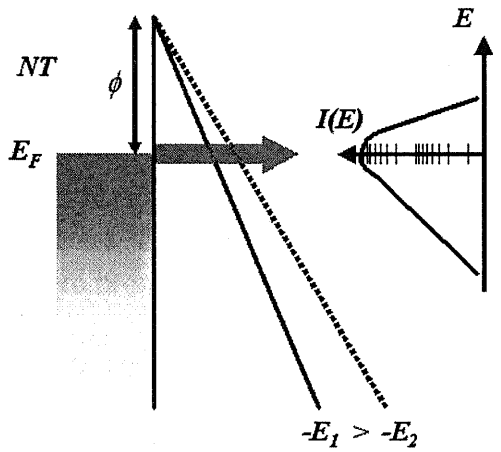

Fig. 5.1 Standard field emission model from a metallic emitter, showing the potential barrier and the corresponding FEED (energy on the vertical axis, current on the horizontal logarithmic axis)

These facts make a thorough comparison of results delicate, particularly because the methods used for synthesis (SWNTs, MWNTs), purification (closed or open ends, presence of contaminating material), and film deposition (alignment, spacing between the tubes) are quite varied. The interpretation is further complicated by the different experimental setups, e.g., the use of planar, spherical or sharp tip anodes, and different interlectrode distances. Finally, the film surfaces used for emission are in some cases quite small (below 100 μm). With such dimensions, one nanotube emitting 10 μA is sufficient to yield an apparent current density of 0.1 A/cm^2. Sufficiently large

emission surfaces (>1 mm^2) have to be considered to ensure that the measurement is representative. I will therefore distinguish between integrated (or macroscopic) and microscopic emission to explain the large variation of observed current densities from micron-to millimeter-sized areas.

5.2.2 Field emission mechanism

Why are nanotubes such exceptional field emitters? The very low turn-on fields measured for nearly all emitters originate certainly from the small diameter and elongated shape of the tubes that lead to a high geometrical field enhancement. In fact, the local electric field just above the emitter surface needed for field emission is around 2-3 V/nm as for metallic emitters, as can be estimated from the applied field and the field amplification factor [12-14]. On the other hand, nanotubes do not behave like very sharp metallic tips. Furthermore, the influence of the structural properties of the tube on the field emission is not clearly assessed at present. This issue is complicated by the fact that the physical and chemical properties are deeply modified by preparation and purification steps [15-18]. Despite these difficulties we will summarize here the principal models that have been proposed for the field emission from carbon nanotubes.

Some authors recorded *I-V* characteristics that follow the Fowler- Nordheim law (at least over a certain current range), from which they concluded that carbon nanotubes behave as metallic emitters [19-21].

Rinzler et al. interpreted the higher efficiency of open MWNTs and their behavior under laser irradiation as emission from a single carbon chain that unravels from the tube edge and produces very high field amplification [15]. This model could not be confirmed yet experimentally, and would probably be valid only for open tubes.

Obraztsov et al. proposed that the graphene layers form sharp bends at the open end of the nanotube, where the carbon atoms show sp^3 like atomic bonds instead of the sp^2 configuration typical for graphene [22-24]. This change in coordination would decrease the height of the potential barrier and could explain the very low work function that the authors estimated from the slope of Fowler-Nordheim plots. Again, this model would be valid only for open MWNT.

We concluded from our observations that the electrons are emitted from sharp energy levels due to localized states at the tube cap as shown in Fig. 10(b) [25]. Luminescence

induced by the electron emission could arise from radiative transitions between two levels participating to the field emission [26]. Actually, theoretical calculations predict the presence of localized states at the tube cap, with a DOS that differs markedly to that of the tube body [26-28]. This was recently confirmed experimentally by STM measurements on MWNTs [29] as well as on SWNTs [15]. The FWHM of these states and their separation is in good agreement with the values measured for the light emission and with FEED observations carried out at 20 °C [37] and at 600 °C [31].

Two points have to be mentioned concerning this hypothesis. If several energy levels participate in the emission, the occupied level nearest to the Fermi energy will supply nearly all the emitted electrons. Since the position of this level would depend strongly on the local atomic configuration (tube diameter, chirality, presence of pentagons and other defects), significant differences of the emitted currents can be expected from one tube to another. Second, these localized states often show far higher carrier densities as compared to the tube body at the Fermi level [28]. As the field emission current depends directly on this carrier density, we speculate that the emitted current would be far lower for a nanotube without such states.

A complete study by Dean et al. suggests complementary mechanisms, and shows clearly that emission behavior of nanotubes is far more complex than the one expected from a very sharp metallic tip with a work function of ~5 eV [37,32]. Different emission regimes on single SWNTs were identified and depended on applied field and temperature. A first regime corresponding to resonant tunneling through an adsorbate (Fig. 2.5.6(b)) was found under "usual" experimental conditions at low temperatures and applied fields. The involved molecule has been identified as water and it appears that this adsorbate-assisted tunneling is the stable field emission mode at room temperature. These molecules desorb either at high fields and emitted currents or at temperatures higher than 400 °C. The other regimes correspond to the intrinsic emission from the cleaned tube and show a far lower emitted current for comparable voltages with strongly reduced current fluctuations. The origin of these (at least two) intrinsic regimes is not clear yet but the emission mechanism involves probably non-metallic electronic states, such as enhanced field emission states above the Fermi level or a non-metallic DOS.

In short, the present understanding is that the emission involves a non-metallic DOS

and/or adsorbate-resonant tunneling. Supplementary informations on the influence of absorbates or bonded groups are required for a better comprehension of the emission. It seems us important to mention again the work of Lovall et al. [33]. They show the way for a complete characterization of nanotubes, where the electronic DOS is measured by FEED and the exact structure of the tube, cap is determined by FIM. This simultaneous determination of the electronic and structural properties of individual nanotubes would without doubt yield valuable insights on the emission mechanism.

5.2.3 Field emission applications

Despite the demonstration that a single MWNT emits monochromatic electrons over long periods of time at low applied fields, we know of only one instance where a single nanotube has been used in a high-resolution electron beam instrument. Fink et al. developed a low energy electron projection microscope where the electrons are extracted by applying a voltage between the sample and a MWNT emitter [34]. The nanotube provided a highly coherent beam that allowed the acquisition of in-line electron holograms of the observed objects with a quality comparable to atom-sized W emitters [35].

It is not proven yet that single nanotubes can be used in other instruments such as scanning or transmission electron microscopes [36]. Nanotube emitters show higher coherence and narrower FEED than cold or Schottky cathodes used in such instruments and might provide an interesting alternative [37].

In contrast to single nanotube devices, applications based on an assembly of nanotubes are divers. Nanotube flat-panel displays were proposed early on as an enticing alternative to other film emitters [1,38]. It took only three years until the first display with 32 × 32 matrix-addressable pixels in diode configuration was realized by Wang et al. [39].

Choi et al. recently demonstrated a fully sealed 4.5 in. three color field-emission display [40,41]. The display, reproduced in Fig. 5.2 has 128 addressable lines and works in diode configuration. Since then, the Samsung research group has shown a 4.5 in. device displaying full-color images [42] and later a 9 in. full-color display with 576 × 242 pixels [43].

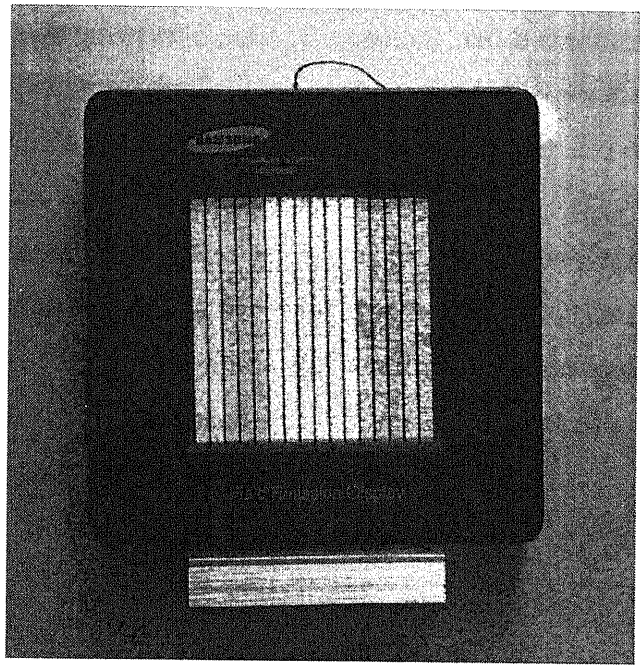

Fig. 5.2 The Samsung 4.5 in. full-color nanotube display (The photograph is courtesy of Dr. Choi, Display Laboratory, Samsung Advanced Institute of Technology)

There are numerous technological hurdles related to the deposition of nanotubes in gated structures. Problems such as display sealing, phosphor lifetime, and charging of spacers are further concerns. Other, simpler devices than flat-panel displays have been demonstrated up to now and there are probably many more under investigation.

One possibility is to use nanotubes in lighting elements, i.e., to produce light by bombarding a phosphor-coated surface with electrons. Such a cathode-ray tube (also called "jumbotron lamp") has been developed by Saito et al. and is reportedly commercially available [44]. The brightness is typically higher by a factor of 2 as compared to conventional thermoionic lighting elements and can be used for giant outdoor displays [45]. Lifetimes of 8000 h have been demonstrated with such devices [46,17].

Field emitters are also of great interest for microwave amplification [47]. This type of application is very demanding because the current density must be at least 0.1 A/cm^2. Zhou et al. constructed a prototype based on a SWNT cathode that is able to reach that lower limit to operate in microwave tubes [48,49].

The same group realized a gas discharge tube that serves as an overvoltage protection

[50]. When the voltage between a nanotube cathode and a counter-electrode reaches a threshold value for field emission, the emitted current induces a discharge in the noble gas-filled inter-electrode gap. It could be demonstrated that this device shows better performance than commercially available elements.

All these achievements underline the potential of carbon nanotube emitters in applications. Nevertheless, the lack of information on some aspects of device realization like device lifetime, fabrication yield and cost show the demand for more studies. Finally, nearly all devices mentioned work in diode configuration. One of the future challenges is hence the fabrication of gated nanotube devices.

5.3 Effect of chemical treatments

When the electric field F between the CNT and a counter electrode is zero, only electrons excited thermally or by some radiation can reach the vacuum level and be emitted from the CNT. However when electric field is applied, the shape of the potential barrier changes as shown in Fig. 5.3. That potential barrier decrease is expressed by $\Delta\phi$. If the external field strength increases, the the potential barrier width decreases so that and electrons can pass through that barrier by the tunnel effect [51].

The chemical treatment generates new trapping states E_{Trap} by the induced functional groups. The deeper trapping sites trap the electrons which were located in the top of the valence band. So that, the amount of electrons in valence band decreases [52,53]. As a result, the tunneling of electrons through the potential barrier takes place at the deeper sites. This leads to decrease the field emission performance.

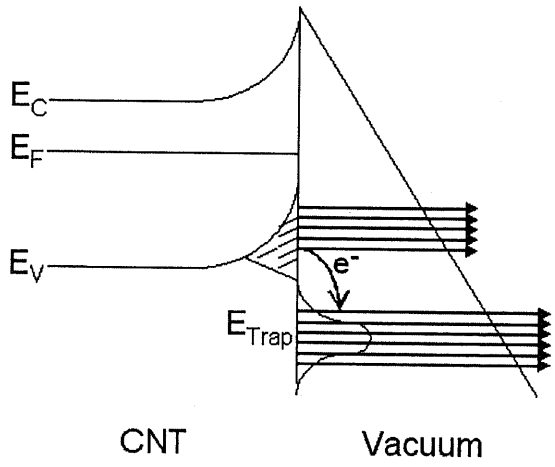

Fig. 5.3 Band diagrams of the chemically treated CNT film

The CNT films treated in liquid phase such as HNO_3-CNT film and HF-CNT film may have carboxyl groups (–COOH). On the other hand, the CNT film treated in gas phase such as O_2-CNT film may have hydroxyl groups (–OH). Since the carboxyl group has more oxygen atoms than the hydroxyl group, it is predicted that the CNT film treated in liquid phase has deeper trap (large electron affinity) than that treated in gas phase. As a result, the CNT film treated in liquid phase degraded the field emission performance. That fact is in good agreement with the result of the field emission measurement.

The field emission properties of original CNT film and chemically treated CNT films

are shown in Fig. 5.4. All of the chemically treated CNT films show the better field emission property than the original CNT film. Although the field emission from O_2-CNT film occurs at the lower electric field, field emission from HNO_3-CNT film and HF-CNT film occurs at the higher electric field. To make clear those phenomena, a threshold of the electric field was defined at a current density of 10 $\mu A/cm^2$.

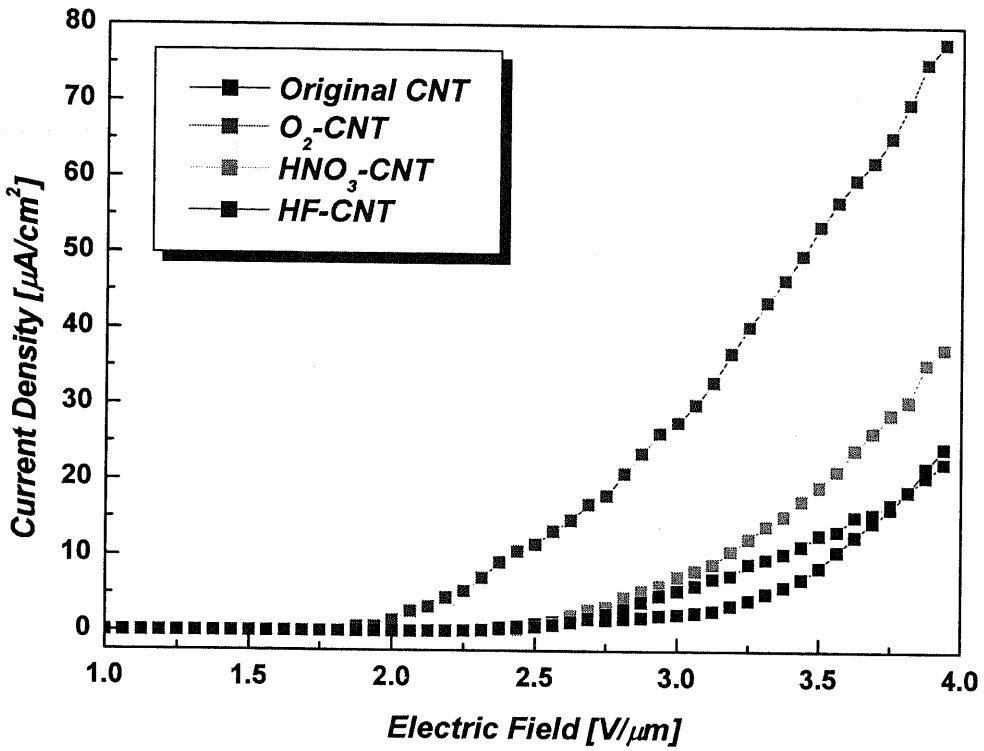

Fig. 5.4 Plot of field emission current vs. electric field for the original CNT and the chemically treated CNT

The threshold of the electric field of the original CNT film, O_2-CNT film, HNO_3-CNT film, and HF-CNT film are 3.55, 2.41, 3.17, and 3.34 V/μm, respectively. As mentioned earlier, the chemical treatment on the CNT films increase the dangling bonds, which play as the electron emission sites, consequently the field emission performance improved. These results can be explained by using the XPS data. Y. Saito et al. reported that the field emission occurs at the pentagon site (need to form a curvature at the CNT cap) or the dangling bond of the CNT cap [54]. The chemical treatment can break the bonds between carbon and carbon, so as to create new bonds between carbon and other

functional groups (or other elements). As the field emission occurs at pentagons or dangling bonds of the cap, increment of the dangling bonds means the improvement of the field emission performance. And it was thought that the difference of the field emission performance between the CNT film treated in liquid phase and the CNT films treated in gas phase was due to the attached functional groups. The CNT films treated in liquid phase such as HNO_3-CNT film and HF-CNT film may have carboxyl groups (–COOH). On the other hand, the CNT film treated in gas phase such as O_2-CNT film may have hydroxyl groups (–OH). Since the carboxyl group has more oxygen atoms than the hydroxyl group, it is predicted that the CNT film treated in liquid phase has deeper trap (large electron affinity) than that treated in gas phase. As a result, the CNT film treated in liquid phase degraded the field emission performance.

5.4 Effect of plasma processes

5.4.1 Ar plasma process

The field emission properties of the original CNT film and the Ar plasma processed CNT films were shown in Fig. 5.5. The field emission performance increased with increasing the Ar plasma processing time. In the case of the Ar plasma processed CNT films for 10 mins and 30 mins, slight performance improvements were observed. On the other hand in the case of the Ar plasma processed CNT film for 60 mins, outstanding improvement of field emission performance was observed. These results can be explained by using the XPS data. Y. Saito et al. reported that the field emission occurs at the pentagon site (need to form a curvature at the CNT cap) or the dangling bond of the CNT cap. Ar plasma process can break the bonds between carbon and carbon, so as to create new bonds between carbon and oxygen. The amount of oxygen and the bonding strength between carbon and oxygen increased with increasing the plasma processing time. As the field emission occurs at pentagons or dangling bonds of the cap, increment of the bonds between carbon and oxygen means the improvement of the field emission performance.

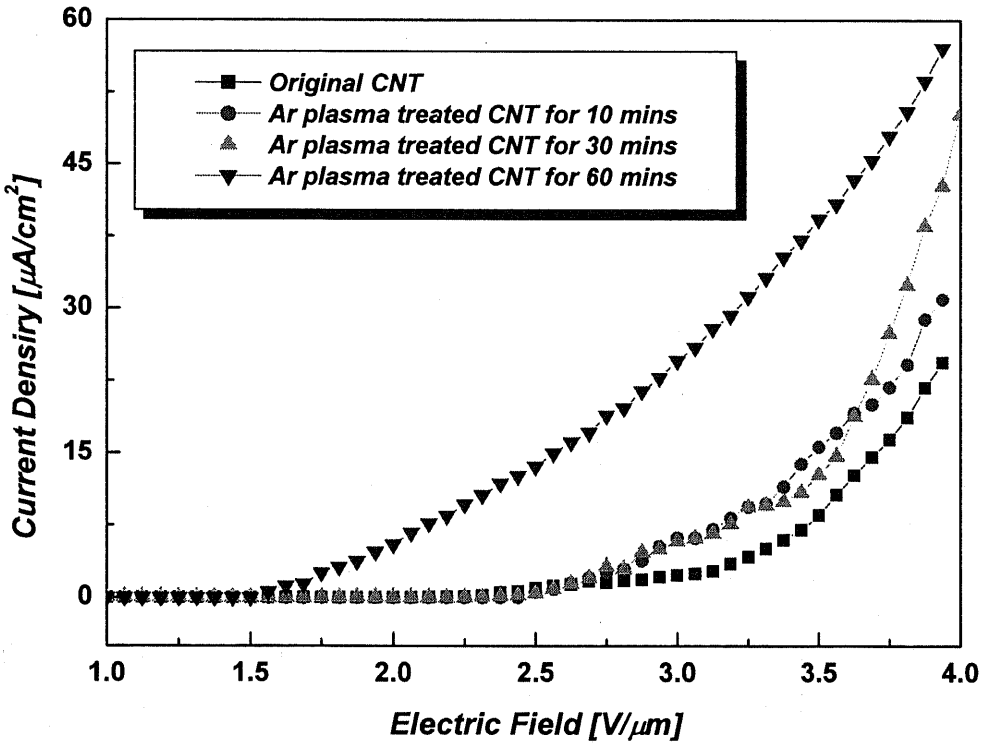

Fig. 5.5 Plot of field emission current vs. electric field for the original CNT film and the Ar plasma processed CNT films.

5.4.2 N_2 plasma process

The field emission properties of the original CNT film and the N_2 plasma processed CNT films were shown in Fig. 5.6. The field emission performance increased with increasing the N_2 plasma processing time steadily. These improvement of the field emission performances on the N_2 plasma processed CNT films could be also explained by the increment of the dangling bonds, which the same as the case of the Ar plasma processed CNT films. From the result of Fig. 4.8 (b), the O/C ratio increased from 0 % to over 100 % for the N_2 plasma processed CNT films for 0 mins to 60 mins, respectively.

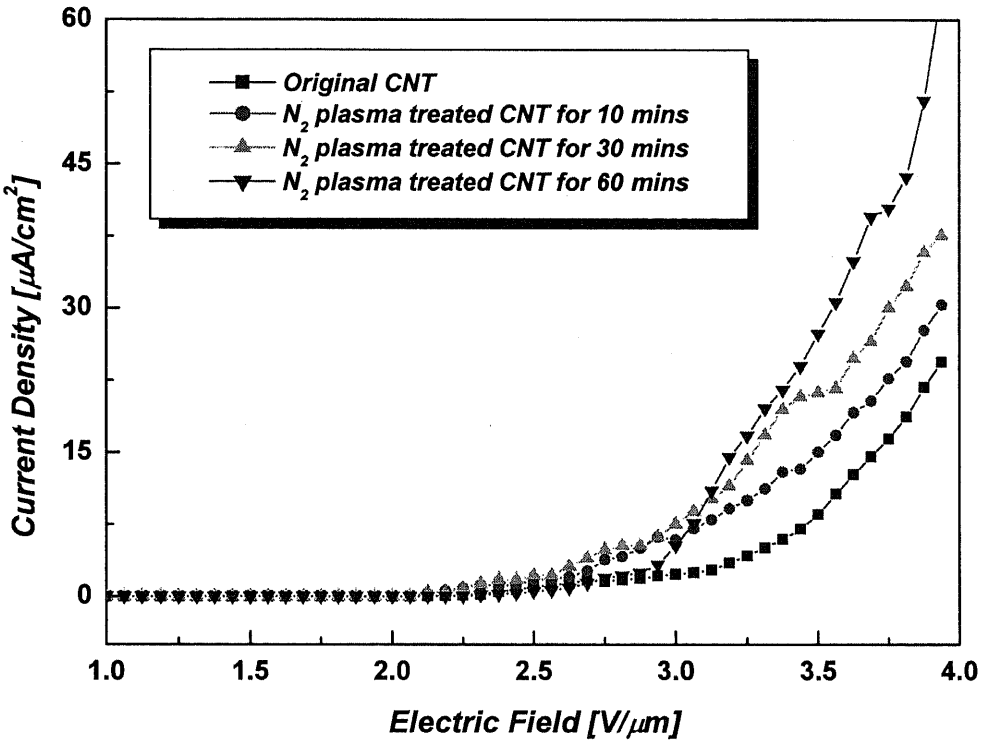

Fig. 5.6 Plot of field emission current vs. electric field for the original CNT film and the N_2 plasma processed CNT films.

5.4.3 H_2 plasma process

The field emission properties of the original CNT film and the H_2 plasma processed CNT films were shown in Fig. 5.7. The field emission performance increased with increasing the H_2 plasma processing time. These improvement of the field emission performances on the N_2 plasma processed CNT films could be also explained by the increment of the dangling bonds, which the same as the case of the Ar plasma processed

CNT films. From the result of Fig. 4.12 (a), the (O 1s)/(C 1s) ratio increased from 0 % to 139 % for the H_2 plasma processed CNT films for 0 mins to 60 mins, respectively.

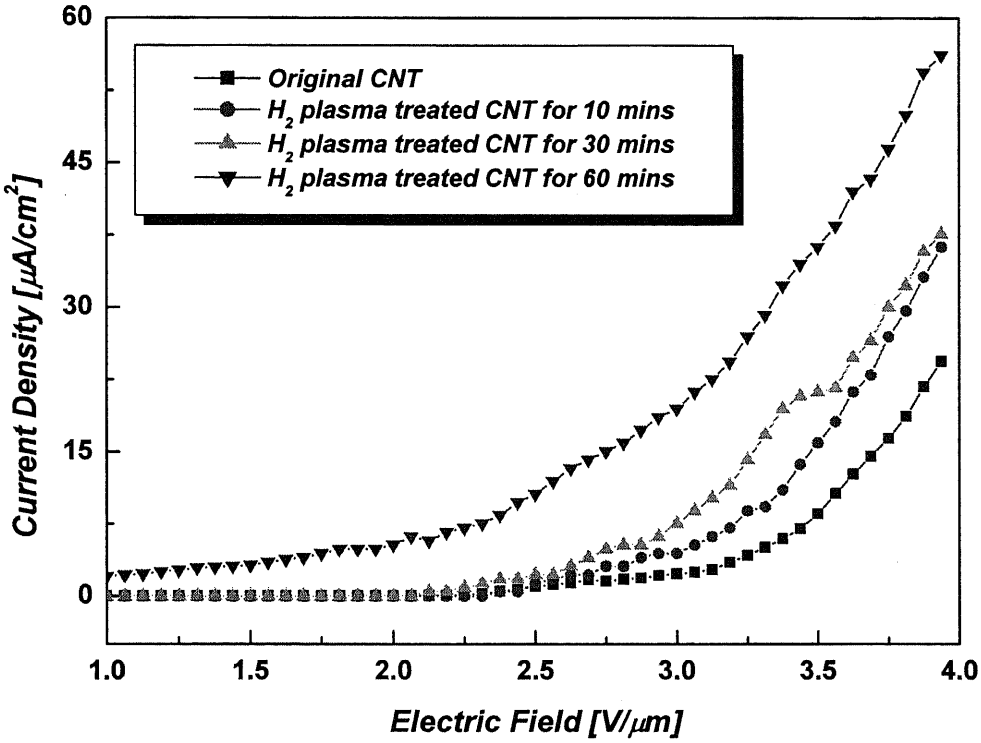

Fig. 5.7 Plot of field emission current vs. electric field for the original CNT film and the H_2 plasma processed CNT films.

5.5 Conclusions

5.5.1 Chemical treatments

In order to verify the effect of the chemical treatment on the field emission property, the field emission current was measured. All of the chemically treated CNT films show the better field emission property than the original CNT film. Although the field emission from O_2-CNT film occurs at the lower electric field, field emission from HNO_3-CNT film and HF-CNT film occurs at the higher electric field. The threshold of the electric field of the original CNT film, O_2-CNT film, HNO_3-CNT film, and HF-CNT film are 3.55, 2.41, 3.17, and 3.34 V/μm, respectively. As the field emission occurs at pentagons or dangling bonds of the cap, increment of the dangling bonds means the improvement of the field emission performance. And it was thought that the difference of the field emission performance between the CNT film treated in liquid phase and the CNT films treated in gas phase was due to the attached functional groups. The CNT films treated in liquid phase such as HNO_3-CNT film and HF-CNT film may have carboxyl groups (–COOH). On the other hand, the CNT film treated in gas phase such as O_2-CNT film may have hydroxyl groups (–OH). Since the carboxyl group has more oxygen atoms than the hydroxyl group, it is predicted that the CNT film treated in liquid phase has deeper trap than that treated in gas phase. As a result, the CNT film treated in liquid phase degraded the field emission performance.

5.5.2 Plasma processes

5.5.2.1 Ar plasma process The field emission performance increased with increasing the Ar plasma processing time. Ar plasma process can break the bonds between carbon and carbon, so as to create new bonds between carbon and oxygen. The amount of oxygen and the bonding strength between carbon and oxygen increased with increasing the plasma processing time. As the field emission occurs at pentagons or dangling bonds of the cap, increment of the number of bonds between carbon and oxygen means the improvement of the field emission performance.

5.5.2.2 N_2 plasma process The field emission performance increased with increasing the N_2 plasma processing time steadily. These improvement of the field emission performances on the N_2 plasma processed CNT films could be also explained by the increment of the dangling bonds, which the same as the case of the Ar plasma processed

CNT films.

5.5.2.3 H_2 plasma process The field emission performance increased with increasing the H_2 plasma processing time. These improvement of the field emission performances on the N_2 plasma processed CNT films could be also explained by the increment of the dangling bonds, which the same as the case of the Ar plasma processed CNT films.

5.6 References

[1] Chernozatonskii L.A., Gulyaev Y.V., Sinitsyn N.I., Torgashov V., Zakharchenko Y.F., Fedorov E.A., Val'chuk V.P., Chem. Phys. Lett., 1995, 233, :63.

[2] Chernozatonskii L.A., Kosakovskaja Z.J., Kiselev A.N., Kiselev N.A., Chem. Phys. Lett., 1994, 228, 1.

[3] Chernozatonskii L.A., Gulyaev Y.V., Kosakovskaya Z., Sintisyn N.I., Torgashov G.V., Fedorov E.A., Zakharchenko Y.F., Val'chuk V.P., Mater. Res. Soc. Symp. Proc., 1995, 359, 99.

[4] Chernozatonskii L.A., Kosakovskaya Z., Gulyaev Y.V., Sinitsyn N.I., Torgashov G.V., Zakharchenko Y.F., J. Vac. Sci. Technol. B, 1996, 14, 2080.

[5] De Heer W.A., Chatelain A., Ugarte D., Science, 1995, 270, 1179.

[6] Obraztsov A.N., Pavlovsky I., Volkov A.P., Obraztsova E.D., Chuvilin A.L., Kuznetsov V.L., J. Vac. Sci. Technol. B, 2000, 18, 1059.

[7] Good R.H., Muller E.W., Handbuch der Physik, 1956, 21, 176.

[8] Dyke W.P., Dolan W.W., Adv. Electron EI Phys., 1956, 8, 89.

[9] Gadzuk J.W., Plummer E.W., Rev. Mod. Phys., 1973, 45, 487.

[10] Modinos A., Field, themoionic, and secondary electron spectroscopy, New York: Plenum Publishing Corporation, 1984.

[11] Gomer R. Surf. Sci., 1994, 299/300, 129.

[12] Kuttel O.M., Groning O., Emmenegger C., Schlapbach L., Appl. Phys. Lett., 1998, 73, 2113.

[13] Bonard J-M., Maier F., Stockli T., Chatelain A., De Heer W.A., Salvetat J-P., Forro L., Ultramicroscopy, 1998, 73, 9.

[14] Bonard J-M., Weiss N., Kind H., Stockli T., Forro L., Kern K., Chatelain A., Adv. Mater., in press.

[15] Rinzler A.G., Hafiner J.H., Nikolaev P., Lou L., Kim S.G., Tomanek D., Nordlander P., Colbert D.T., Smalley R.E., Science, 1995, 269, 1550.

[16] de Pablo P.J., Howell S., Crittenden S., Walsh B., Graugnard E., Reifenberger R., Appl. Phys. Lett., 1999, 75, 3941.

[17] Saito Y., Uemura S., Carbon, 2000, 38, 169.

[18] Rinzler A.G., Hafner J.K., Colbert D.T., Smalley R.E., Mat. Res. Soc. Symp. Proc., 1995, 359, 61.

[19]Saito Y., Hamaguchi K., Hata K., Tohji K., Kasuya A., Nishina Y., Uchida K., Tasaka Y., Ikazaki F., Yumura M., Ultramicroscopy, 1998, 73, 1.

[20]Wang Q.H., Corrigan T.D., Dai J.Y., Chang R.P.H., Krauss A.R., Appl. Phys. Lett., 1997, 70, 3308.

[21]Kuttel O.M., Groning O., Emmenegger C., Nilsson L., Maillard E., Diederich L., Schlapbach L., Carbon, 1999, 37, 745.

[22]Obraztsova E.D., Bonard J-M., Kuznetsov V.L., Zaikovskii V.I., Pimenov S.M., Pozarov A.S., Terekhov S.V., Konov V.I., Obraztsov A.N., Volkov A.S., Nanostructured Mater., 1999, 12, 567.

[23]Obraztsov A.N., Volkov A.P., Pavlovskii I.Y., Chuvilin A.L., Rudina N.A., Kuznetsov V.L., JETP. Lett., 1999, 69, 411.

[24]Obraztsov A.N., Pavlovsky I., Volkov A.P., Obraztsova E.D., Chuvilin A.L., Kuznetsov V.L., J. Vac. Sci. Technol. B, 2000, 18, 1059.

[25]de Pablo P.J., Howell S., Crittenden S., Walsh B., Graugnard E., Reifenberger R., Appl. Phys. Lett., 1999, 75, 3941.

[26]Bonard J-M., Stockli T., Maier F., De Heer W.A., Chatelain A., Salvetat J-P., Forro L., Phys. Rev. Lett., 1998, 81, 1441.

[27]Tamura R., Tsukada M., Phys. Rev. B, 1995, 52, 6015.

[28]Carroll D.L., Redlich P., Ajayan P.M., Charlier J.C., Blase X., De A., Vita R., Phys. Rev. Lett., 1997, 78, 2811.

[29]De Vita A., Charlier J-C., Blase X., Car R., Appl. Phys. A, 1999, 68, 283.

[30]Cassell A.M., Franklin N.R., Tombler T.W., Chan E.M., Han J., Dai H., J. Am. Chem. Soc., 1999, 121, 7975.

[31]Dean K.A., Groning O., Kuttel O.M., Schlapbach L., Appl. Phys. Lett., 1999, 75, 2773.

[32]Dean K.A., von Allmen P., Chalamala B.R., J. Vac. Sci. Technol. B, 1999, 17, 1959.

[33]Lovall D., Buss M., Graugnard E., Andres R.P., Reifenberger R., Phys. Rev. B, 2000, 61, 5683.

[34]Fink H-W., Stocker W., Schmid H., Phys. Rev. Lett. 1990, 56, 1204.

[35]Schmid H., Fink H-W., Appl. Phys. Lett., 1997, 70, 2679.

[36]Fransen M.J., Towards high-brightness, monochromatic electron sources. Delft University of Technology, 1998.

[37]Fransen M.J., van Rooy T.L., Kruit P., Appl. Surf. Sci., 1999, 146, 312.

[38]De Heer W.A., Chatelain A., Ugarte D., Science, 1995, 270, 1179.

[39]Wang Q.H., Setlur A.A., Lauerhaas J.M., Dai J.Y., Seelig E.W., Chang R.P.H., Appl. Phys. Lett., 1998, 72, 2912.

[40]Choi W.B., Chung D.S., Kang J.H., Kim H.Y., Jin Y.W., Han I.T., Lee Y.H., Jung J.E., Lee N.S., Park G.S., Kim J.M., Appl. Phys. Lett., 1999, 75, 3129.

[41]Chung D.S., Choi W.B., Kang J.H., Kim H.Y., Han I.T., Park Y.S., Lee Y.H., Lee N.S., Jung J.E., Kim J.M., J. Vac. Sci. Technol., 2000, B18, 1054.

[42]Choi W.B., Chung D.S., Kang J.H., Kim H.Y., Jin Y.W., Han I.T., Lee Y.H., Jung J.E., Lee N.S., Park G.S., Kim J.M., EuroFE'99 meeting, Toledo, Spain, 15-19 November, 1999.

[43]Kim J.M., Lee N.S., Choi W.B., Jung J.E., Han I.T., Jung D.S., Park S.H., Hong S.S., Kim H.Y., 14th International Winterschool on Electronic Properties of Novel Mater. (IWEPNM 2000), Kirchberg, Austria, 4-11 March, 2000.

[44]Saito Y., Uemura S., Hamaguchi K., Jpn. J. Appl. Phys., 1998, 37, L346.

[45]Bonard J.M., Salvetat J.P., Stockli T, Forro L., Chatelain A., Appl. Phys. A, 1999, 69, 245.

[46]Murakami H., Hirakawa M., Yamakawa H., Appl. Phys. Lett., 2000, 76, 1776.

[47]Jensen K.L., Phys. Plasma, 1999, 6, 2241.

[48][78] Zhou O., 14th International Winterschool on Electronic Properties of Novel Mater. (IWEPNM 2000), Kirchberg, Austria, 4-11 March, 2000.

[49]Zhou O. et al. (UNC Chapel Hill), Zhu W. (Lucent Technologies), pending US patents.

[50]Rosen R., Simendinger W., Debbault C., Shimoda H., Fleming L., Stoner B., Zhou O., Appl. Phys. Lett., 2000, 76, 1663.

[51]P.W. Hawkes and E. Kasper, Theory of electron emission, in: Principles of electron optics: Applied Geometrical Optics, Vol. 2, Chap. 44, Academic Press (1989)

[52]J. Fain, S. Sanzelle, Th. Pilleyre, D. Miallier and M. Montret, Radiation Measurements 30 (1999) 487-495

[53]E. N. Agafonov, A. N. Georgobiani, and L. S. Lepnev, Semiconductors 36(6) (2002) 655–658

[54]Y. Saito and S. Uemura, Carbon 38 (2000)

6. Conclusions

In this work, the effect of surface treatment on the field emission property of carbon nanotube films prepared by the chemical vapor deposition method was investigated.

6.1 CNT synthesis By introducing ammonia gas during the CNT synthesis process, the pure CNT films including no impurities such as amorphous carbon could be prepared. The role of the ammonia gas in this CVD process was thought to be the next two possibilities. First, the ammonia gas elevates the hydrogen ratio in the mixed gas during the CNT synthesis process, so that we can control the CNT reaction rate. Also, the ammonia gas, which has an etching ability, etches the catalyst particles and makes them active during the synthesis process.

6.2 Chemical treatment The surface treatment of the CNT films by chemical treatment was investigated by using the XPS analysis. A strong oxygen peak, a weak nitrogen peak, and a fluorine peak in trace level were observed for the O_2 treated CNT film, the HNO_3 treated CNT film, and the HF treated CNT film, respectively. Carbon shifts such as C-O, COO-, or CHF-CHF were observed from the C 1s narrow scan spectra for O_2-CNT film, HNO_3-CNT film, and HF-CNT film. This fact implies that every element observed in the XPS wide scan spectra has a chemical bond with the carbon on the CNT films.

In order to verify the effect of the chemical treatment on the field emission property, the field emission current was measured. All of the chemically treated CNT films show the better field emission property than the original CNT film. Although the field emission from O_2-CNT film occurs at the lower electric field, field emission from HNO_3-CNT film and HF-CNT film occurs at the higher electric field. The threshold of the electric field of the original CNT film, O_2-CNT film, HNO_3-CNT film, and HF-CNT film are 3.55, 2.41, 3.17, and 3.34 V/μm, respectively. As the field emission occurs at pentagons or dangling bonds of the cap, increment of the dangling bonds means the improvement of the field emission performance. And it was thought that the difference of the field emission performance between the CNT film treated in liquid phase and the CNT films treated in gas phase was due to the attached functional groups. The CNT

films treated in liquid phase such as HNO_3-CNT film and HF-CNT film may have carboxyl groups (–COOH). On the other hand, the CNT film treated in gas phase such as O_2-CNT film may have hydroxyl groups (–OH). Since the carboxyl group has more oxygen atoms than the hydroxyl group, it is predicted that the CNT film treated in liquid phase has deeper trap than that treated in gas phase. As a result, the CNT film treated in liquid phase degraded the field emission performance.

6.3 Plasma process Ar, N_2, and H_2 plasma processes were conducted as a surface treatment, its change of the surface state on the plasma processed CNT film was investigated by using XPS analysis. In all of the plasma processed CNT films, a very strong oxygen peak was observed. From the additional experiment, the origin of this strong oxygen peak thought to be come from the water vapor attached at the chamber surface of the plasma process setup.

6.3.1 Ar plasma process In the case of the original CNT film, there was very small oxygen peak, but in the case of the Ar plasma processed CNT films, the strong oxygen peak was observed. In order to evaluate the plasma time effect on the surface composition, the O1s/C1s ratio and the F1s/C1s ratio were obtained from the XPS wide scan spectra. The O1s/C1s ratio and the F1s/C1s ratio were increased from 2.64 % to 59.16 % and from 0 % to 10.44 % with increasing plasma processing time, respectively. These results imply that the Ar plasma process could change the surface composition effectively. From the result of the C 1s narrow scan spectra, every peak was curve fitted and divided into sp^2, sp^3, and carbon shift. In the case of original-CNT film, no carbon shift was observed. In the case of the Ar plasma processed CNT films however, the oxygen related carbon shift was observed. This oxygen related carbon shift at higher binding energy implies increment of amount of the oxygen. The field emission performance increased with increasing the Ar plasma processing time. Ar plasma process can break the bonds between carbon and carbon, so as to create new bonds between carbon and oxygen. The amount of oxygen and the bonding strength between carbon and oxygen increased with increasing the plasma processing time. As the field emission occurs at pentagons or dangling bonds of the cap, increment of the number of bonds between carbon and oxygen means the improvement of the field emission performance.

6.3.2 N_2 plasma process The N_2 plasma process was done to verify the origin of the oxygen peak using ion etching in the XPS inspection chamber. The water vapors in the air don't play an important role in the adhesion of the oxygen to the CNT surface during the plasma process. Therefore we can conclude that the origin of the oxygen peak in the XPS spectra is from the water vapor attached to the chamber wall. The field emission performance increased with increasing the N_2 plasma processing time steadily. These improvement of the field emission performances on the N_2 plasma processed CNT films could be also explained by the increment of the dangling bonds, which the same as the case of the Ar plasma processed CNT films.

6.3.3 H_2 plasma process In the case of the original CNT film, there was very small oxygen peak, but in the case of the H_2 plasma processed CNT films, a very strong oxygen peak was observed. This result is similar to that of Ar and N_2 plasma processed CNT films. The oxygen related carbon shift moves toward the higher binding energy with increasing H_2 plasma processing time. Thus, the gap between the carbon shift and the sp^2 peak increased with increasing plasma processing time. This means that the bonding strength between carbon and oxygen became stronger with increasing H_2 plasma processing time. The field emission performance increased with increasing the H_2 plasma processing time. These improvement of the field emission performances on the N_2 plasma processed CNT films could be also explained by the increment of the dangling bonds, which the same as the case of the Ar plasma processed CNT films.

6.4 General Conclusions By introducing ammonia gas during the CNT synthesis process, the pure CNT films including no impurities such as amorphous carbon could be prepared. The chemical treatment and the plasma process could change the surface state of the CNT films effectively. As the surface treatments increase the dangling bonds on the CNT film's surface, the field emission performance increased. Therefore these surface treatments can be used to improve the field emission performance of the CNT films.

Paper List

International Journal

1. Effect of field emission properties of the chemically modified multi wall carbon nanotubes, Sunwoo LEE and Tetsuji ODA, *Thin Solid Films, (In review)*

2. XPS Investigation and Field Emission Property of the Ar Plasma Processed Carbon Nanotube Films, Sunwoo LEE and Tetsuji ODA, *Journal of Physics D: Applied Physics, (In review)*

Proceedings and Conferences

1. Electron Emission Properties of Carbon Nanotubes Synthesized by Chemical Vapor Deposition, Sunwoo LEE and Tetsuji ODA, *Proceedings of 2002 Annual Meeting of The Institute of electrostatics Japan*, Aug. 2002, Toyohashi, Japan (in English)
2. Effect of Chemical Treatments on the field Emission Property of Carbon Nanotubes, Sunwoo LEE and Tetsuji ODA, *Proceedings of 2003 Annual Meeting of The Institute of electrostatics Japan*, Mar. 2003, Tokyo, Japan (in Japanese)
3. Chemically modified multi wall carbon nanotubes; Field emission properties and XPS investigation, Sunwoo LEE and Tetsuji ODA, *NT03*, Jul. 2003, Seoul, Korea (in English)
4. XPS Analysis of the Chemically Treated Carbon Nanotubes, Sunwoo LEE and Tetsuji ODA, *Proceedings of 2003 Annual Meeting of The Institute of electrostatics Japan*, Aug. 2003, Noda, Japan (in Japanese)
5. H_2 Plasma Processed Carbon Nanotube Films; XPS analysis and Field emission property, Sunwoo LEE and Tetsuji ODA, *Proceedings of 2003 Annual Meeting of The Institute of electrostatics Japan*, Mar. 2004, Tokyo, Japan (in English)

Acknowledgements

I would like to express my sincere gratitude to a number of persons for their support, collaboration, encouragement, and friendship while carrying out my studies in the past three years at the Department of Electronics Engineering.

Before everyone, I would like to thank my supervisor, Prof. *T. Oda*, to whom I am indebted for giving constant support, guidance, incredible freedom for doing research, numerous opportunities, and being concerned with my career development.

I am grateful to Technical Assistant *T. Takahashi* and Research Associate *R. Ono* for their advice and help to construct the experimental setups, and also to Research Associate *H. Tsunakawa* and Mr. *S. Ohtsuka* for teaching the TEM and SEM operation.

My gratitude should also go to all the current and former members of the ODA Laboratory, and especially I would like to thank to Mr. *S.B. Han* and Mr. *K. Yamashita* for their co-work and friendship.

I would like to express my sincere grateful to the *Ministry of Education, Culture, Sports, Science, and Technology* for its great assistance in terms of scholarship provided to me during my whole period of study.

Finally, I would like to thank and devote this work to my lovely family, especially to my wife Ms. *S.J. Jang* in Korea.

Sunwoo LEE
December 9, 2003